Distribution Category:
Magnetic Fusion Energy Systems
(UC-424)

ANL/FPP/TM-276
ITER/US/95/IV-BL-16-A

ARGONNE NATIONAL LABORATORY
9700 South Cass Avenue
Argonne, Illinois 60439-4801

SUMMARY REPORT FOR ITER TASK - D4: ACTIVATION CALCULATIONS FOR THE STAINLESS STEEL ITER DESIGN

by

Hosny Attaya
Fusion Power Program/Technology Development Division

February 1995

Work supported by
Office of Fusion Energy
U.S. Department of Energy
under Contract W-31-109-Eng-38

DISCLAIMER

TABLE OF CONTENTS

LIST OF TABLES

LIST OF FIGURES

Page

Summary Report for ITER Task - D4
Activation Calculations for the Stainless Steel ITER Design

Hosny Attaya

EXECUTIVE SUMMARY

Detailed activation analysis for ITER has been performed as a part of ITER Task D4. The calculations have been performed for the shielding blanket (SS/water) and for the breeding blanket (Li/V) options. The activation code RACC-P, which has been modified under ITER Task-D-10 for pulsed operation, has been used in this analysis. The spatial distributions of the radioactive inventory, decay heat, biological hazard potential, and the contact dose were calculated for the two designs for different operation modes and targeted fluences.

A one-dimensional toroidal geometrical model has been utilized to determine the neutron fluxes in the two designs. The results are normalized for an inboard and outboard neutron wall loadings of 0.91 and 1.2 MW/m^2, respectively.

The point-wise distributions of the decay gamma sources have been calculated everywhere in the reactor at several times after the shutdown of the two designs and are then used in the transport code ONEDANT to calculate the biological dose everywhere in the reactor. The point-wise distributions of all the responses have also been calculated. These calculations have been performed for neutron fluences of 3.0 MWa/m^2, which corresponds to the target fluence of ITER, and 0.1 MWa/m^2, which is anticipated to correspond to the beginning of an extended maintenance period.

The decay heat results show that a large fraction of this energy (50 to 90%) is produced by photons. This implies that this energy would be transported to different parts of the reactor, thus relieving the energy concentration at high intensity source

locations such as the first wall. Accurate modeling for the decay gamma transport is required to produce realistic spatial distribution of the decay heat which may be used in LOCA and LOFA analyses.

The results of the pulsed operation, using the new version of RACC, show large reductions in the radioactivity and the decay heat for pure pulsed operation. The continuous operation assumption, usually used in the radioactivity calculations, overestimates the different activation responses at the final shutdown and for about one week after shutdown by a factor of more than 2.

1. Introduction

Part of this design task is to perform activation calculations for the different parts of ITER to provide information needed for the engineering design, maintenance assessment, safety analysis, and radwaste management. For this purpose, detailed activation analyses have been carried out for the two ITER designs, the SS/water design and the LiV (breeding) design. For both designs, the radial build, the neutron wall loading, and the operation scenarios, used in these calculations, were provided by the JCT.

The activation code RACC-P [1], which has been modified under ITER Task-D-10 for pulsed operation [2], has been used in this analysis. The spatial distributions of the radioactive inventory, decay heat, biological hazard potential, and the contact dose were calculated for the two designs for different operation modes and targeted fluences. In this report the activation results of the stainless steel-water design (SS/water) are presented.

2. Calculational Procedure

There is no reliable multidimensional deterministic transport computer code that is capable of adequately modeling the complicated tokamak geometry and calculating the neutron flux, which is the key input for the activation calculations, accurately. On the other hand, utilizing the neutron flux calculated by 3-D Monte Carlo methods in the activation calculations would impregnate its results with the large statistical errors inherent to the calculated Monte Carlo flux. Thus, for the activation calculations, a one-dimensional cylindrical toroidal geometrical model has been used in the neutron transport calculations. In this model, the cylinder axis is the vertical axis of the reactor, and the inboard and the outboard blankets/shields are modeled with their midplane compositions. The neutron source is extended between the midplane plasma boundaries. This allows for the mutual neutronics coupling between the inboard and the outboard blankets/shields as well as the geometrical toroidal effect on the calculated neutron flux.

It is important to realize the limitations of this modeling and to understand the employed approximations in order to interpret the obtained activation results correctly. The first obvious assumption in this model is the full coverage of the FW/blanket/shield, i.e., no account is made for the large penetrations in the reactor. The second assumption is the discount of any poloidal variations of the neutron wall loading, the neutron source incident angle, and the radial build of the blanket/shield. The model deals with and produces average vertical (poloidal) values representing part of the system rather than localized values that could deviate considerably from the system average. Another assumption is the nucleonics decoupling of that part of the system, modeled in the calculations, from the rest of the system. The larger the modeled part is, the less effect this assumption has. These assumptions, in general, tend to overestimate the radioactivity.

3. Material Composition

The weight and the atomic compositions of the different materials used in these calculations are given in Table 1. In this table, the mass density (g/cc) and the atomic density (atoms-barn/cc) are listed first for each material, then the mass and atomic densities of each element are given in percentage or in ppm (marked by *).

Table 2 shows the volume compositions of the different mixtures made up from the basic materials (Table 1), and assigned to different geometrical zones. The names and acronyms used in these two tables are keys to understanding all of the graphics outputs.

Table 1. Materials' compositions

Alloy:	SS316-L	Incl625	SS316lw	v4cr4ti	r-epxy
ρ :	7.855[a] :8.528-2[b]	8.44 :8.632-2	7.855 :8.543-2	6.1 :7.235-2	1.9006 :8.421-2
	:	:	:	:	:
H	.... :........	.... :........	.... :........	.... :........	1.90 : 25.69
B	* 10.00 : * 51.30	.... :........	* 10.00 : * 51.21	.... :........	.... :........
C	0.02 : 0.08	0.10 : 0.49	0.01 : 0.05	* 50.00 : 0.02	19.85 : 22.47
N	0.07 : 0.28	.... :........	0.19 : 0.75	0.01 : 0.04	2.52 : 2.45
O	* 20.00 : * 69.33	.... :........	* 20.00 : * 69.21	0.03 : 0.10	37.82 : 32.13
Mg	.... :........	.... :........	.... :........	.... :........	2.53 : 1.41
Al	0.30 : 0.62	0.40 : 0.87	0.30 : 0.62	0.02 : 0.04	9.26 : 4.67
Si	0.46 : 0.91	0.50 : 1.05	0.10 : 0.20	0.04 : 0.07	19.63 : 9.50
P	0.03 : 0.05	0.02 : 0.04	* 30.00 : * 53.63	* 4.00 : * 6.56	.... :........
S	0.01 : 0.02	0.02 : 0.04	* 14.00 : * 24.17	* 3.00 : * 4.75	1.43 : 0.61
Cl	.... :........	.... :........	.... :........	* 1.00 : * 1.43	.... :........
K	* 5.00 : * 7.09	.... :........	* 5.00 : * 7.08	* 0.10 : * 0.13	.... :........
Ti	0.04 : 0.05	0.40 : 0.49	0.04 : 0.05	4.00 : 4.24	.... :........
V	* 40.00 : * 43.55	.... :........	* 40.00 : * 43.48	91.89 : 91.58	.... :........
Cr	17.10 : 18.24	22.00 : 24.91	17.17 : 18.28	4.00 : 3.91	.... :........
Mn	1.70 : 1.72	0.50 : 0.54	1.48 : 1.49	.... :........	.... :........
Fe	64.43 : 63.99	5.00 : 5.27	66.33 : 65.77	* 40.00 : * 36.37	.... :........
Co	0.03 : 0.03	1.00 : 1.00	0.03 : 0.03	.... :........	.... :........
Ni	13.20 : 12.47	57.05 : 57.24	12.14 : 11.45	* 3.00 : * 2.60	.... :........
Cu	0.10 : 0.09	.... :........	0.10 : 0.09	* 2.00 : * 1.60	5.05 : 1.08
As	* 5.00 : * 3.70	.... :........	* 5.00 : * 3.70	* 2.00 : * 1.36	.... :........
Zr	* 20.00 : * 12.16	.... :........	* 20.00 : * 12.14	* 1.00 : * 0.56	.... :........
Nb	* 20.00 : * 11.94	4.00 : 2.54	0.05 : 0.03	* 0.50 : * 0.27	.... :........
Mo	2.50 : 1.45	9.00 : 5.52	2.03 : 1.17	* 4.00 : * 2.12	.... :........
Ag	* 2.00 : * 1.03	.... :........	* 2.00 : * 1.03	* 0.01 : * 0.00	.... :........
Cd	* 2.00 : * 0.99	.... :........	* 2.00 : * 0.99	.... :........	.... :........
Sn	* 20.00 : * 9.34	.... :........	* 20.00 : * 9.33	.... :........	.... :........
Sb	* 5.00 : * 2.28	.... :........	* 5.00 : * 2.27	.... :........	.... :........
Ba	* 5.00 : * 2.02	.... :........	* 5.00 : * 2.02	.... :........	.... :........
Tb	* 5.00 : * 1.75	.... :........	* 5.00 : * 1.74	.... :........	.... :........
Ta	* 5.00 : * 1.53	* 50.00 : * 16.27	* 5.00 : * 1.53	* 0.20 : * 0.06	.... :........
W	* 10.00 : * 3.02	.... :........	* 10.00 : * 3.01	* 1.00 : * 0.28	.... :........
Ir	* 5.00 : * 1.44	.... :........	* 5.00 : * 1.44	.... :........	.... :........
Pb	* 8.00 : * 2.14	.... :........	* 8.00 : * 2.14	.... :........	.... :........
Bi	* 8.00 : * 2.12	.... :........	* 8.00 : * 2.12	.... :........	.... :........

a) density (g/cc.)
b) atomic density (atoms-barn/cc).

	nb3sn	b4c	cube	L_nak68	wc
	9. :5.455-2	2.52 :1.373-1	8.87461 :8.679-2	0.81691 :1.748-2	15.62606 :9.614-2
	:	:	:	:	:
Be	.... :........	.... :........	0.50 : 3.42	.... :........	.... :........
B	.... :........	78.26 : 80.00	.... :........	.... :........	.... :........
C	.... :........	21.74 : 20.00	.... :........	.... :........	6.14 : 50.03
Na	.... :........	.... :........	.... :........	55.55 : 68.00	.... :........
K	.... :........	.... :........	.... :........	44.45 : 32.00	.... :........
Ni	.... :........	.... :........	2.00 : 2.10	.... :........	.... :........
Cu	.... :........	.... :........	97.50 : 94.48	.... :........	.... :........
Nb	70.13 : 75.00	.... :........	.... :........	.... :........	.... :........
Sn	29.87 : 25.00	.... :........	.... :........	.... :........	.... :........
W	.... :........	.... :........	.... :........	.... :........	93.86 : 49.97

Table 2. Zonal volume compositions (%).

Mix:	SSWP	coil	B4C_Pb	Incon	WNaK	Cua	SS_H20	SS	H20
material	%	%	%	%	%	%	%	%	%
ss316-L	....	....	....	....	....	....	60.	100.	......
incl625	....	....	...	100.	....	....	....	....	......
ss316lw	100.	47.	...	....	....	....	....	....	.....
r-epxy	....	13.3	....	....	....	....	....	....	......
nb3sn	....	10.5	....	....	....	....	....	....	......
b4c	....	....	40.	....	....	....	....	....	......
cube	....	....	....	....	....	100.	....	....	......
L_nak68	....	....	....	....	20.	....	....	....	......
wc	....	....	....	....	80.	....	....	....	.....
h2o	....	....	....	....	....	....	40.	....	100.
cu_ITR	....	12.	....	....	....	....	....	....	......
pb_p	....	....	60.	....	....	....	....	....	......
lhe	....	17.2	....	....	....	....	....	....	......

Mix:	Vall	Li	WC	BeZ
Material	%	%	%	%
v4cr4ti	100.	....	....	....
wc	....	....	100.	....
L_li	....	100.	....	....
be100	....	....	....	100.

4. The SS/Water Design

4.1 Radial Build and Neutron Flux

The radial build of this design at the midplane is given in Table 3 which lists the thickness, the mix name, the number of fine intervals, the radial extents, the cross section area, and the mass of each zone. There are 46 zones in this model. The zone numbers are used in many figures and this table should be consulted to identify the different zones. Radioactivity calculations have been made for all zones and for all the fine intervals within each zone in order to determine accurate spatial distribution for the decay heat and the γ source.

The transport code ONEDANT [3] has been used to calculate the neutron flux. Figure 1 shows a schematic of the midplane radial build-up of ITER SS/Water design together with the neutron and photon fluxes. In this figure, for illustrative purposes and in order to show the characteristics of these fluxes and the effects of the different materials on them, all the photon groups are collapsed into only one group, and the neutron groups are collapsed into 5 major energy groups whose lower energy limits are 10 MeV, 1 MeV, 0.12 MeV, 0.87 eV, and 10^{-4}eV. More detailed descriptions of the flux are shown in Figures 2 and 3 where isometric views of the inboard and the outboard neutron fluxes are shown as a function of the radius and the lethargy.

4.2 Fine Mesh Results

As indicated above, fine mesh calculations have been made in order to determine accurately the γ source distribution to be used for the contact dose calculations. Also, for any serious LOCA analysis, the spatial distribution of the decay heat is required. Figures 4-6 show the results of these calculations for the radioactivity, the decay heat, and the point-source contact dose, respectively. The latter is based on the dose at one meter radius in the air from a point γ source which is taken as the specific γ intensity at each interval. Thus, these γ's do not suffer any attenuation and the resultant dose is useful only in the context of a large system, in identifying the spatial distribution of the γ source intensity in the system.

As seen in these figures, there are orders of magnitude attenuations of the different responses within thick zones. This indicates that using the average flux in a thick zone to calculate the radioactivity of that zone would underestimate the activity level in the zone.

4.3 System Analysis

The total radioactivity, the total decay heat, and the total air biological hazard potential of this design after operating up to a neutron fluence of 3 MWa/m^2 are shown as a function of time after shutdown in Figs. 7-9. The inhalation biological hazard potential (BHP_{air}) for the public, is based on the US Federal Regulations (10CFR20).

There is about 8 MCi/cm of radioactivity after the shutdown. The isotopic contributions to this activity are shown in the top part of the figure and the zonal contributions (see Table 3) are shown in the bottom part. In this figure and similar ones, only isotopes or zones that contribute more than 10% to the total response, at any time, are shown. The shadowed area at the top represents the contributions of all other isotopes or zones not shown in the figure.

The 0.5 cm Cu layer (zone 22 and 25) used on the FW produces more than 40% of the total radioactivity in the design after shutdown and for about one day. It dominates the radioactivity also at about 100 years after shutdown, since it yields a large fraction of the ^{63}Ni in the system.

At shutdown, there is about 50 kW/cm of radiation power. About 60 to 90% of this power is produced by photons. Usually, in the LOCA analyses [4,5], the decay heat is assumed localized where it is produced. This leads to a large concentration of heat that in turn produces hot spots. The fact that a large fraction of this heat is generated by photons, which have larger range than the charged particles, may level the heat concentration throughout the system.

The BHP_{air} is dominated by the SS zones except in the very short time after shutdown, where it is dominated by the Be zones because of the production of ^{8}Li and ^{6}He.

4.4 Pulsed Operation

Three operational scenarios were suggested by the JCT to reach the target design fluence of 3 MWa/m^2. The first is simply the continuous operation mode. Assuming a burn time and dwell time of 1000 and 2039 seconds, the second scenario assumes 103652 cycles. The third scenario consists of 101777 cycles followed by two weeks of continuous operation. We show the results of these scenarios for the inboard FW, for which a total of 3.25 years of operation is required to reach the target fluence.

The specific activity, the decay heat, and the point-source contact dose in the inboard FW for the three operation scenarios are shown in Figs. 10-12. It is evident that the continuous operation mode overestimates the specific activity, the decay heat, and the dose, at the final shutdown and for about one week after shutdown by about a factor of 2.4 more than the pure pulse operation mode. Adding a short period of continuous operation (two weeks as in the third scenario) decreases this factor considerably. The difference between the different operation scenarios decreases afterward and vanishes, as expected [6], after a long cooling time.

One expects that for an experimental device such as ITER, there would be longer shut-down periods between pulses and a limited numbers of long burn-time pulses. This would make the radioactivity inventory even less than that of the pure pulsed scenario. Thus, in order to alleviate safety constraints on the ITER design, it is important to have a reasonable estimate of the operation scenario of ITER.

4.5 Contact Dose

The γ sources have been calculated for all the fine meshes and for two neutron fluences of 3 MWa/m^2 and 0.1 MWa/m^2 and for different times after shutdown. The γ sources, at each time step after shutdown are then used in the ONEDANT code to calculate the γ flux and the dose equivalent rate everywhere in the reactor. Figure 13 shows the dose distribution after the 3 MWa/m^2 fluence and Fig. 14 shows the dose distribution after the 0.1 MWa/m^2 fluence. The recommended dose rate limit of 2.5 mrem/hr for a full time worker can not be achieved anywhere for a long time after shutdown.

4.6 Detailed Zones' Results

For each zone in the design, the radioactivity, the decay heat, the BHP_{air}, and the point-source contact dose are shown in Appendix A. Because of the interest in the water activation due to the production of the high energy γ's of ^{16}N from the $^{16}O(n,p)\ ^{16}N$ reaction, the water zones at the front and at the back of the inboard and outboard shields are included. The zones are ordered (in Appendix A) from the front (plasma side) to the back of the inboard and the outboard shields respectively.

Table 3. The radial build of the SS/Water design.

Z #	dr	Mix	intv	R1	R2	xs-area	Mass
	cm			cm	cm	m^2	kg/cm
	287.5	vac	29	0.0	287.5		
1	89.4	coil	9	287.5	376.9	18.66023	1109.47
2	0.1	INSUL	1	376.9	377.0	0.02368	0.45
	13.5	vac	14	377.0	390.5		
3	5.0	B4C_Pb	5	390.5	395.5	1.23465	96.45
4	5.0	VV-incl	5	395.5	400.5	1.25035	105.53
5	30.5	SS_H2O	31	400.5	431.0	7.96731	407.37
6	5.0	VV-incl	5	431.0	436.0	1.36188	114.94
	5.0	vac	5	436.0	441.0		
7	6.9	SS	7	441.0	447.9	1.92687	151.36
8	3.1	H2O	4	447.9	451.0	0.87543	8.75
9	4.2	SS	5	451.0	455.2	1.19570	93.92
10	3.0	H2O	3	455.2	458.2	0.86086	8.61
11	7.0	SS	7	458.2	465.2	2.03066	159.51
12	3.0	H2O	3	465.2	468.2	0.87971	8.80
13	5.5	SS	6	468.2	473.7	1.62749	127.84
14	3.0	H2O	3	473.7	476.7	0.89573	8.96
15	5.0	SS	5	476.7	481.7	1.50545	118.25
16	3.0	H2O	3	481.7	484.7	0.91081	9.11
17	2.3	SS	3	484.7	487.0	0.70212	55.15
18	2.0	H2O	2	487.0	489.0	0.61324	6.13
19	1.0	SS	1	489.0	490.0	0.30756	24.16
20	3.6	H2O	4	490.0	493.6	1.11243	11.12
21	0.1	SS(FW)	1	493.6	493.7	0.03102	2.44
22	0.5	Cua	1	493.7	494.2	0.15518	13.77
23	0.8	BeZ	1	494.2	495.0	0.24861	4.60
	11.6	vac	2	495.0	506.6		
	608.4	source	61	506.6	1115.0		
	16.3	vac	2	1115.0	1131.3		
24	0.8	BeZ	1	1131.3	1132.1	0.56885	10.52
25	0.5	Cua	1	1132.1	1132.6	0.35574	31.57
26	0.1	SS(FW)	1	1132.6	1132.7	0.07117	5.59
27	3.6	H2O	4	1132.7	1136.3	2.56618	25.66
28	1.0	SS	1	1136.3	1137.3	0.71427	56.11
29	2.0	H2O	2	1137.3	1139.3	1.43043	14.30
30	2.3	SS	3	1139.3	1141.6	1.64810	129.46
31	3.0	H2O	3	1141.6	1144.6	2.15469	21.55
32	5.0	SS	5	1144.6	1149.6	3.60372	283.07
33	3.0	H2O	3	1149.6	1152.6	2.16977	21.70
34	5.5	SS	6	1152.6	1158.1	3.99260	313.62
35	3.0	H2O	3	1158.1	1161.1	2.18579	21.86
36	7.0	SS	7	1161.1	1168.1	5.12218	402.35
37	3.0	H2O	3	1168.1	1171.1	2.20464	22.05
38	4.2	SS	5	1171.1	1175.3	3.09600	243.19
39	3.1	H2O	4	1175.3	1178.4	2.29225	22.92
40	6.9	SS	7	1178.4	1185.3	5.12379	402.47
	37.5	vac	38	1185.3	1222.8		
41	5.0	VV-incl	5	1222.8	1227.8	3.84939	324.89
42	46.9	SS_H2O	47	1227.8	1274.7	36.87201	1885.27
43	5.0	VV-incl	5	1274.7	1279.7	4.01244	338.65
44	5.0	B4C_Pb	5	1279.7	1284.7	4.02815	314.68
	15.3	vac	14	1284.7	1300.0		
45	0.1	INSUL	1	1300.0	1300.1	0.08168	1.55
46	89.4	coil	9	1300.1	1389.5	75.53967	4491.30
Total						210.06052	12031.01

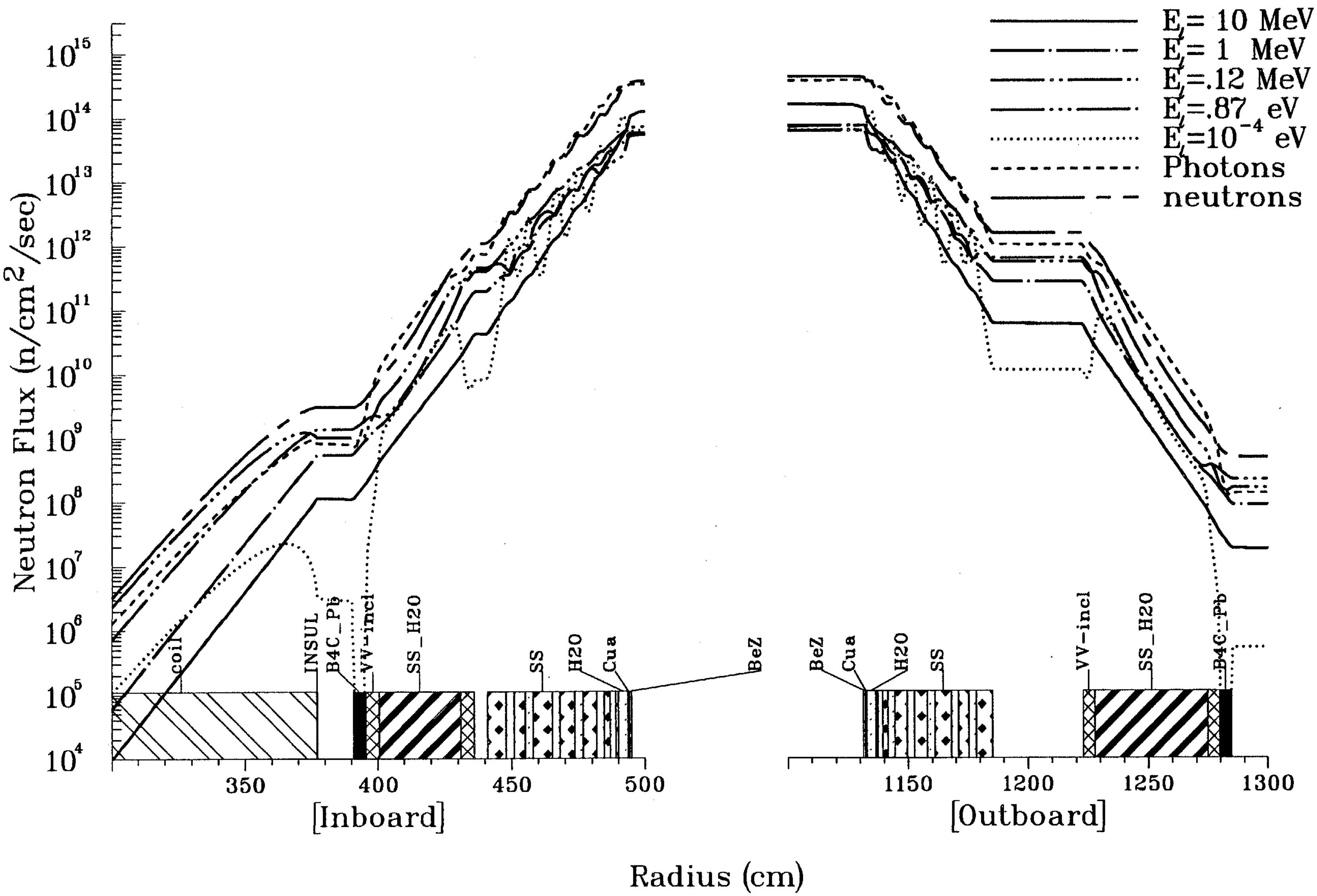

Figure 1. The midplane radial build of ITER, the neutron, and the photons fluxes (SS/water design).

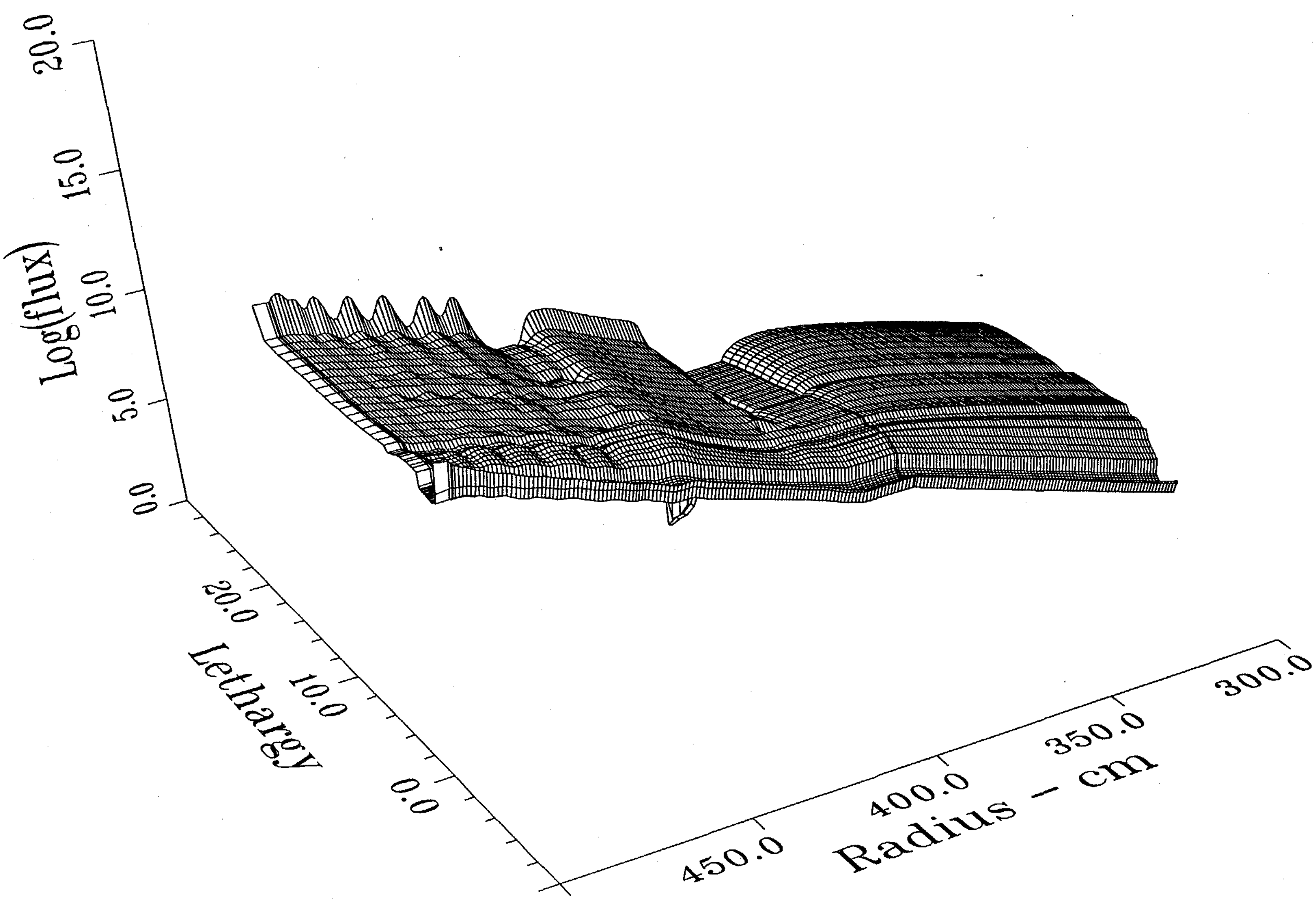

Figure 2. Isometric view of the inboard neutron flux (logarithmic scale) as a function of the lethargy and radius (SS/water design).

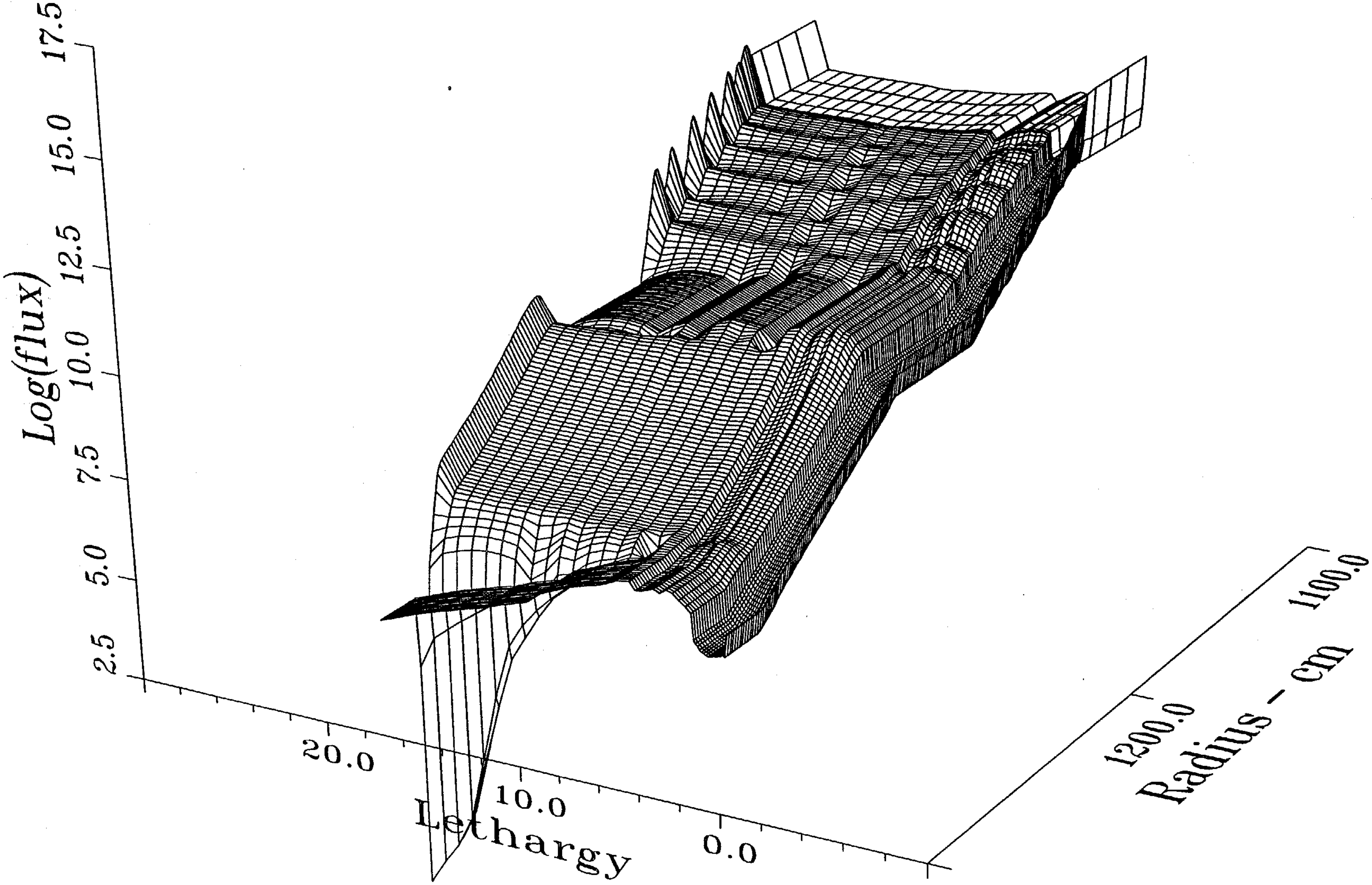

Figure 3. Isometric view of the outboard neutron flux (logarithmic scale) as a function of the lethargy and radius (SS/water design).

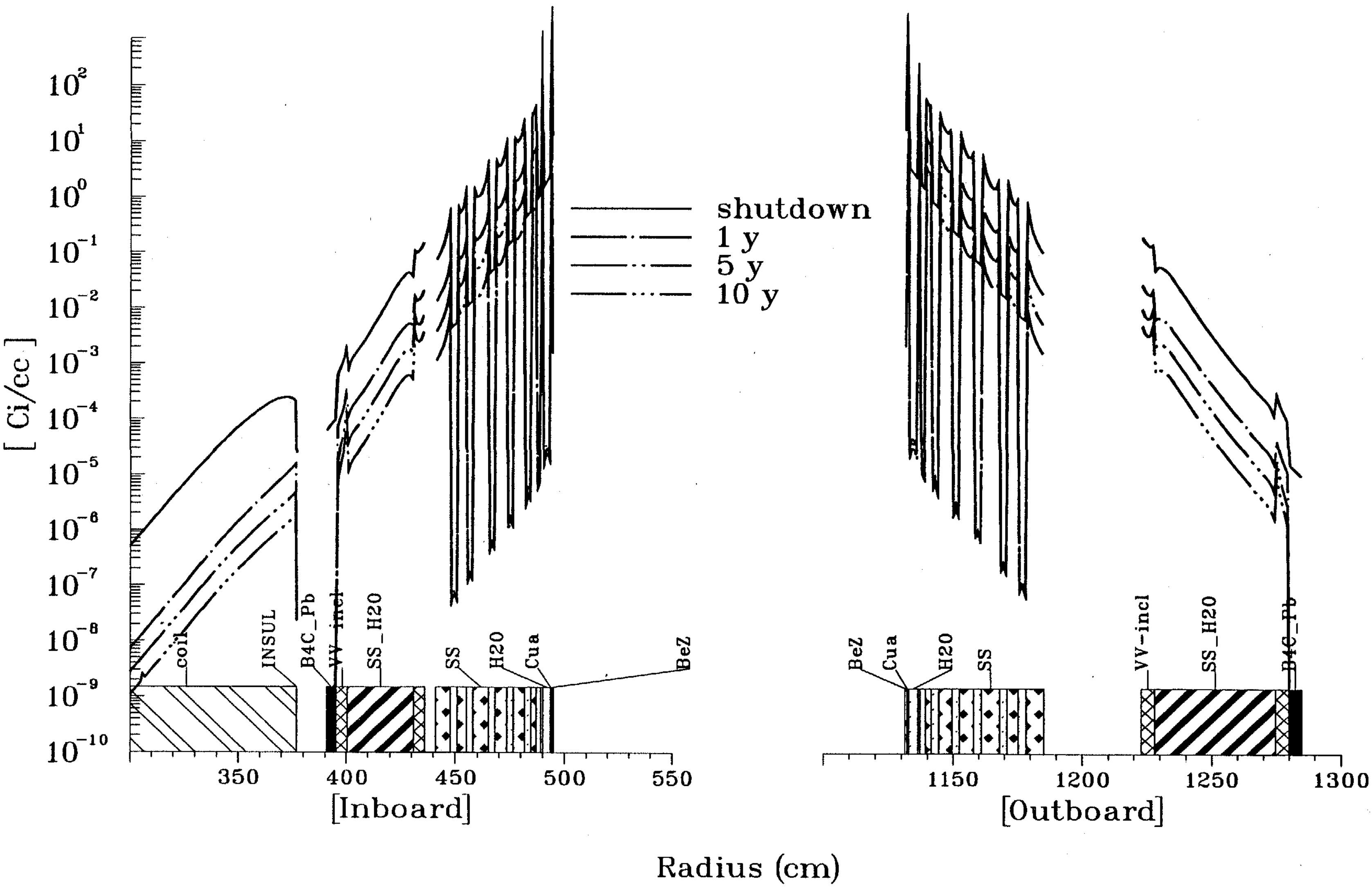

Attaya@ANL:xspw2 950131 14:47:c jpfine 950201 11:12:c wbinss

Figure 4. The specific radioactivity distribution at different times after shutdown (SS/water design).

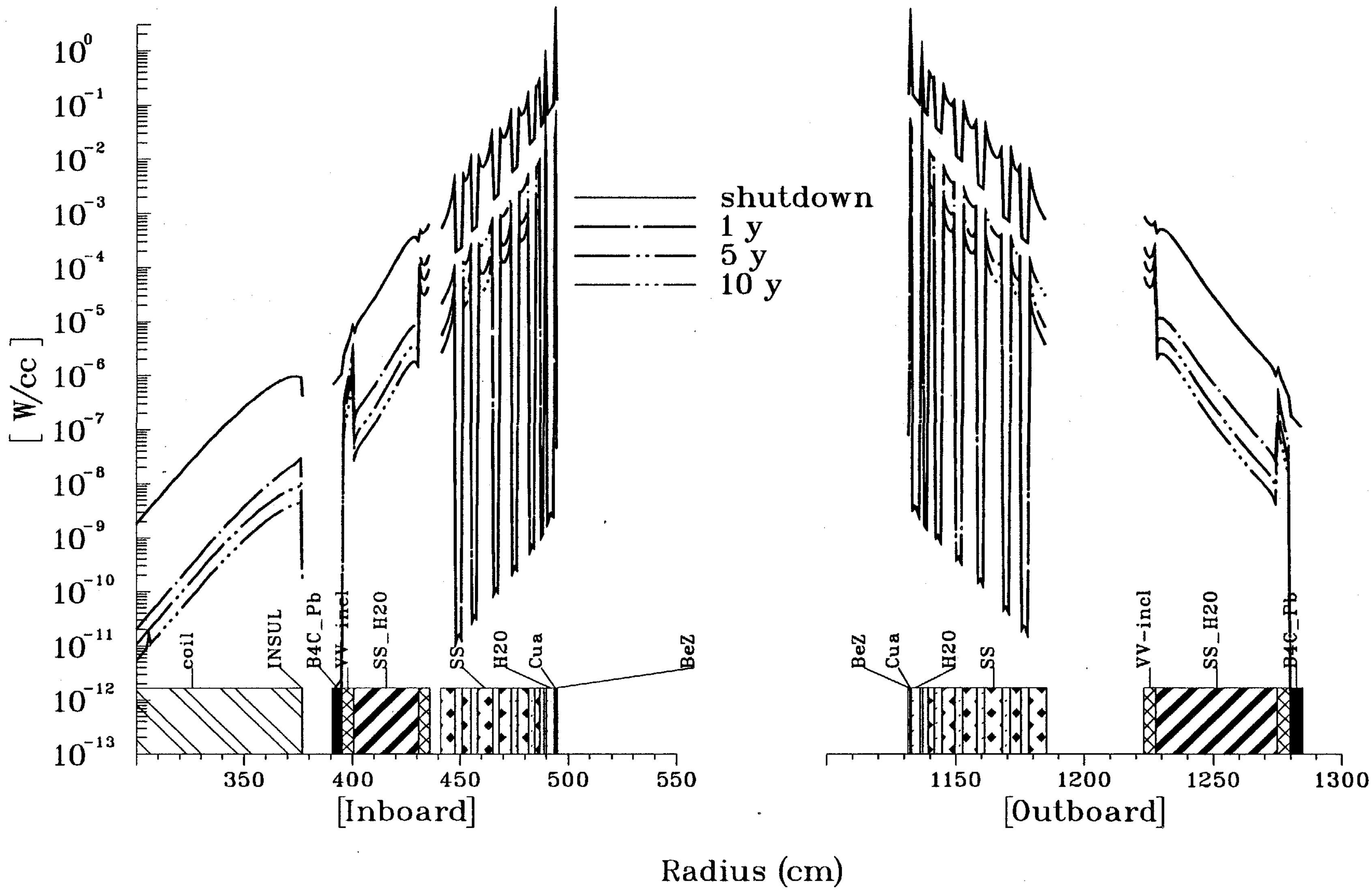

Attaya@ANL:xspw2 950131 14:47:c jpfine 950201 11:25:c wbinss

Figure 5. The specific decay heat distribution at different times after shutdown (SS/water design).

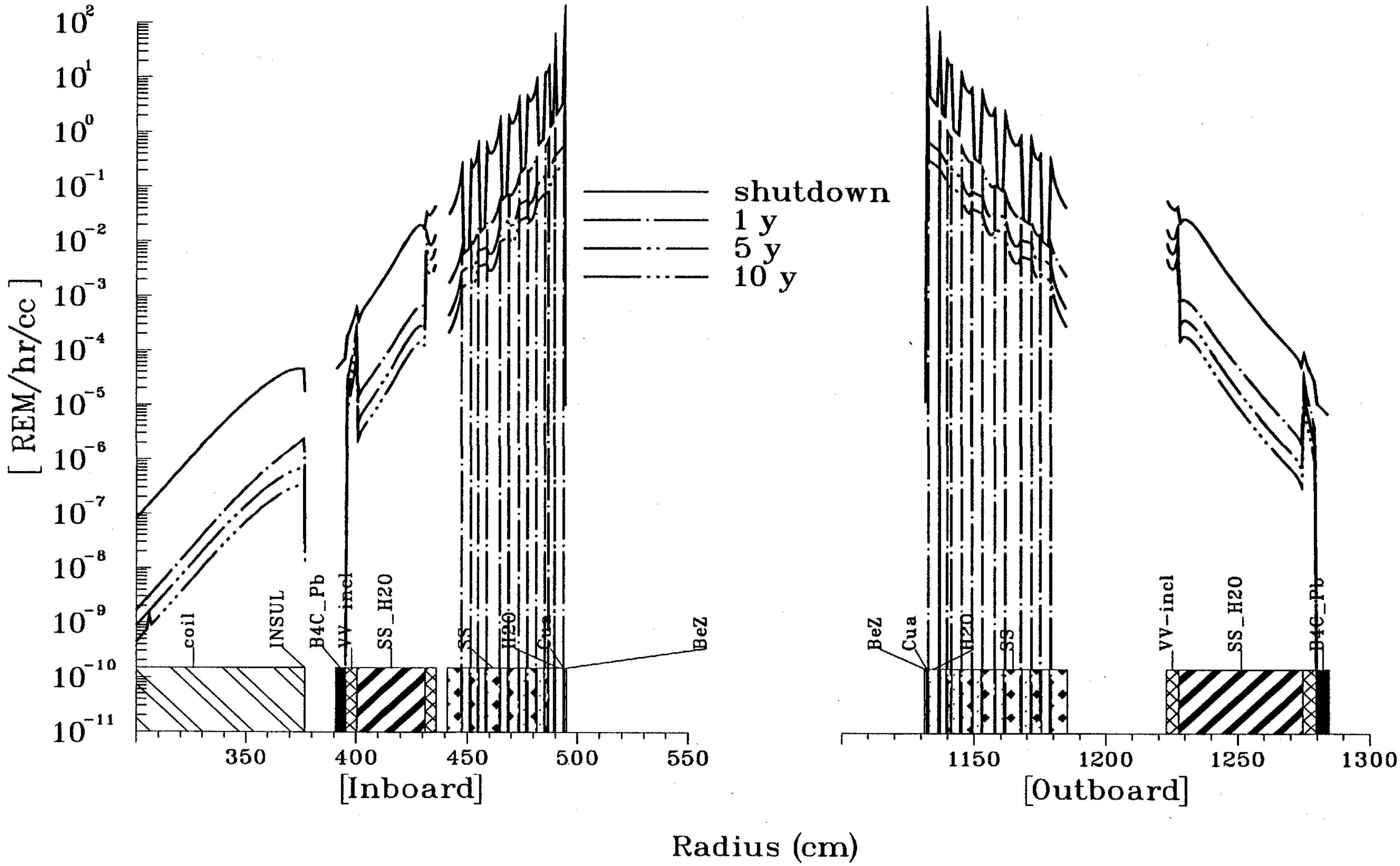

Attaya@ANL:xspw2 950131 14:47:c jpfine 950201 11:32:c wbinss

Figure 6. The point-source contact dose distribution at different times after shutdown (SS/water design).

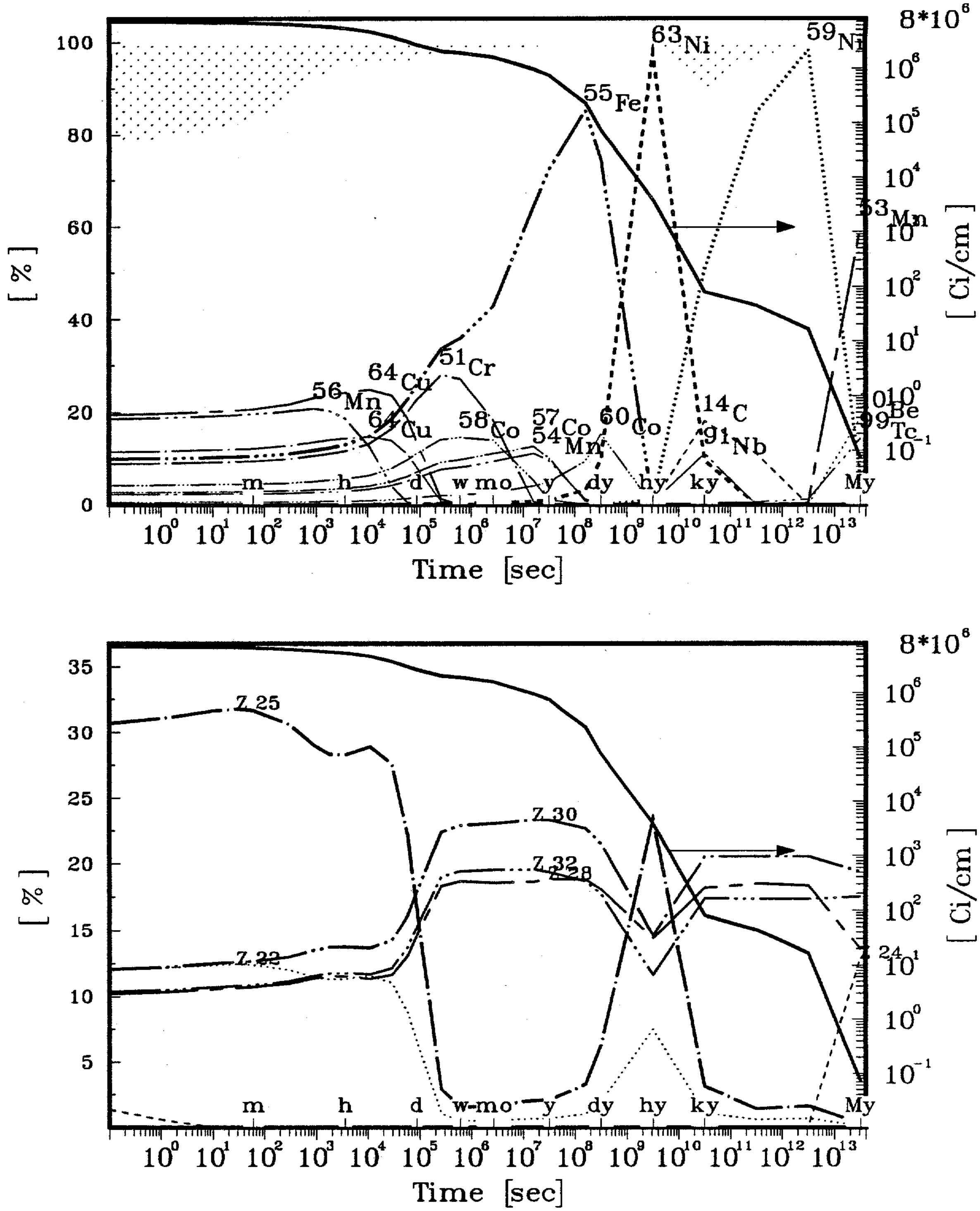

Figure 7. The total radioactivity (per cm height) in the system, top: isotopic contributions, bottom: zonal contributions (SS/water design).

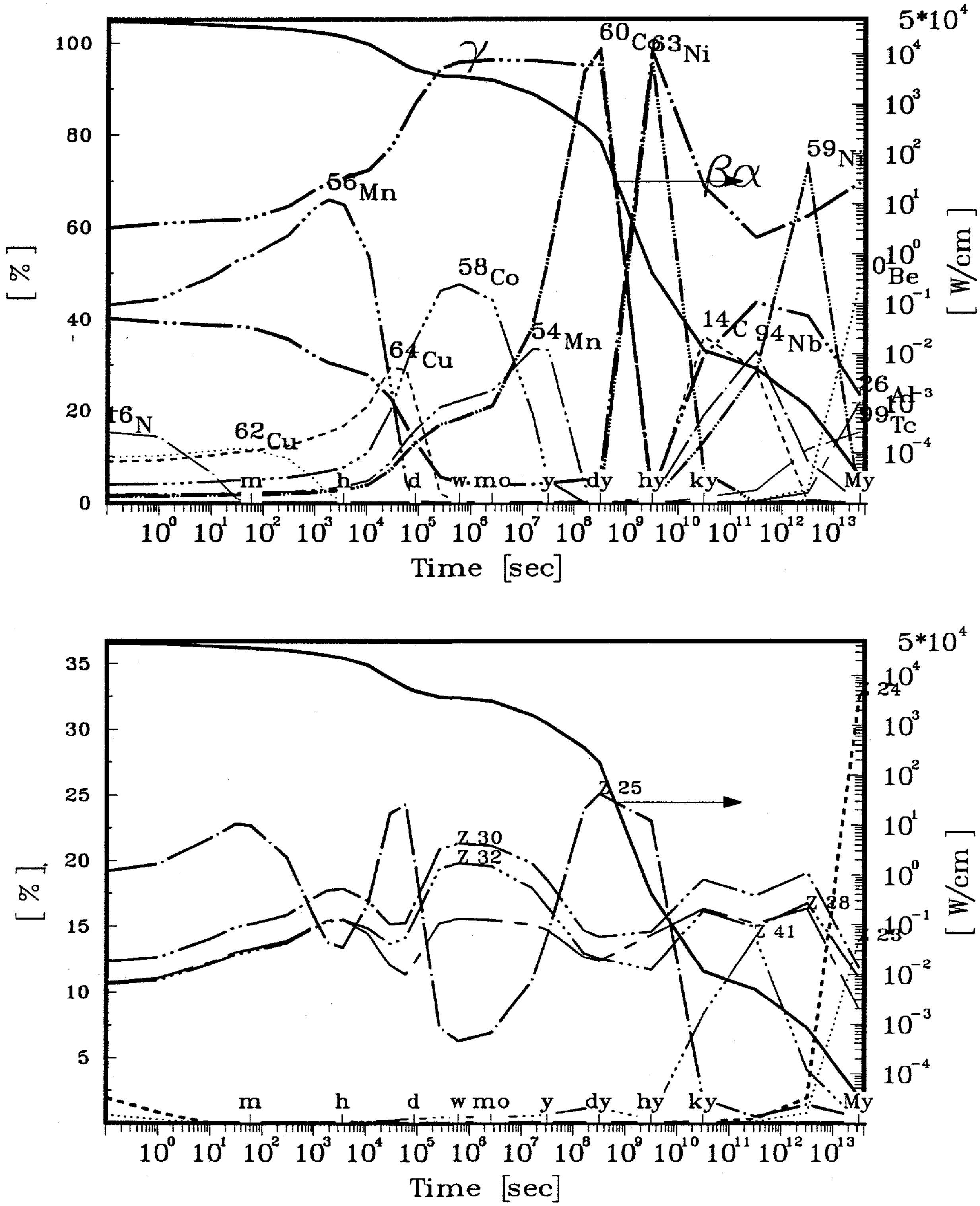

Figure 8. The total decay heat (per cm height) in the system, top: isotopic contributions, bottom: zonal contributions (SS/water design).

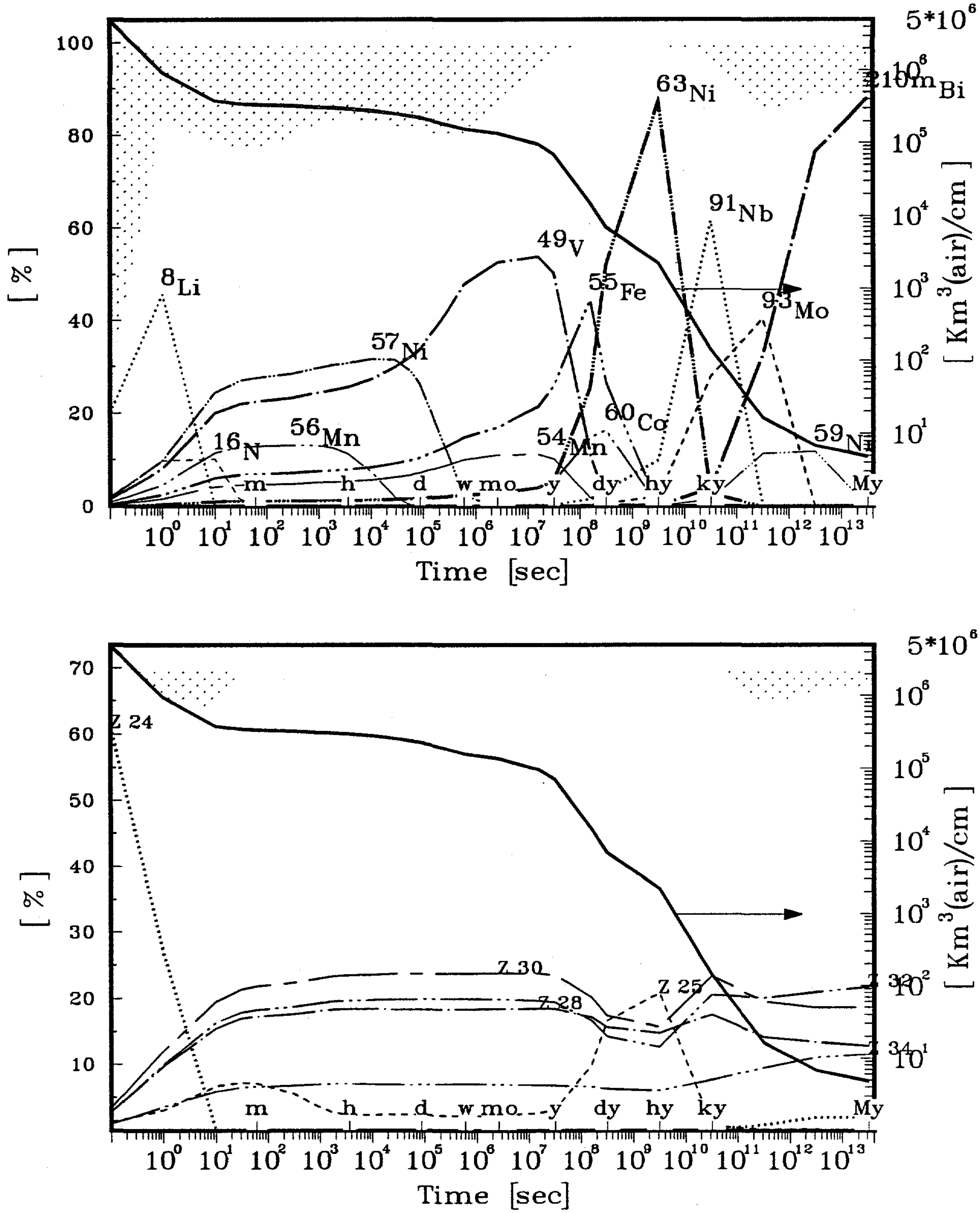

Figure 9. The total air BHP (per cm height) in the system, top: isotopic contributions, bottom: zonal contributions (SS/water design).

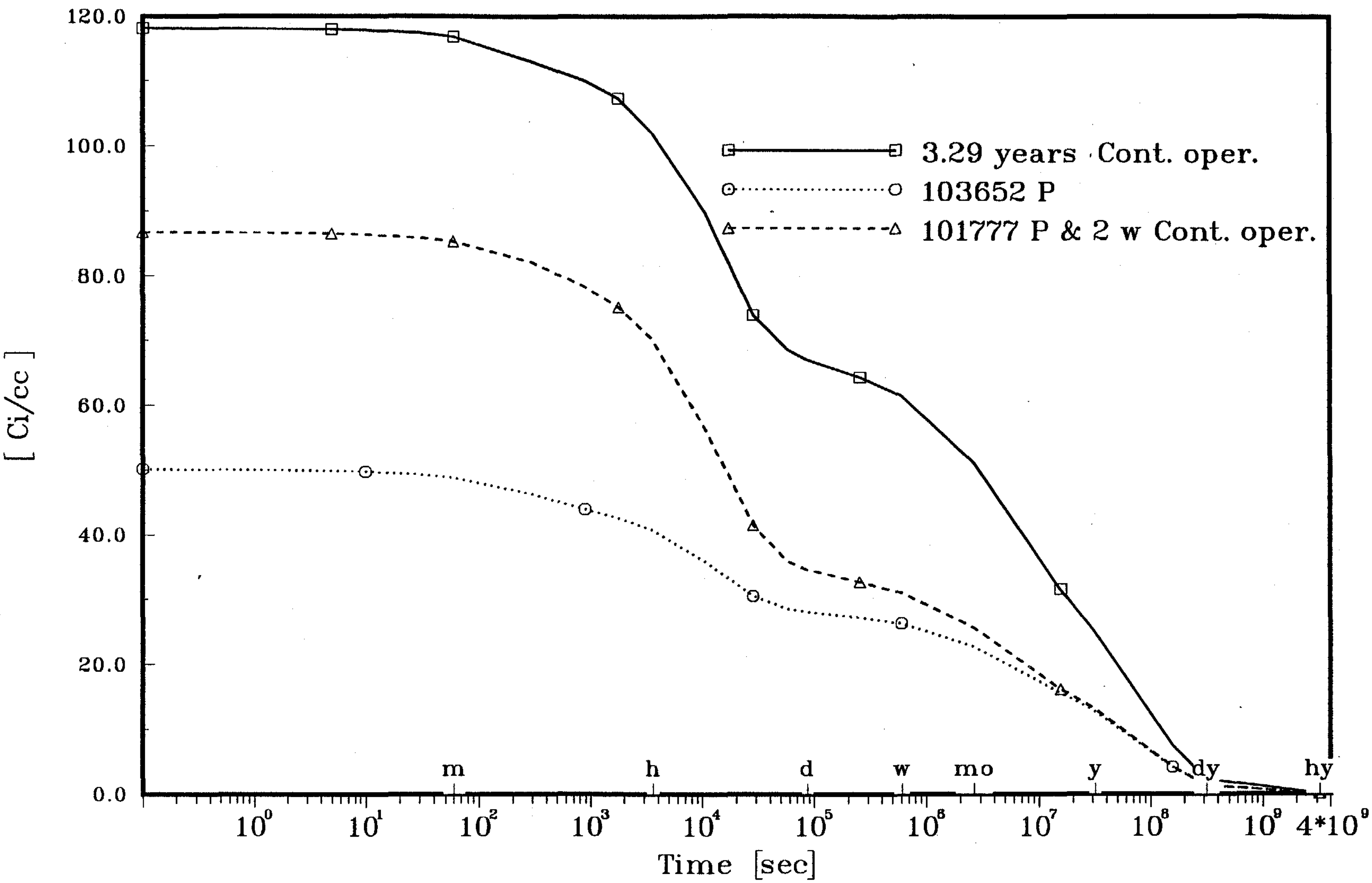

Figure 10. The radioactivity in the inboard FW after different operational scenarios (SS/water design).

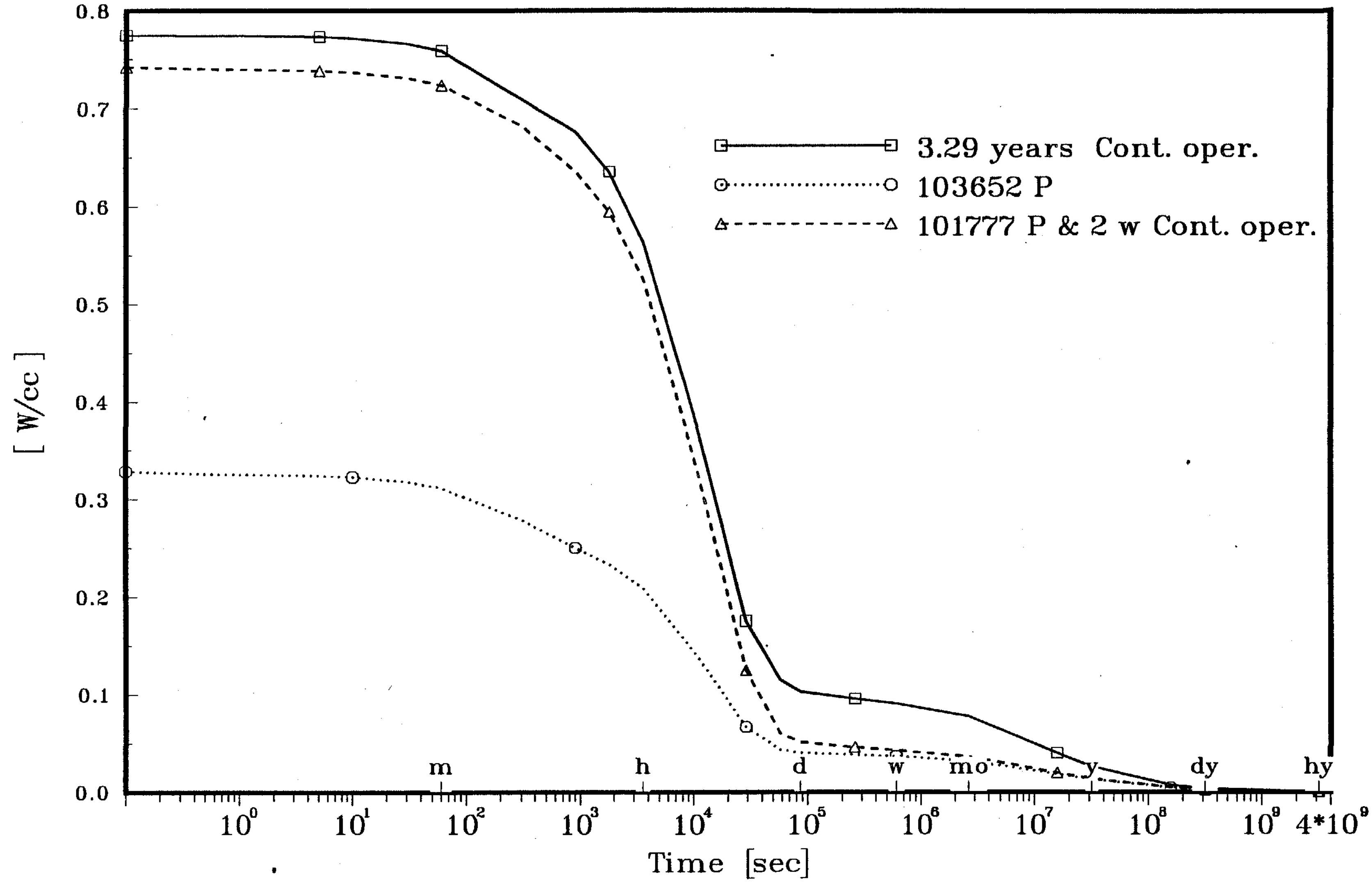

Figure 11. The decay heat in the inboard FW after different operational scenarios (SS/water design).

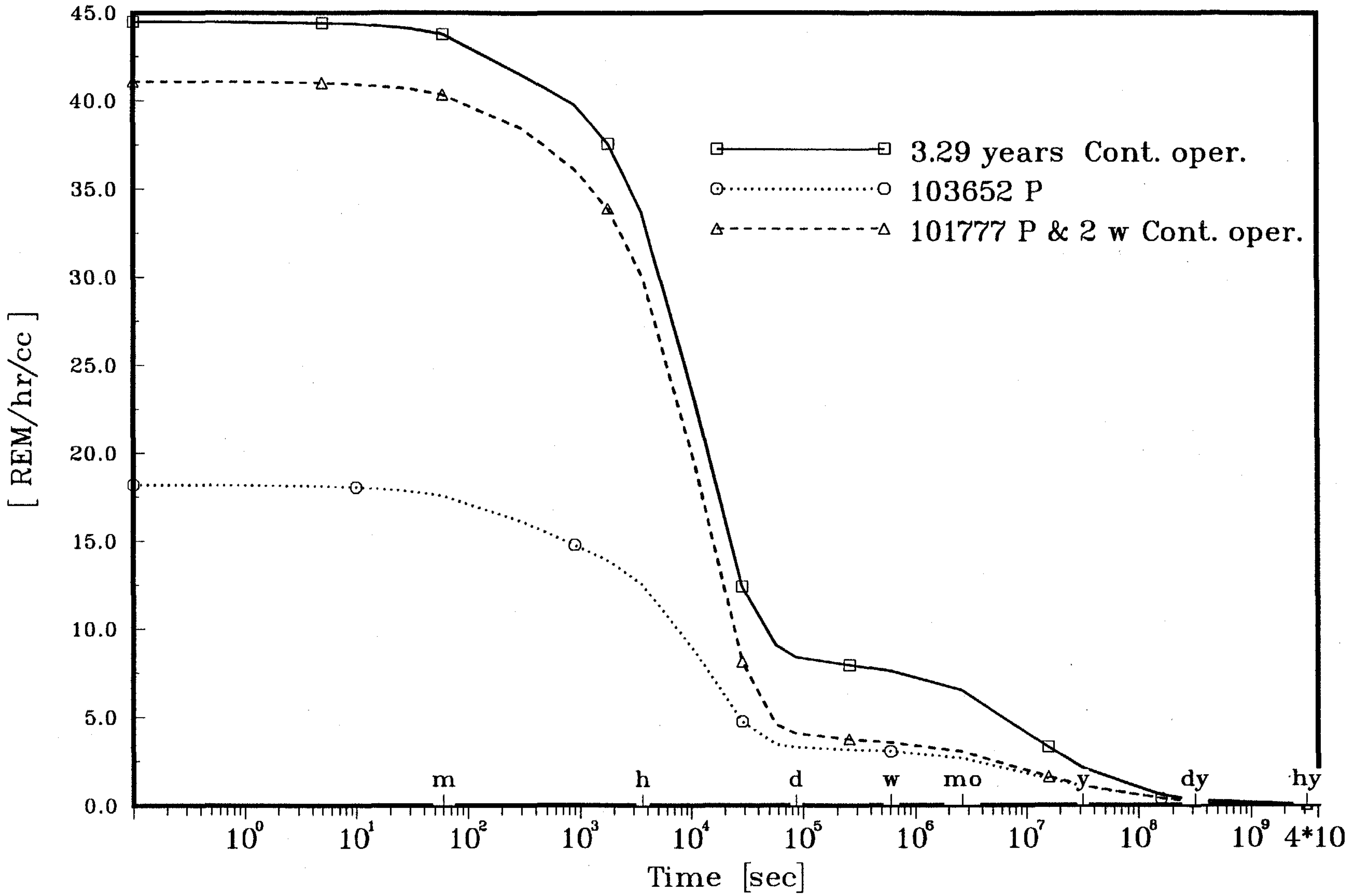

Figure 12. The point-source contact dose of the inboard FW after different operational scenarios (SS/water design).

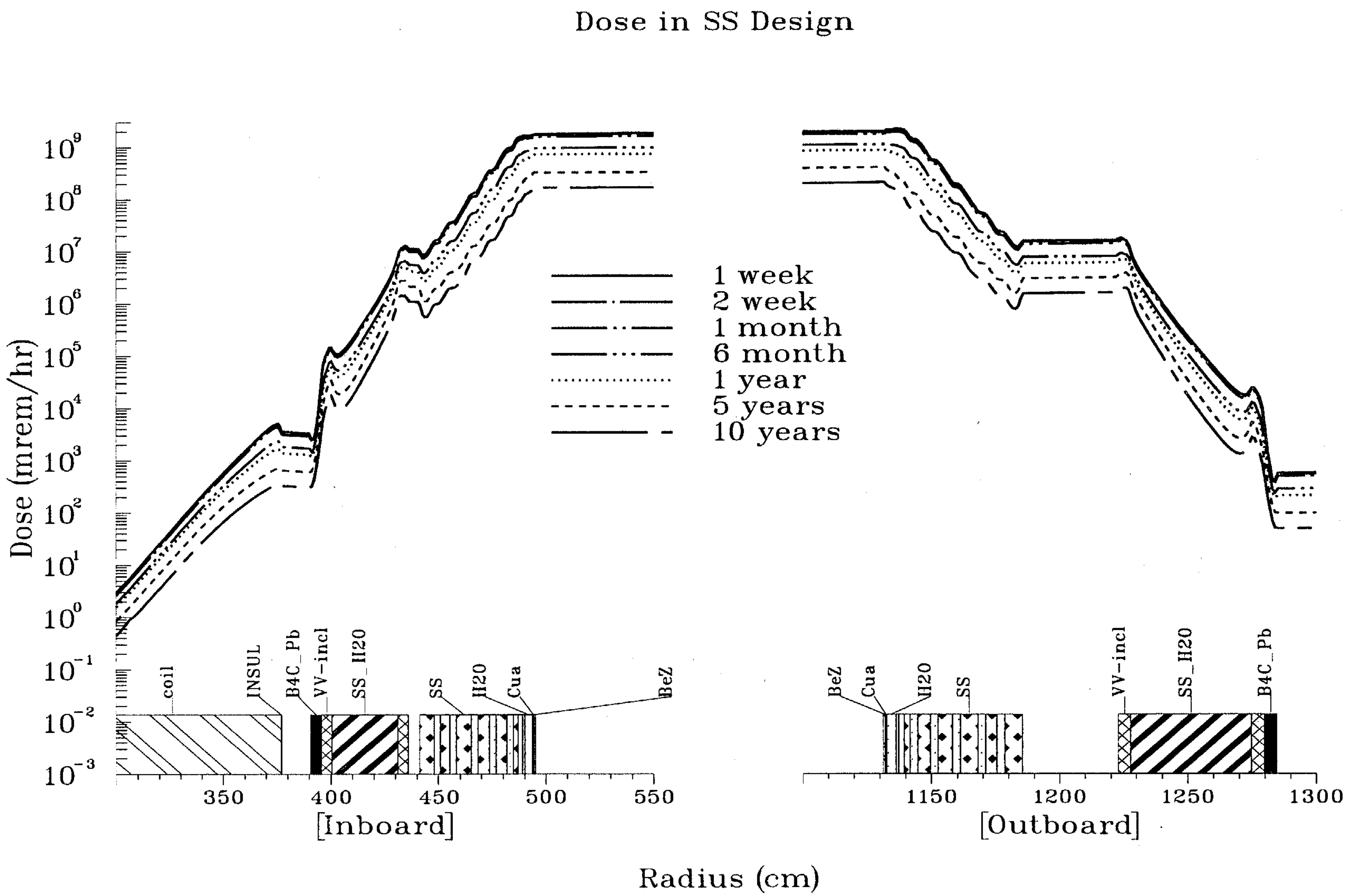

Figure 13. The contact dose (with photon transport) at different times after shutdown and after 3.29 FPYs (3 MWa/m^2 - SS/water design).

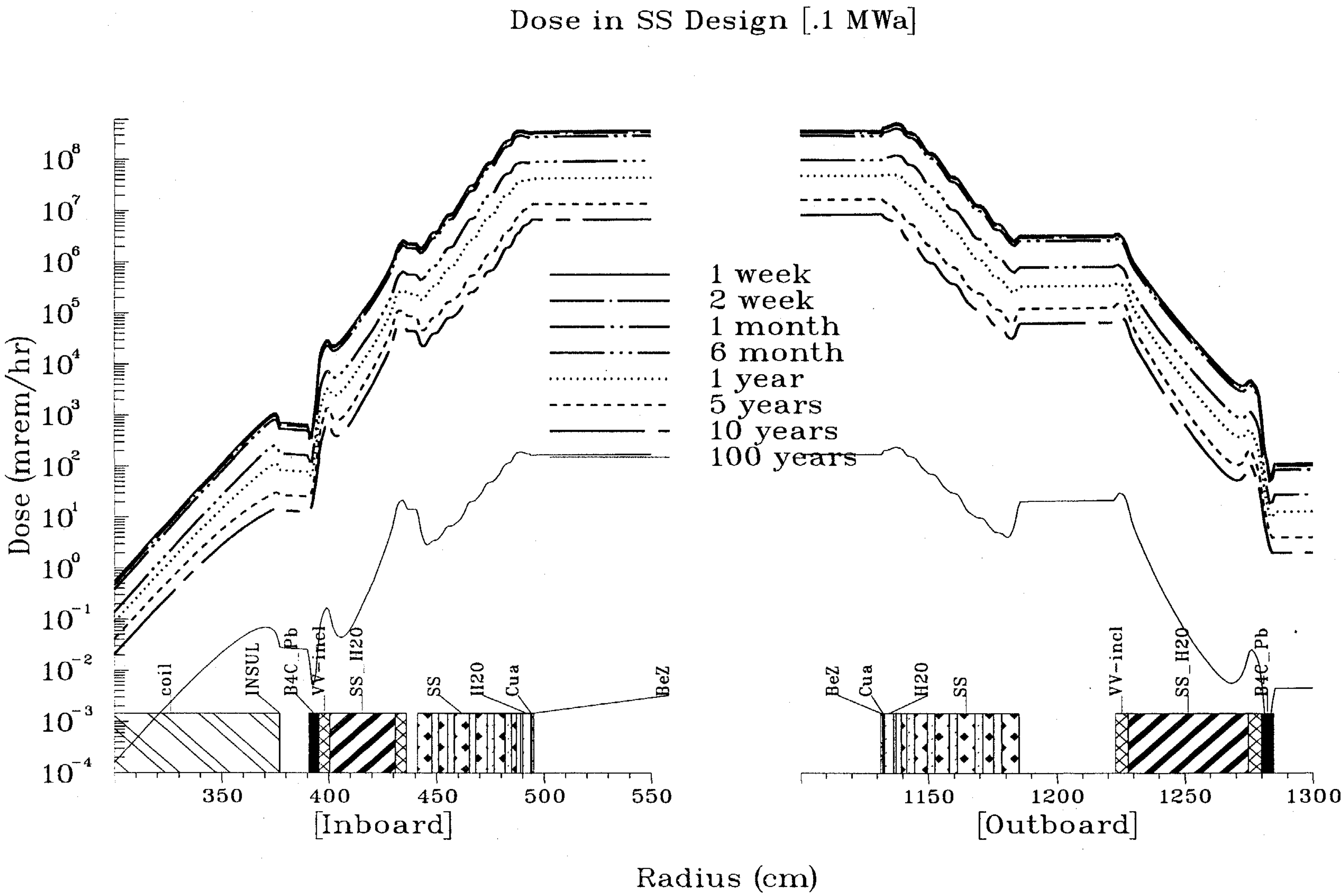

Figure 14. The contact dose (with photon transport) at different times after shutdown and after .11 FPYs (.1 MWa/m^2 - SS/water design).

5. Summary and Conclusions

Detailed activation analysis for ITER has been performed as a part of the ITER Task D4. The calculations have been performed for the shielding blanket (SS/water) and for the breeding blanket (Li/V) options. The activation code RACC-P, which has been modified under ITER Task-D-10 for pulsed operation, has been used in this analysis. The spatial distributions of the radioactive inventory, decay heat, biological hazard potential, and the contact dose were calculated for the two designs for different operation modes and targeted fluences.

A one-dimensional toroidal geometrical model has been utilized to determine the neutron fluxes in the two designs. The results are normalized for an inboard and outboard neutron wall loadings of 0.91 and 1.2 MW/m^2, respectively.

The point-wise distributions of the decay gamma sources have been calculated everywhere in the reactor at several times after the shutdown of the two designs and are then used in the transport code ONEDANT to calculate the biological dose everywhere in the reactor. The point-wise distributions of all the responses have also been calculated. These calculations have been performed for neutron fluences of 3.0 MWa/m^2, which corresponds to the target fluence of ITER, and 0.1 MWa/m^2, which is anticipated to be the beginning of an extended maintenance period.

The decay heat results show a large fraction of this energy (50 to 90%) is produced by photons. This implies that this energy would be transported to different parts of the reactors, relieving the energy concentration at high intensity source locations such as the first wall. Accurate modeling for the decay gamma transport is required to produce realistic spatial distribution of the decay heat which may be used in LOCA and LOFA analyses.

The results of the pulsed operation, using the new version of RACC, show a large reduction in the radioactivity and the decay heat for pure pulsed operation. The continuous operation assumption, usually used in the radioactivity calculations, overestimates the different activation responses at the final shutdown and for about one week after shutdown by a factor of more than 2.

Appendix A

SS/Water Design

Detailed Zones' Results

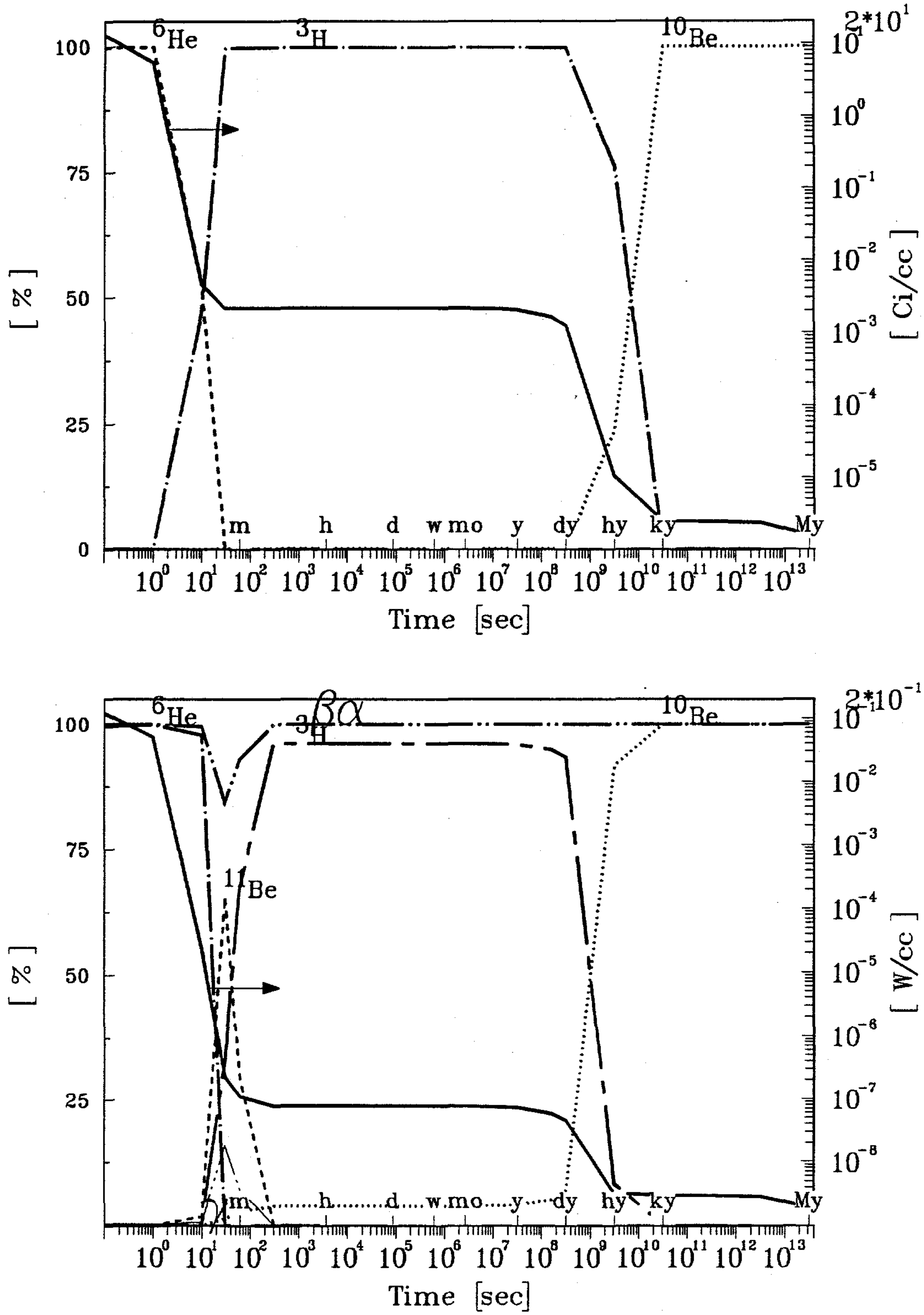

23

Figure 15. The specific radioactivity (top) and the specific decay heat (bottom) in zone # 23 (I_Be - SS/water).

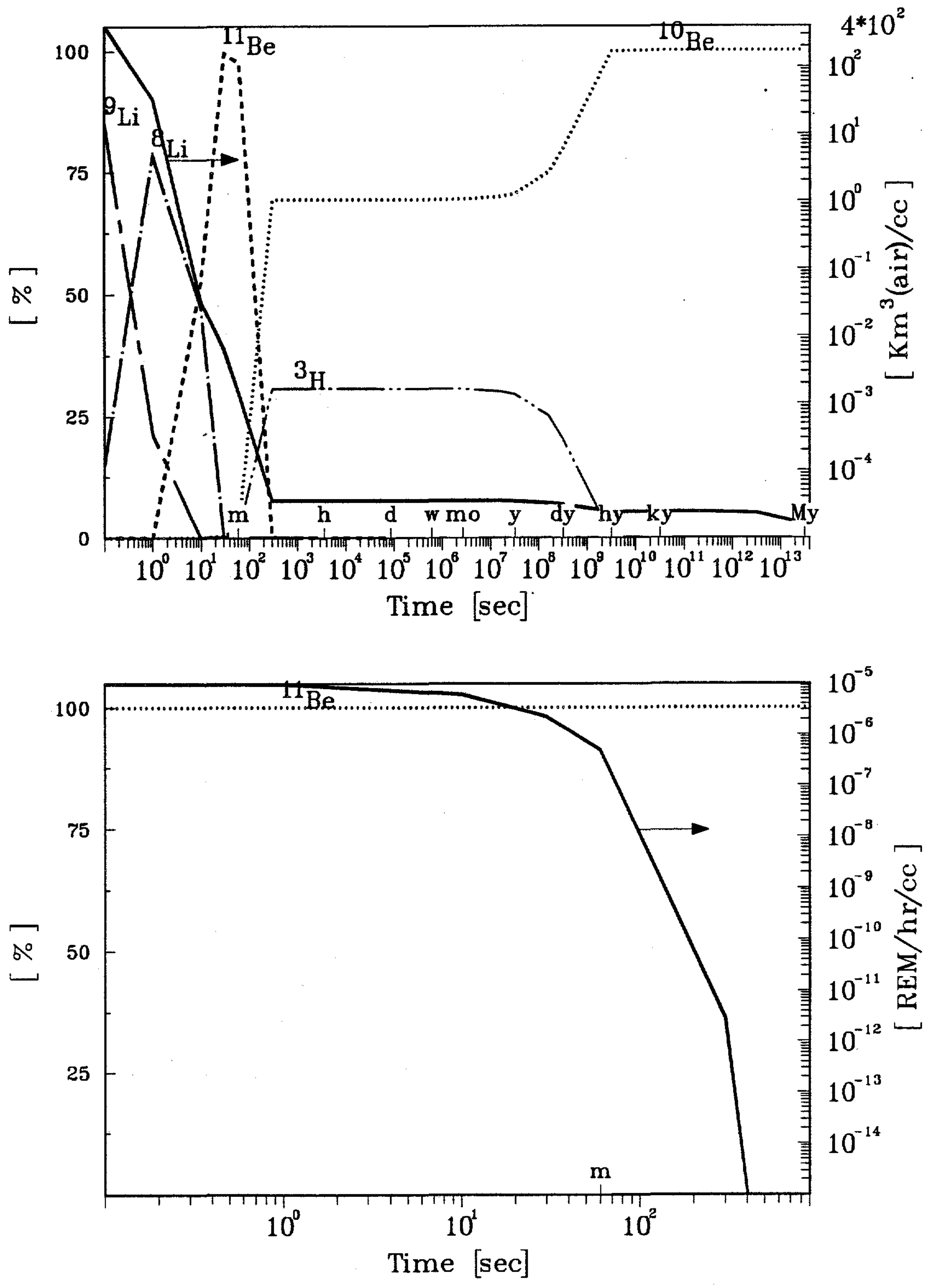

Figure 16. The specific air-BHP (top) and the point-source contact dose (bottom) in zone # 23 (I_Be - SS/water).

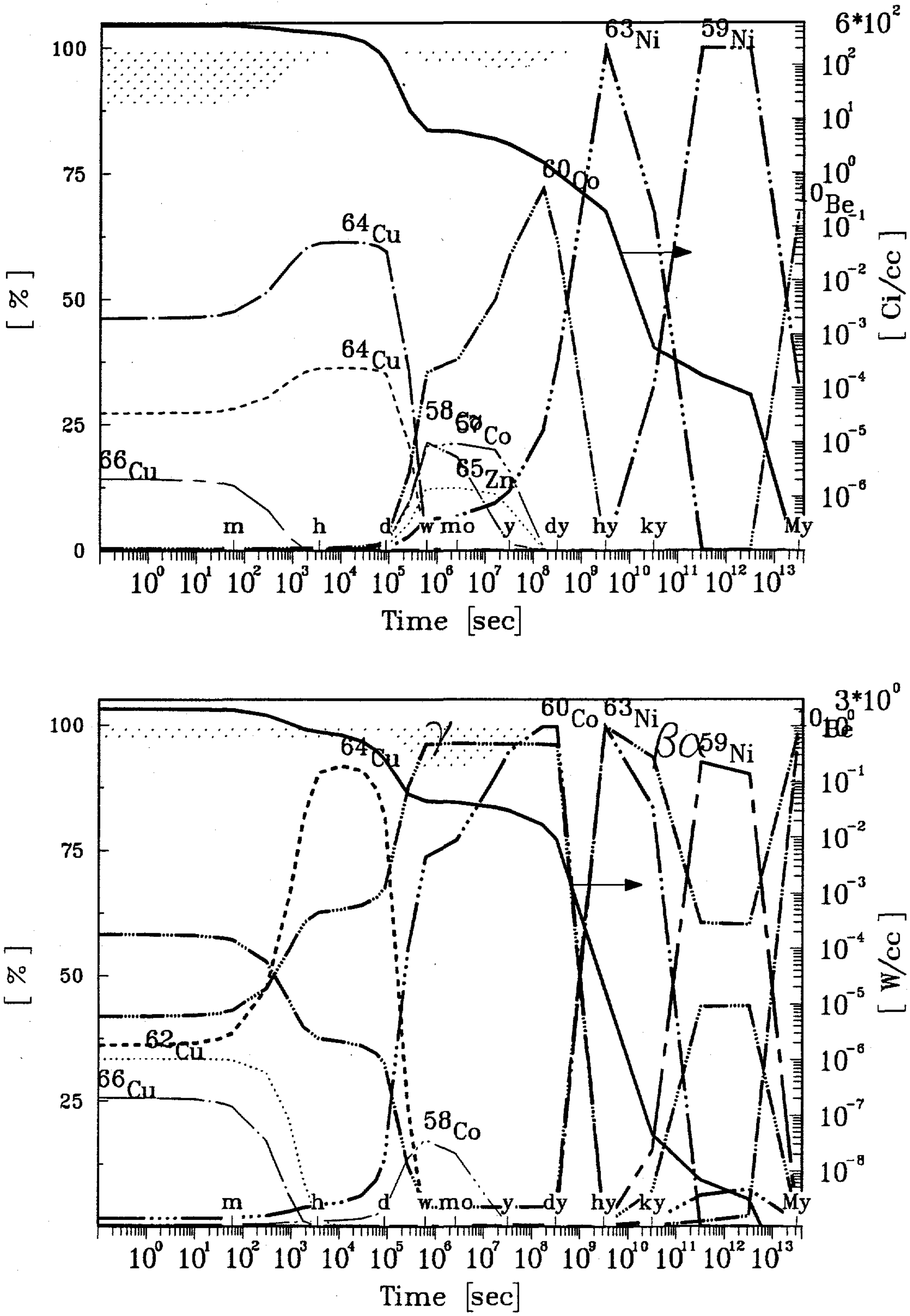

22

Figure 17. The specific radioactivity (top) and the specific decay heat (bottom) in zone # 22 (I_Cua - SS/water).

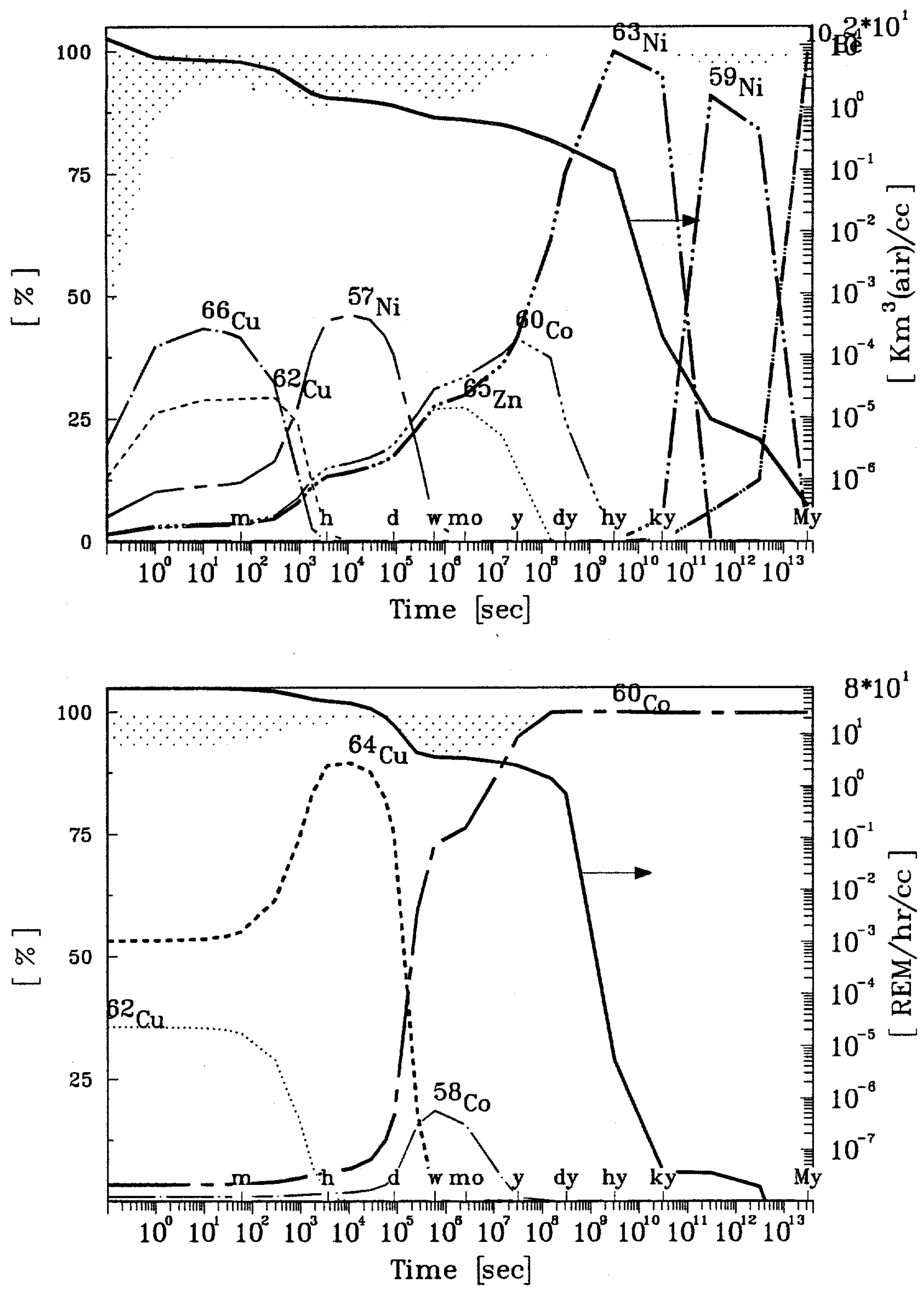

22

Figure 18. The specific air-BHP (top) and the point-source contact dose (bottom) in zone # 22 (I_Cua - SS/water).

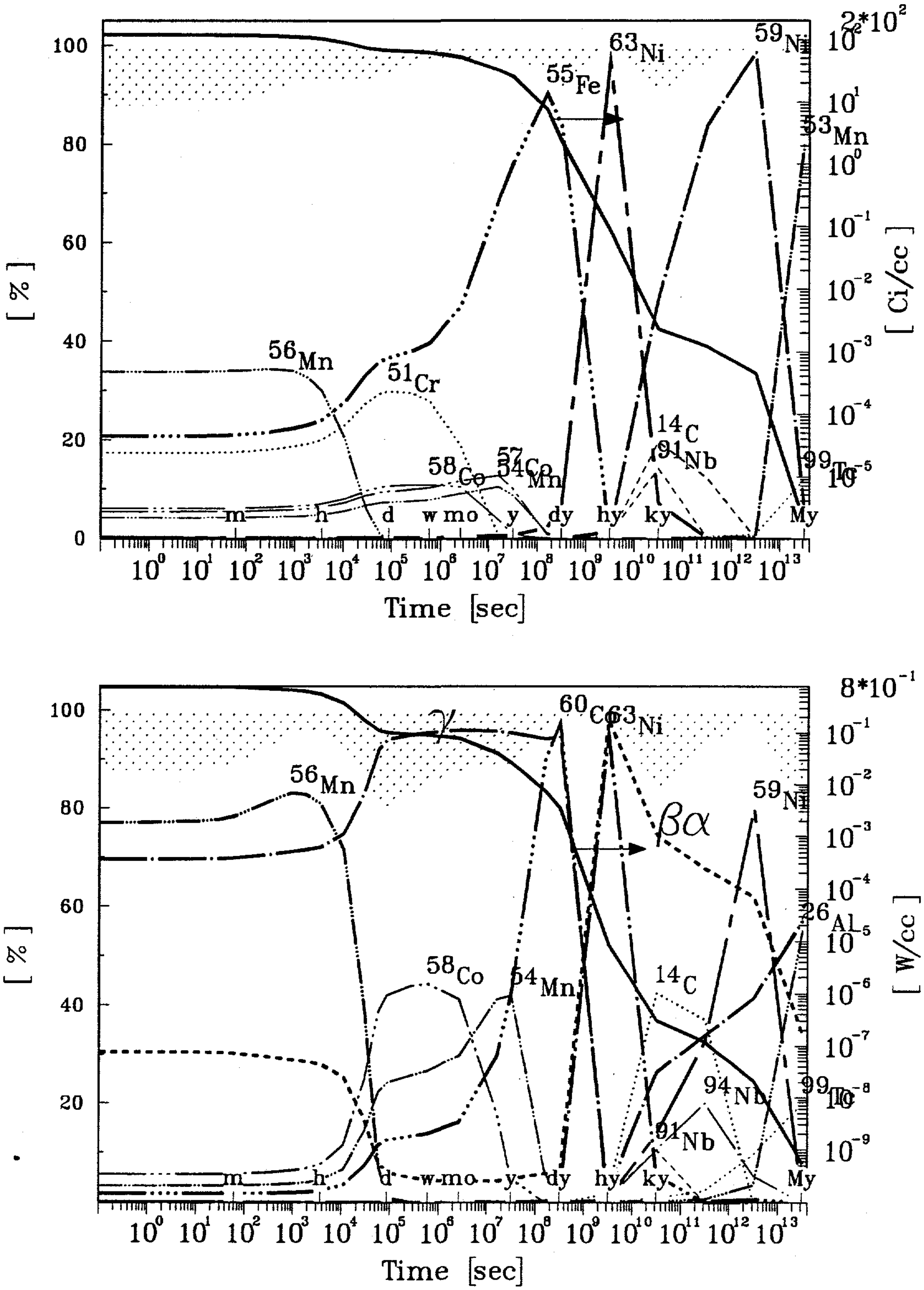

21

Figure 19. The specific radioactivity (top) and the specific decay heat (bottom) in zone # 21 (I_SS (FW)- SS/water).

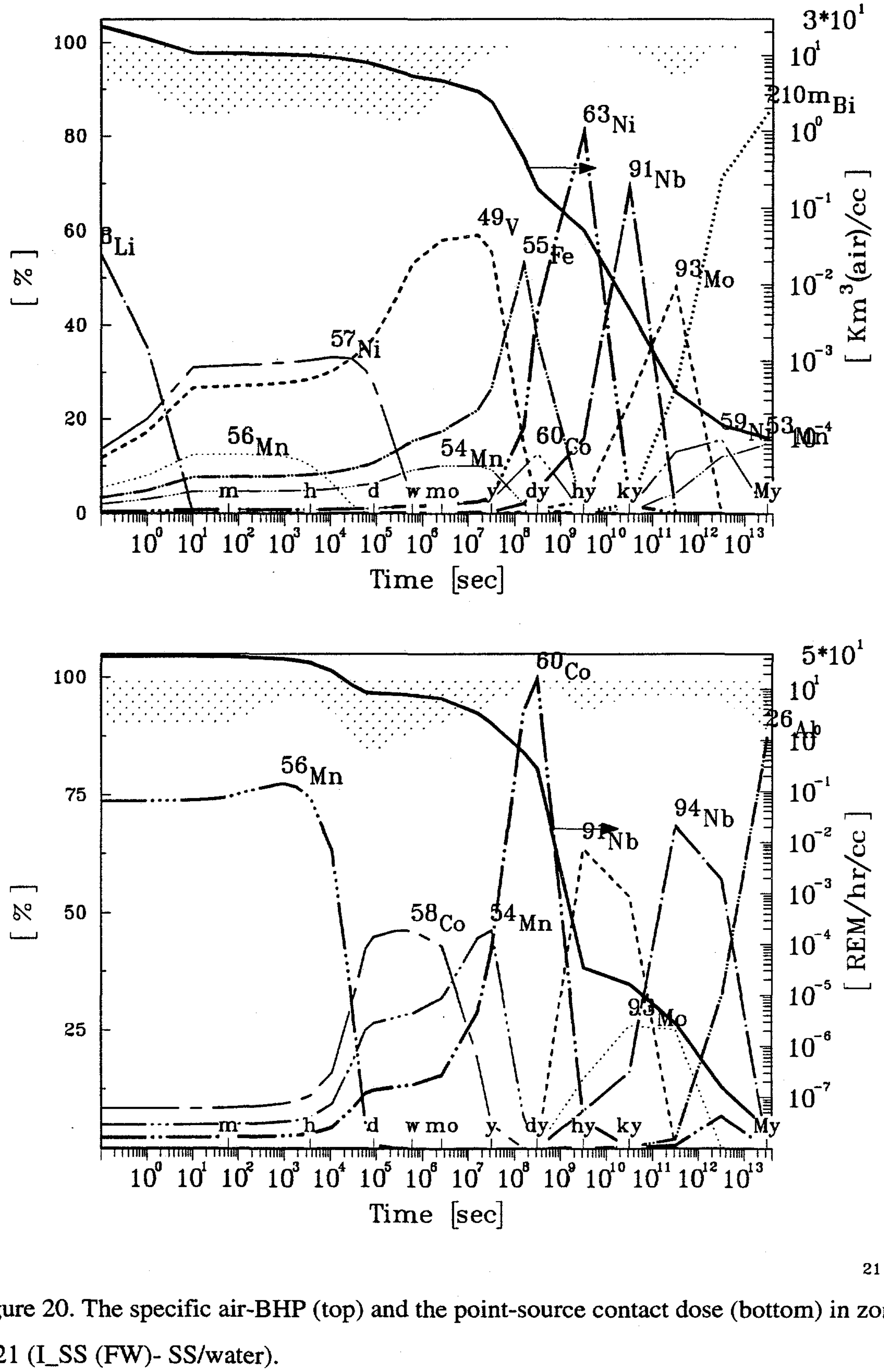

21

Figure 20. The specific air-BHP (top) and the point-source contact dose (bottom) in zone # 21 (I_SS (FW)- SS/water).

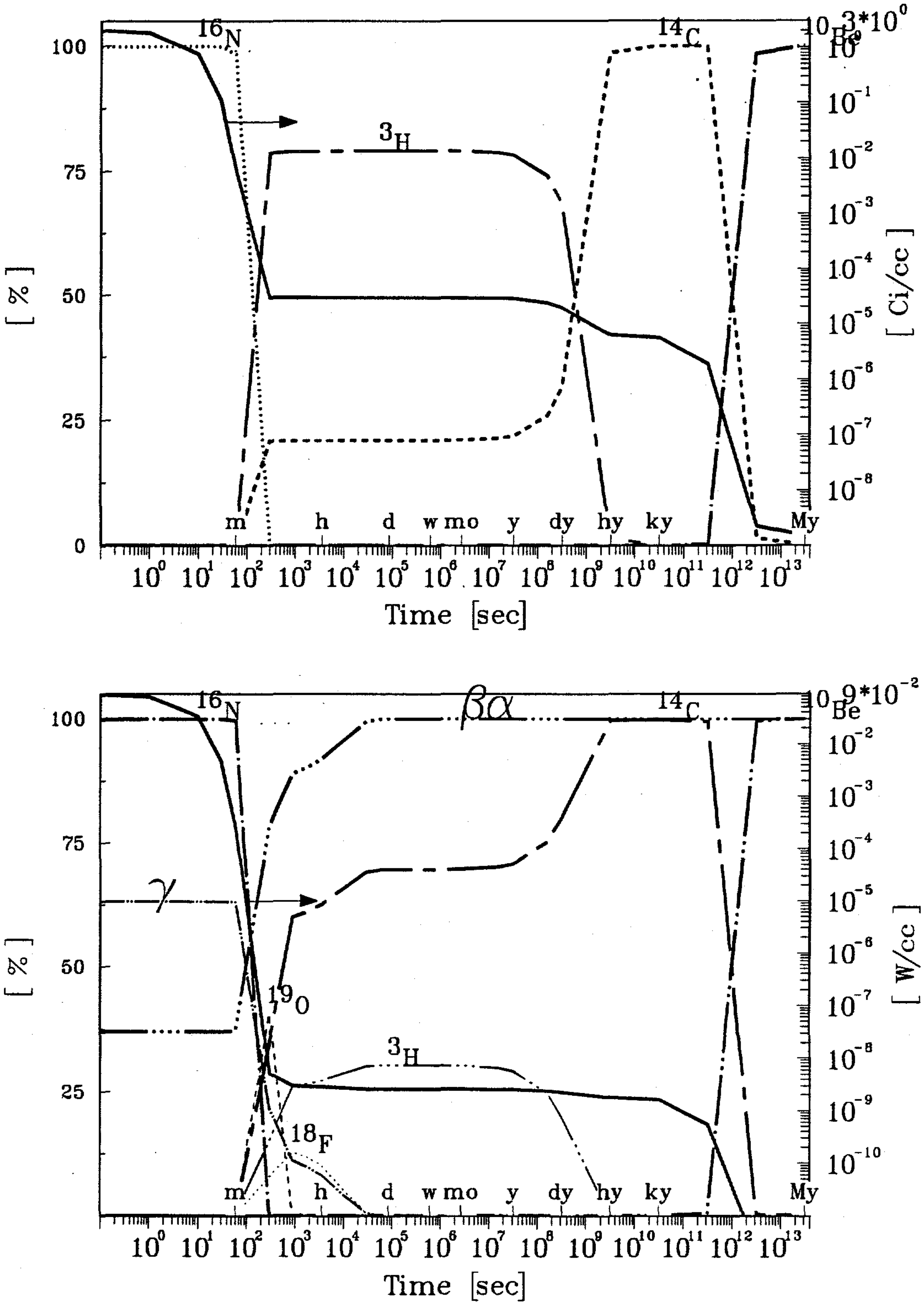

20

Figure 21. The specific radioactivity (top) and the specific decay heat (bottom) in zone # 20 (I_H2O - SS/water).

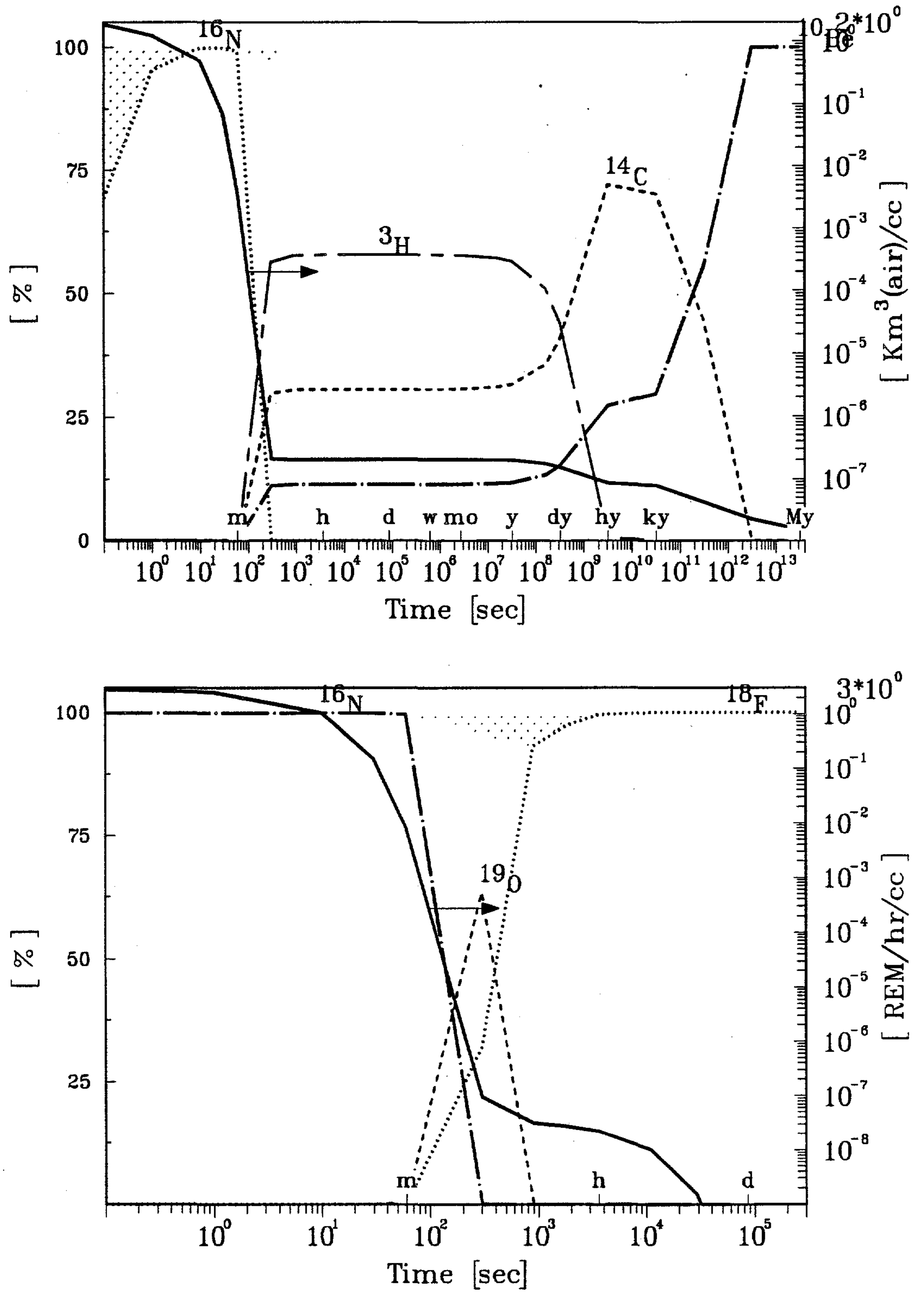

Figure 22. The specific air-BHP (top) and the point-source contact dose (bottom) in zone # 20 (I_H2O - SS/water).

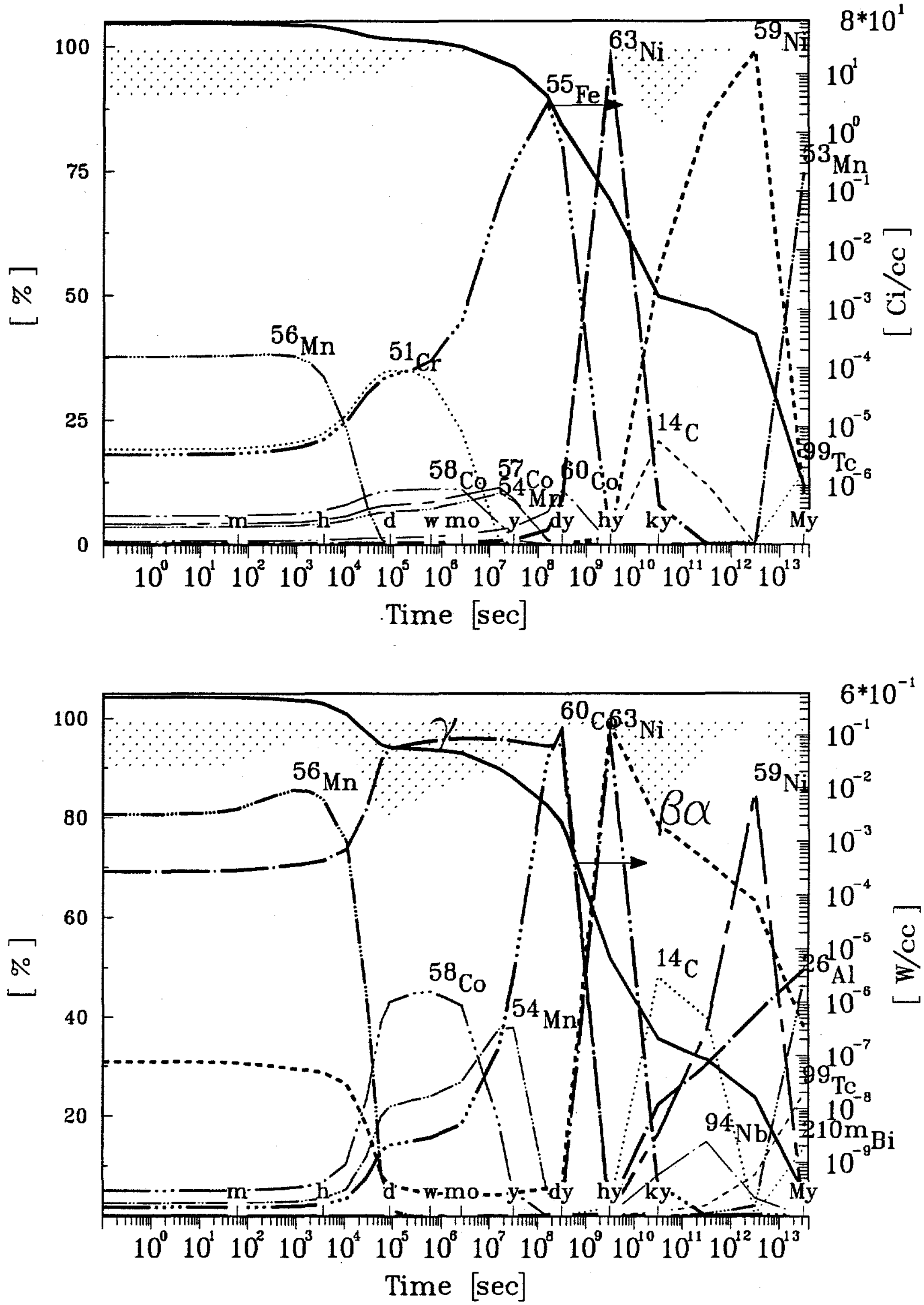

19

Figure 23. The specific radioactivity (top) and the specific decay heat (bottom) in zone # 19 (I_SS - SS/water).

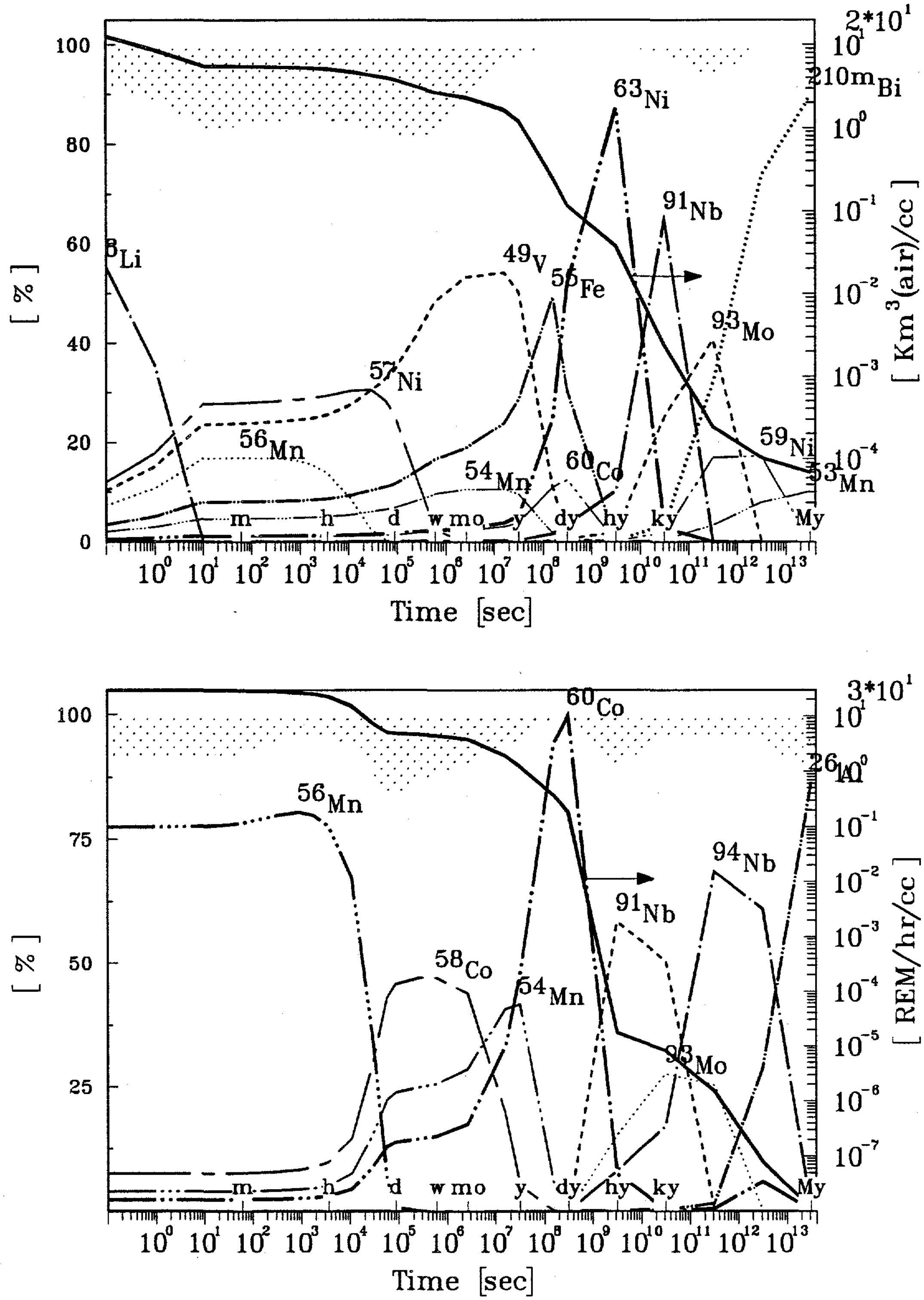

Figure 24. The specific air-BHP (top) and the point-source contact dose (bottom) in zone # 19 (I_SS - SS/water).

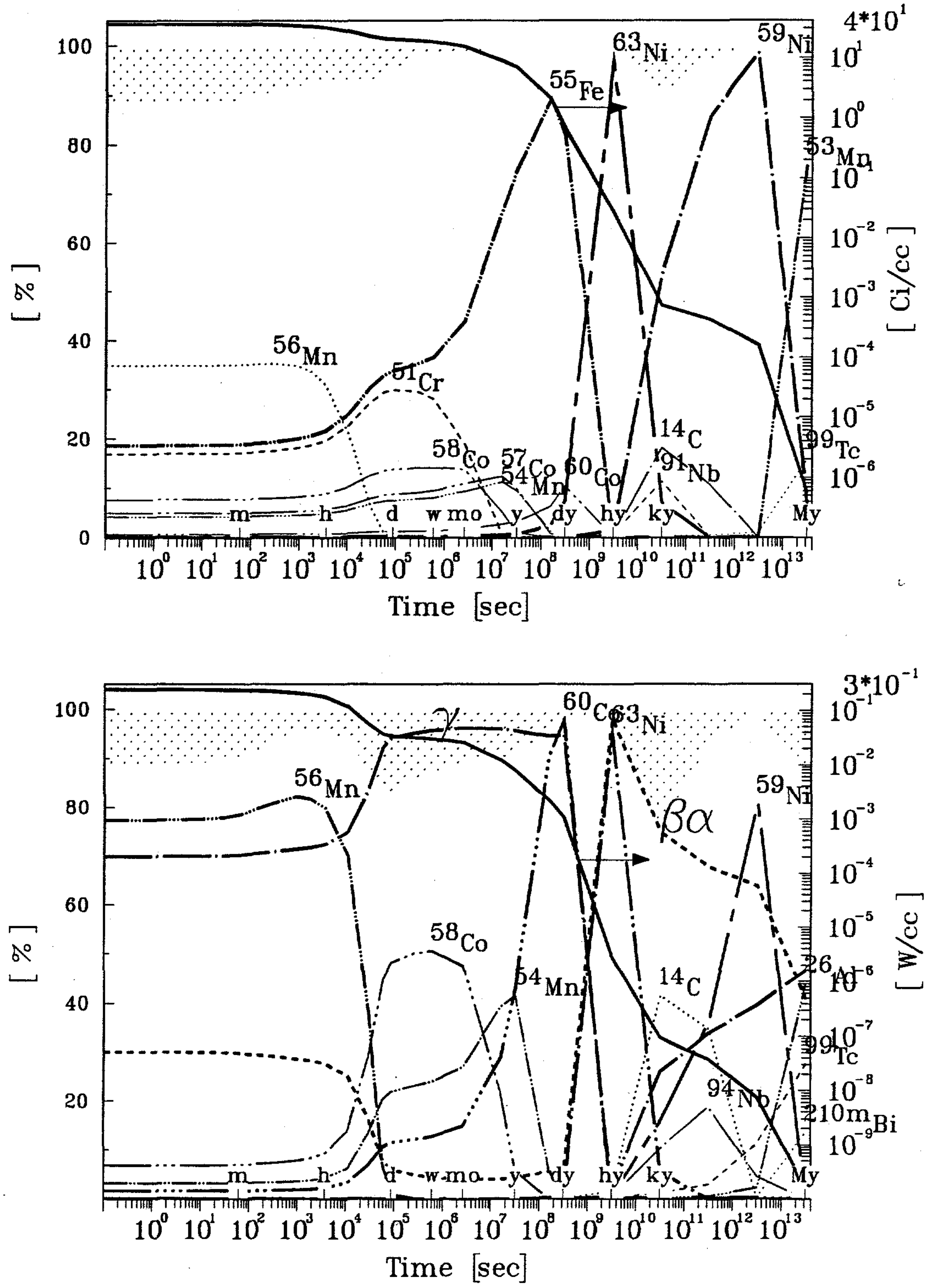

17

Figure 25. The specific radioactivity (top) and the specific decay heat (bottom) in zone # 17 (I_SS - SS/water).

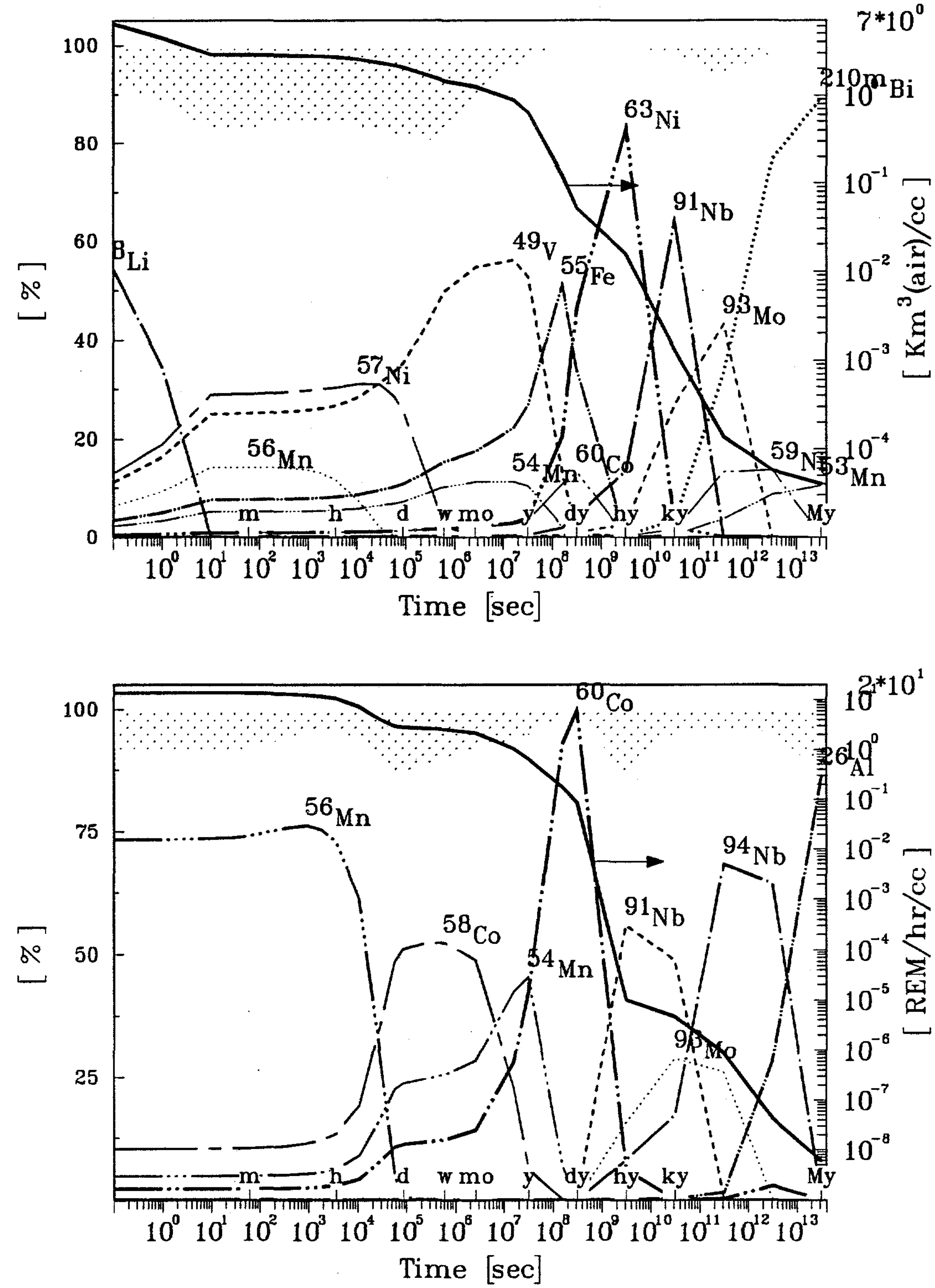

Figure 26. The specific air-BHP (top) and the point-source contact dose (bottom) in zone # 17 (I_SS - SS/water).

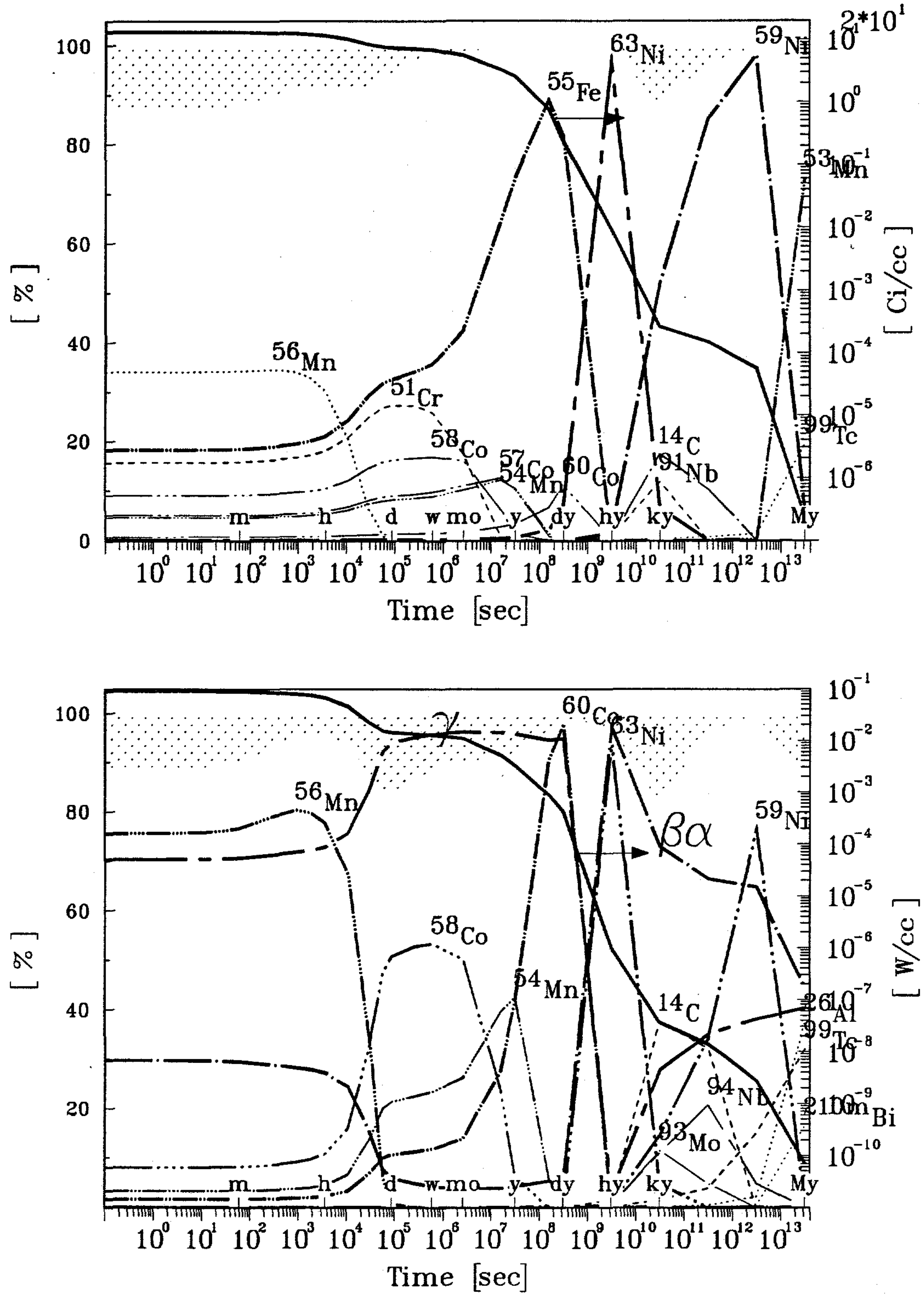

15

Figure 27. The specific radioactivity (top) and the specific decay heat (bottom) in zone # 15 (I_SS - SS/water).

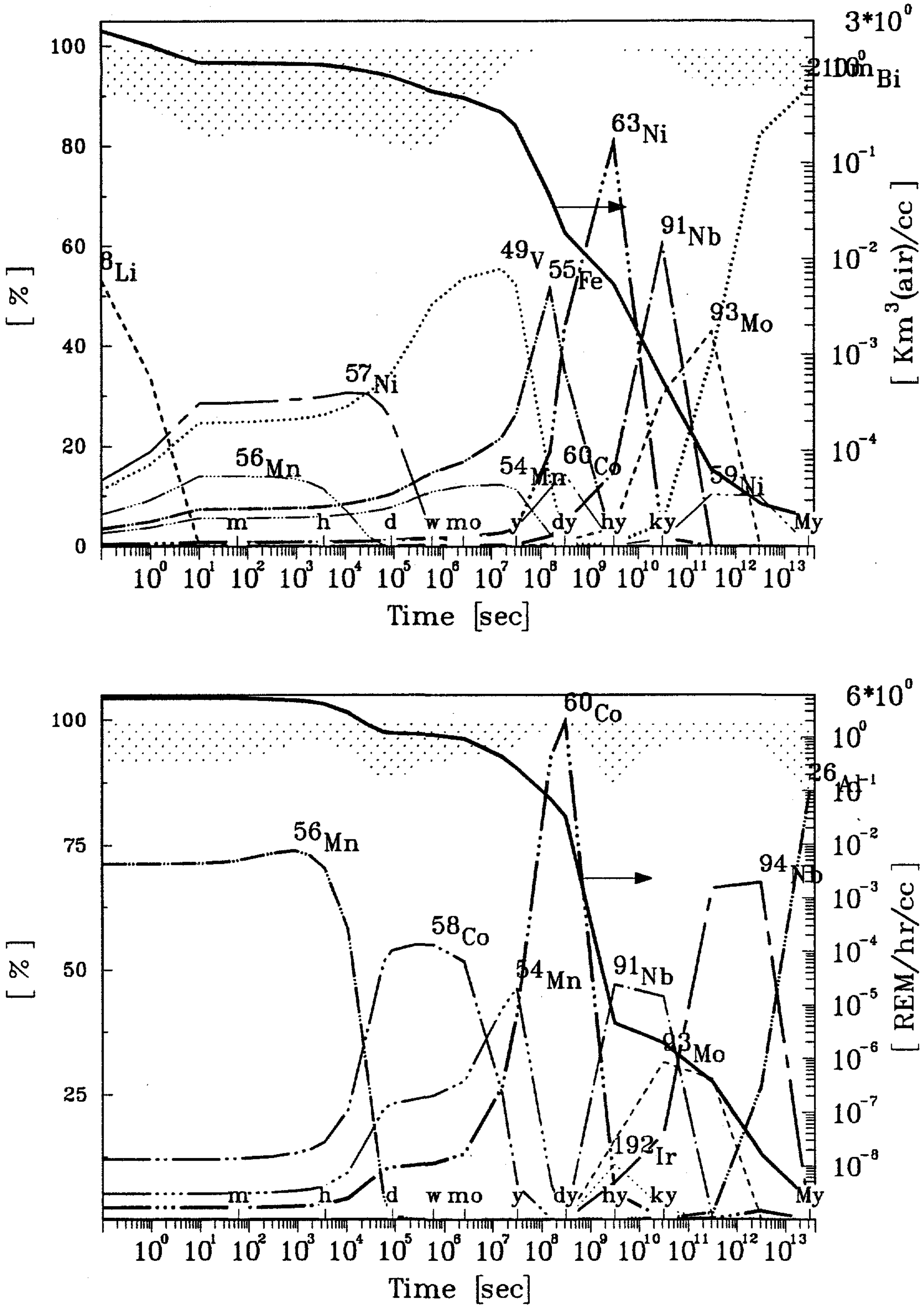

15

Figure 28. The specific air-BHP (top) and the point-source contact dose (bottom) in zone # 15 (I_SS - SS/water).

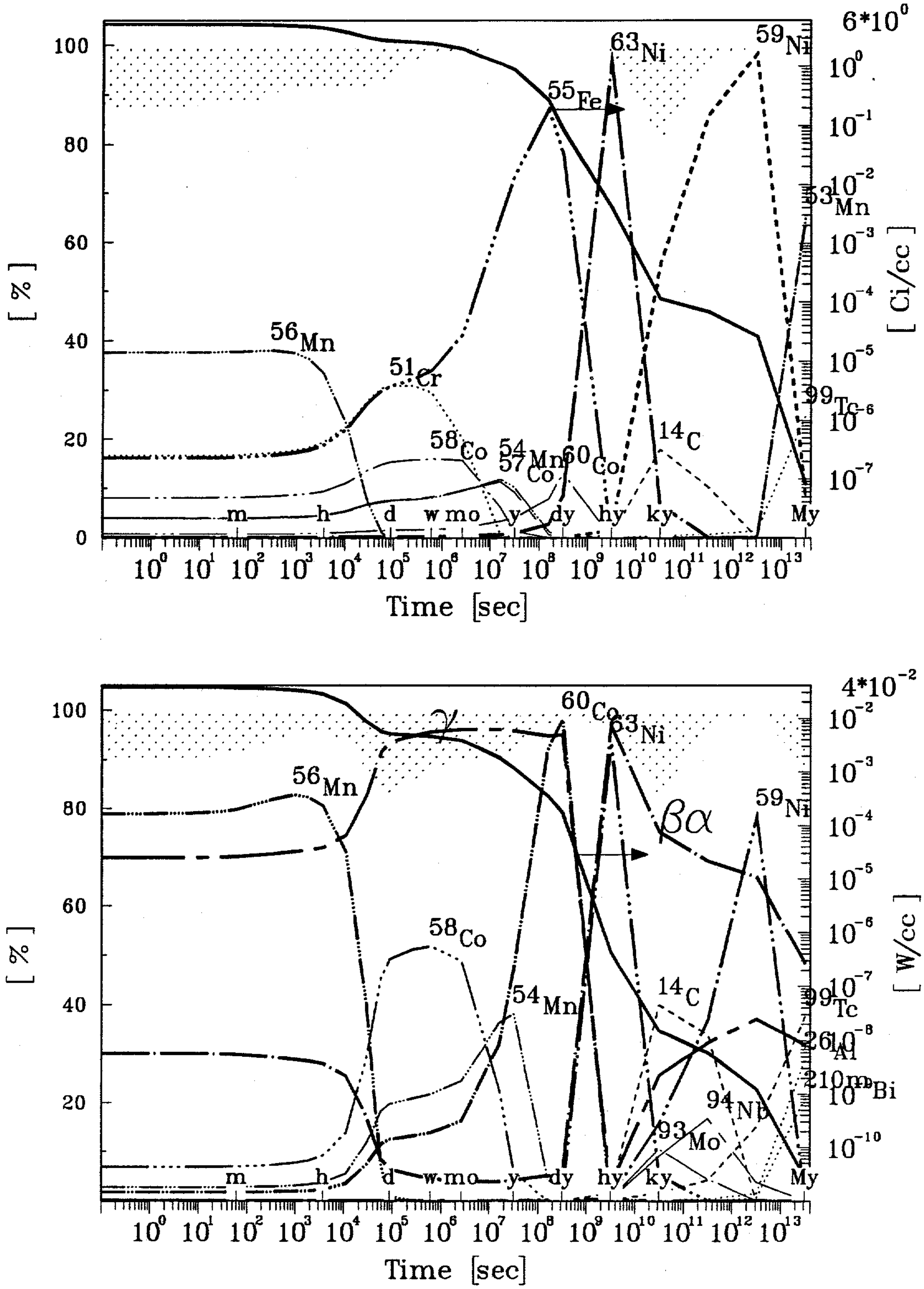

13

Figure 29. The specific radioactivity (top) and the specific decay heat (bottom) in zone # 13 (I_SS - SS/water).

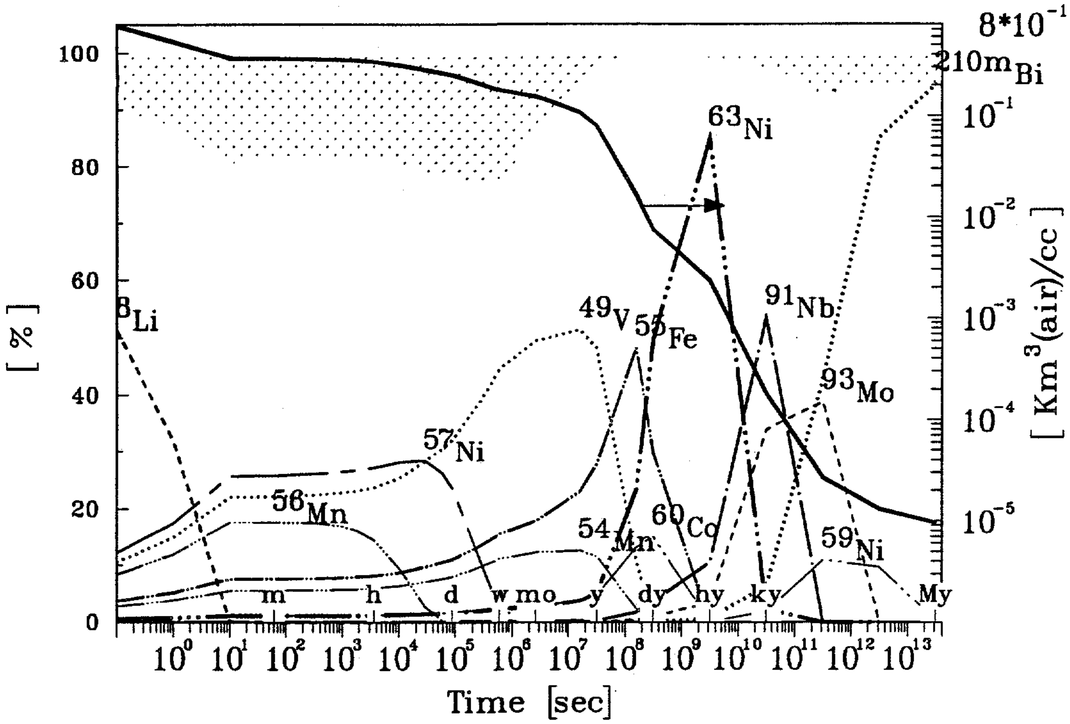

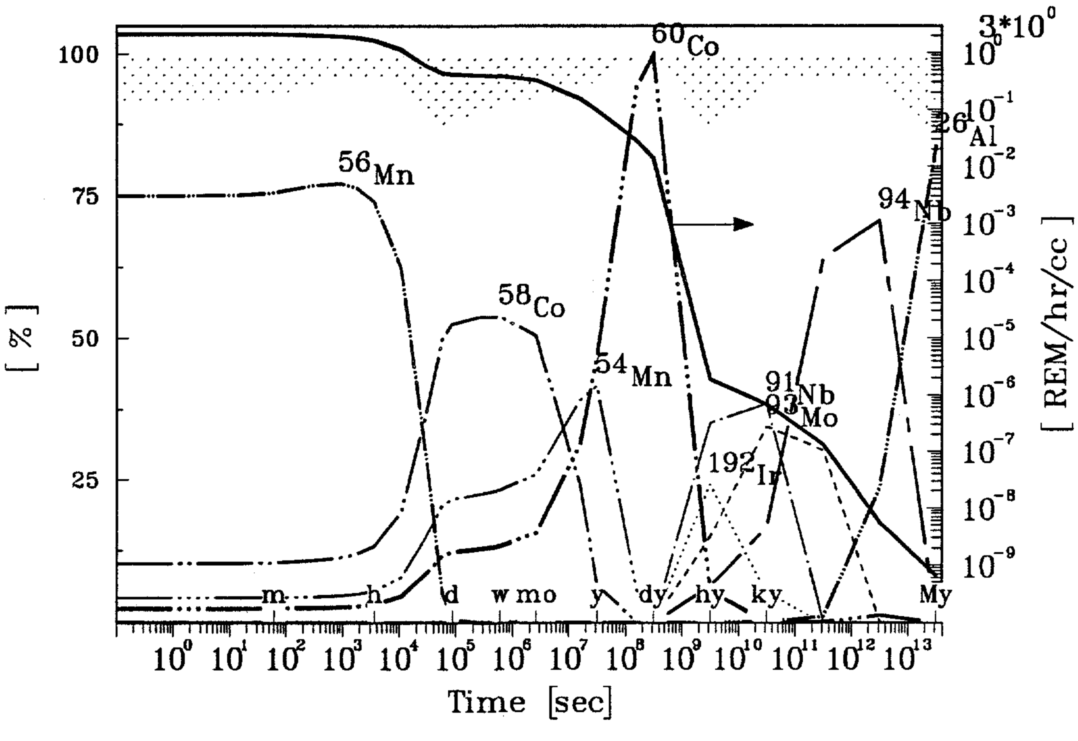

13

Figure 30. The specific air-BHP (top) and the point-source contact dose (bottom) in zone # 13 (I_SS - SS/water).

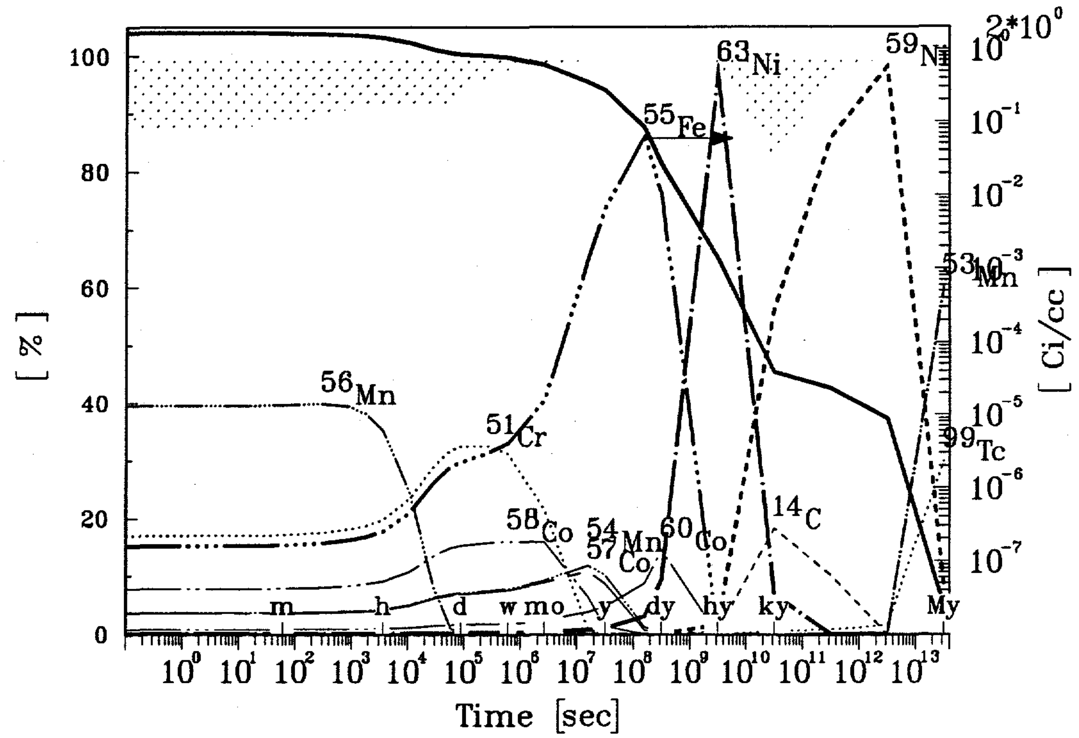

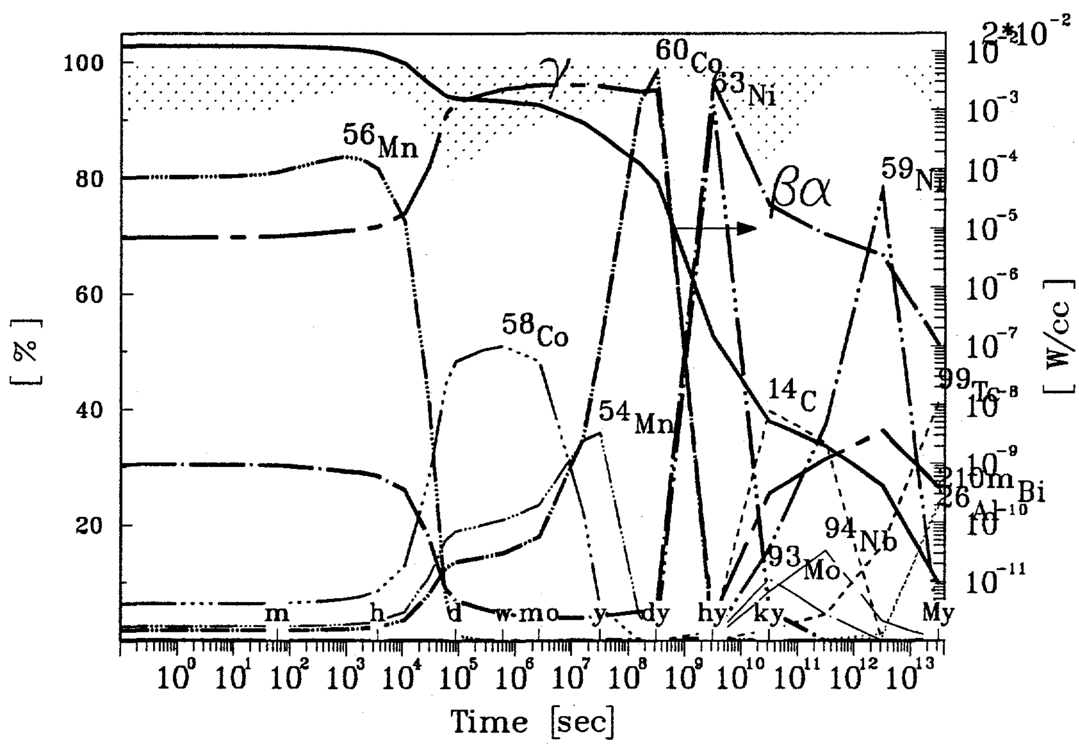

11

Figure 31. The specific radioactivity (top) and the specific decay heat (bottom) in zone # 11 (I_SS - SS/water).

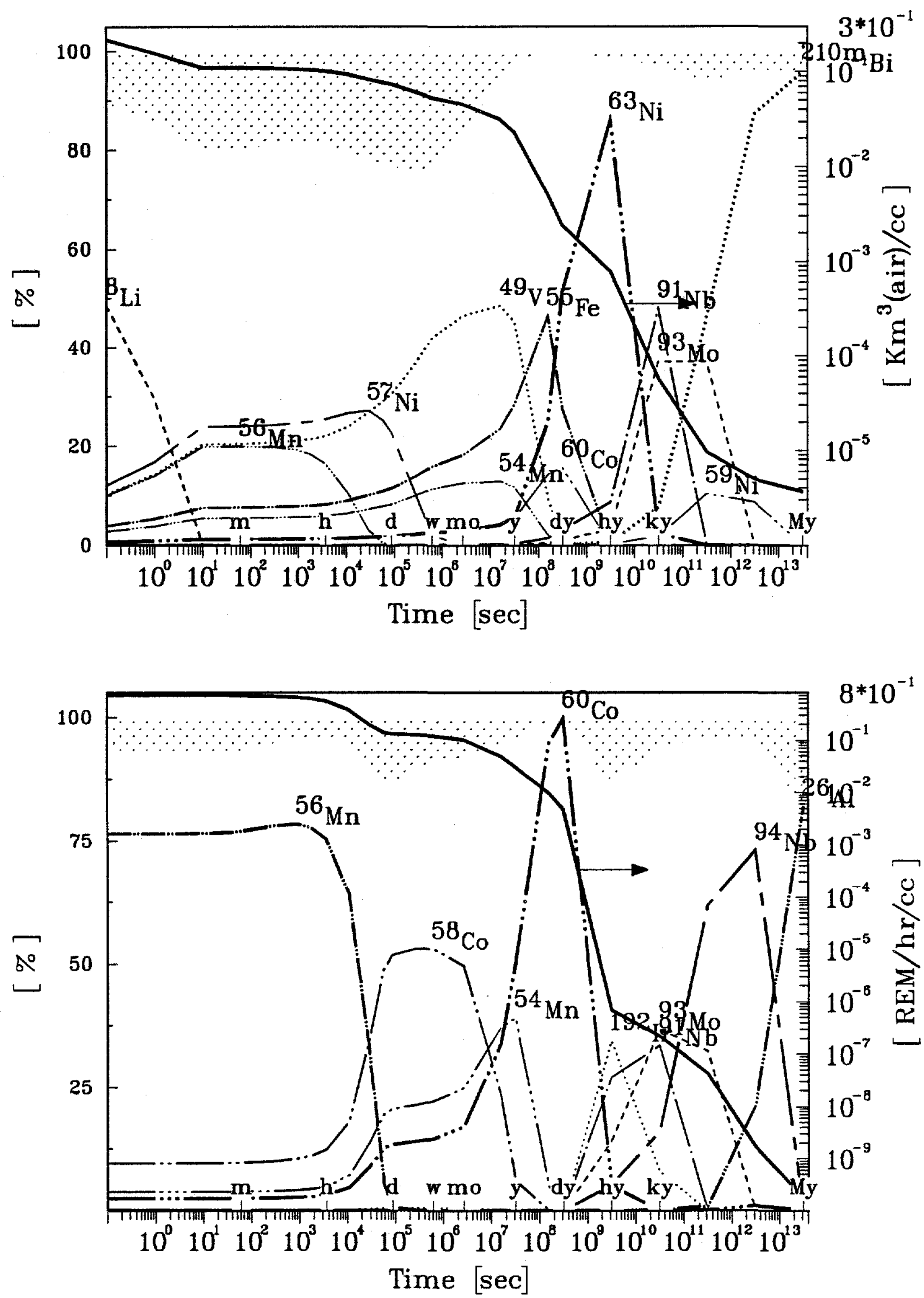

11

Figure 32. The specific air-BHP (top) and the point-source contact dose (bottom) in zone # 11 (I_SS - SS/water).

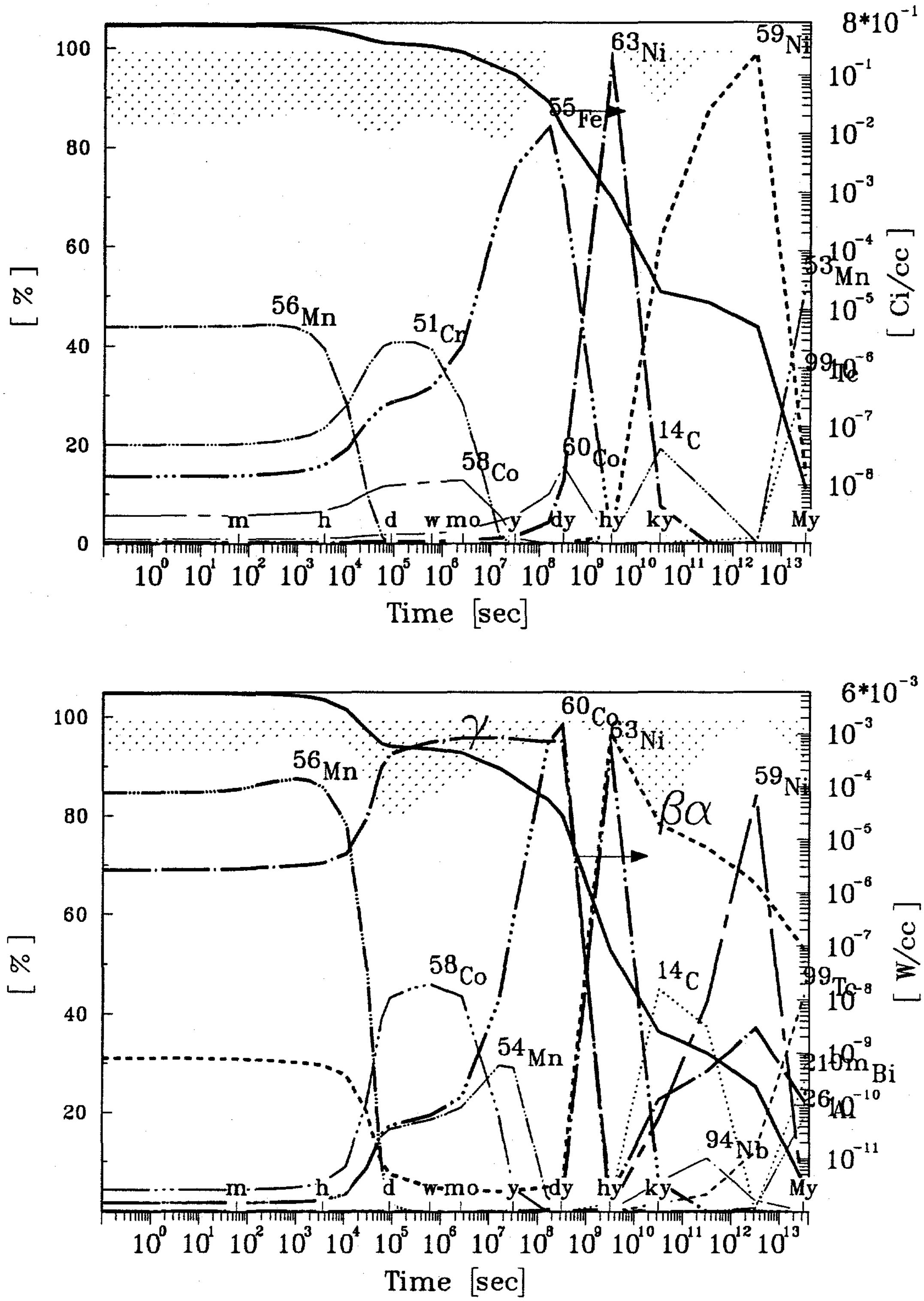

9

Figure 33. The specific radioactivity (top) and the specific decay heat (bottom) in zone # 9 (I_SS - SS/water).

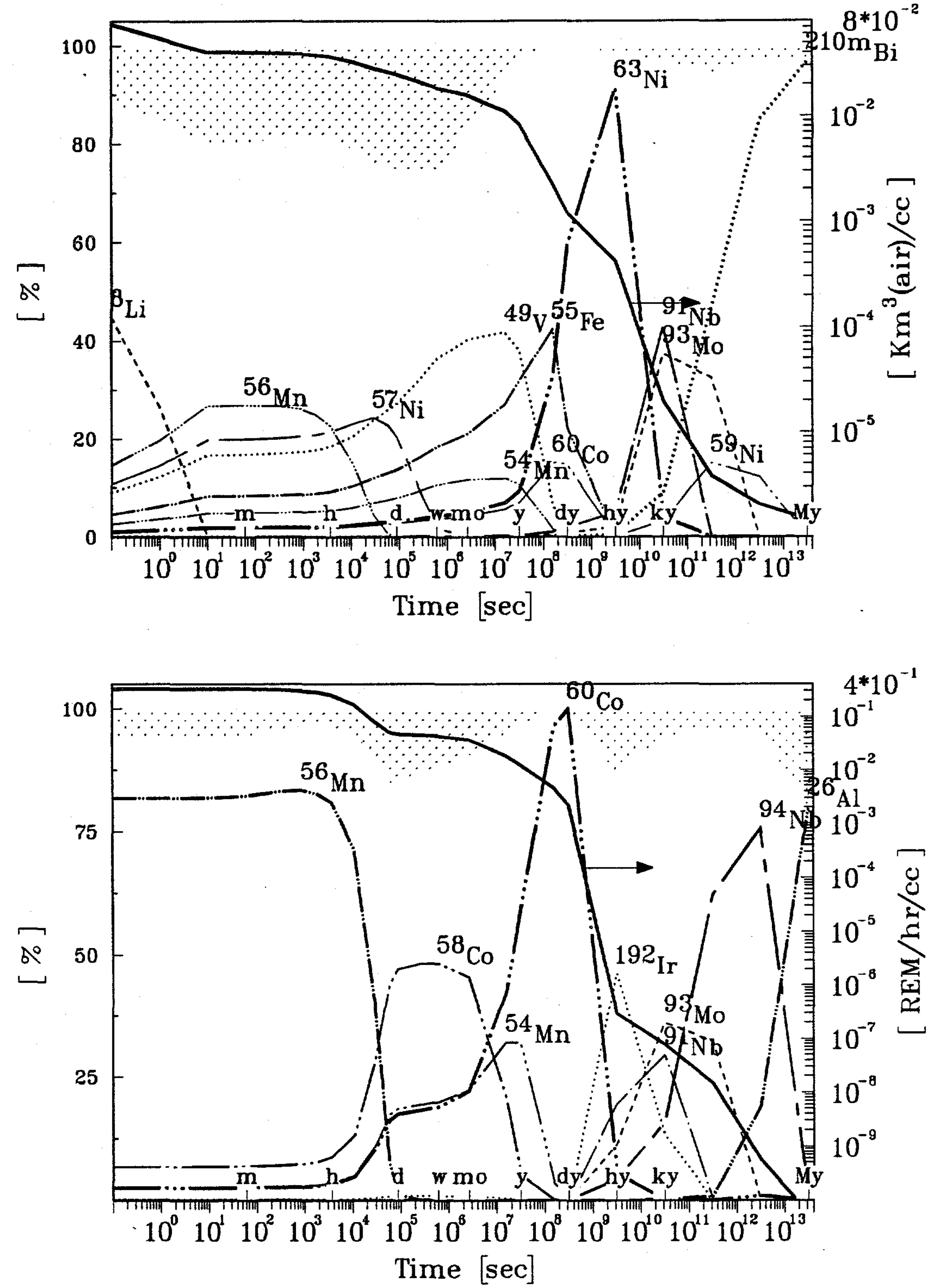

Figure 34. The specific air-BHP (top) and the point-source contact dose (bottom) in zone # 9 (I_SS - SS/water).

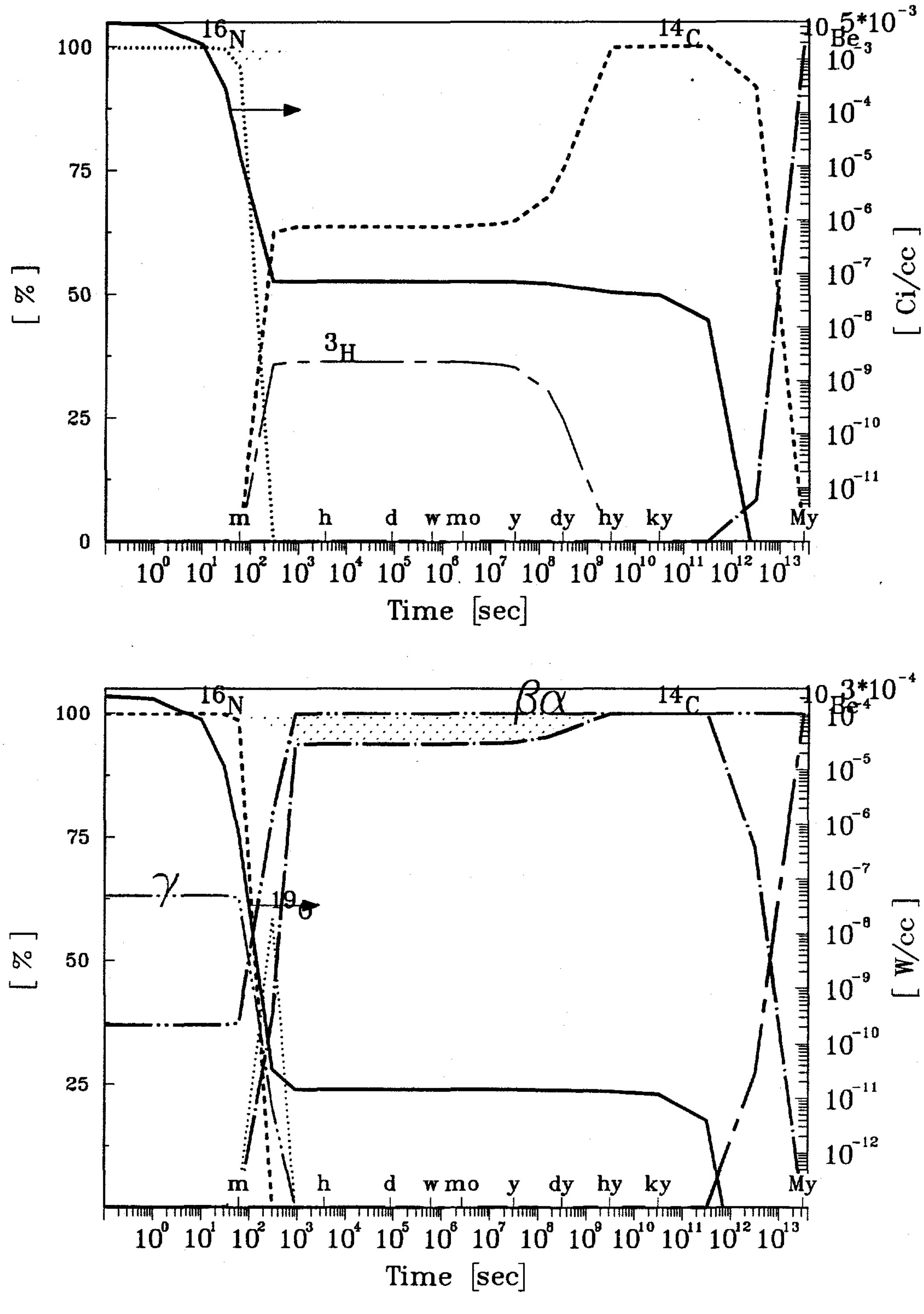

Figure 35. The specific radioactivity (top) and the specific decay heat (bottom) in zone # 8 (I_H2O - SS/water).

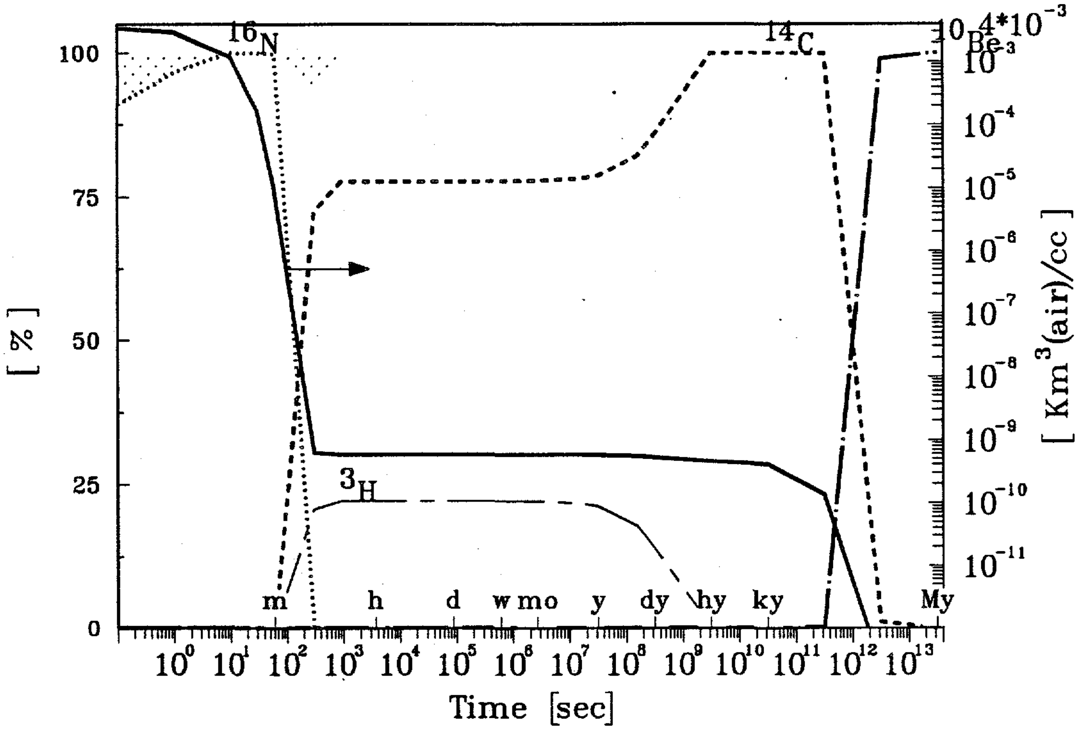

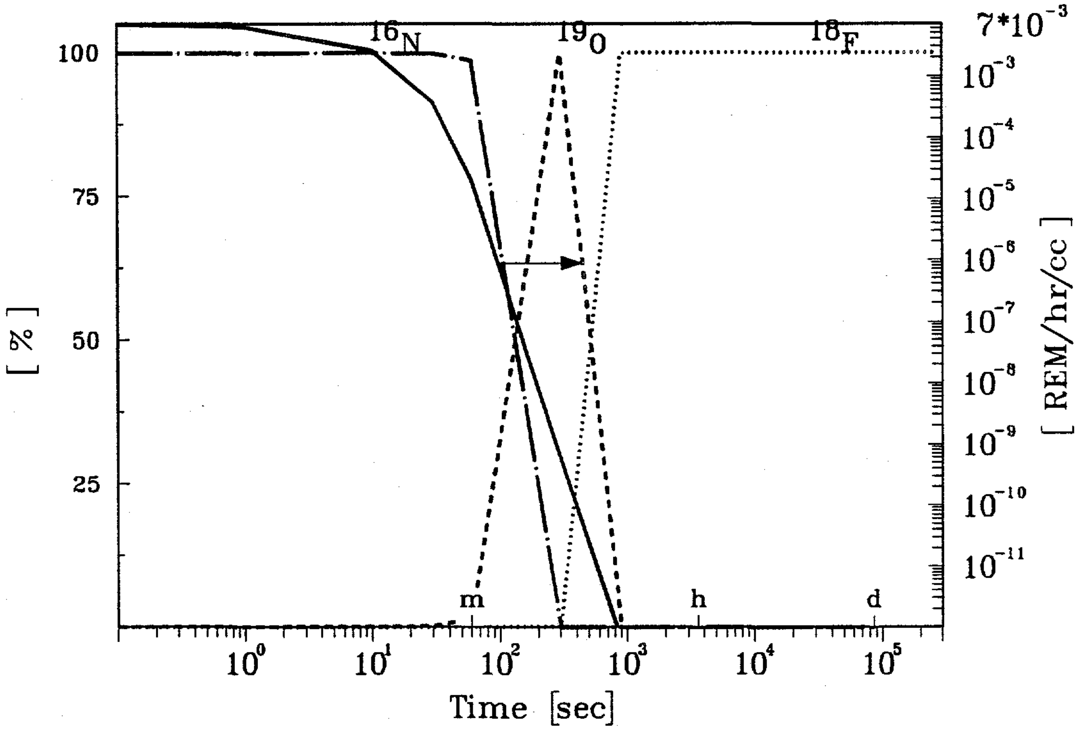

Figure 36. The specific air-BHP (top) and the point-source contact dose (bottom) in zone # 8 (I_H2O - SS/water).

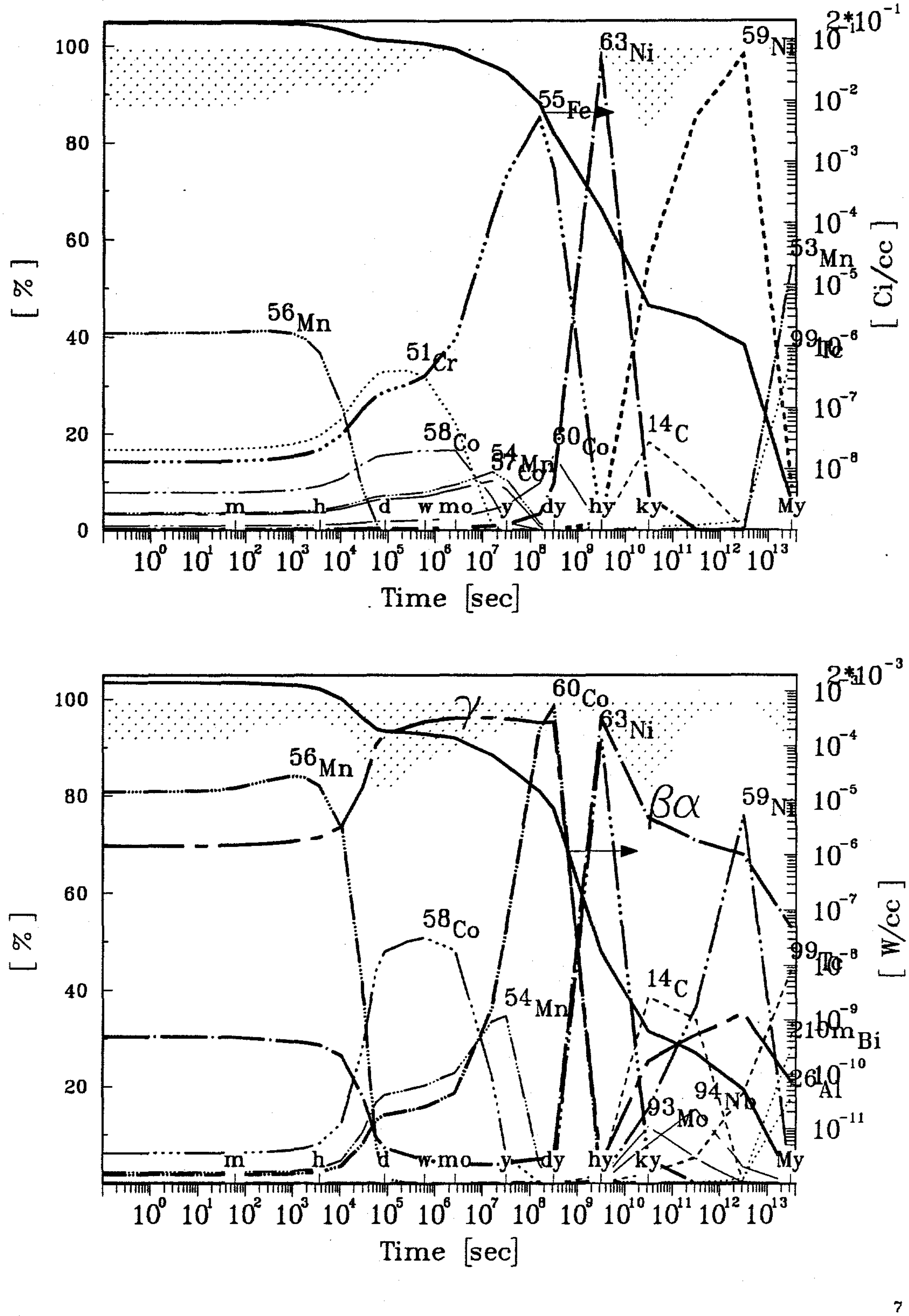

7

Figure 37. The specific radioactivity (top) and the specific decay heat (bottom) in zone # 7 (I_SS - SS/water).

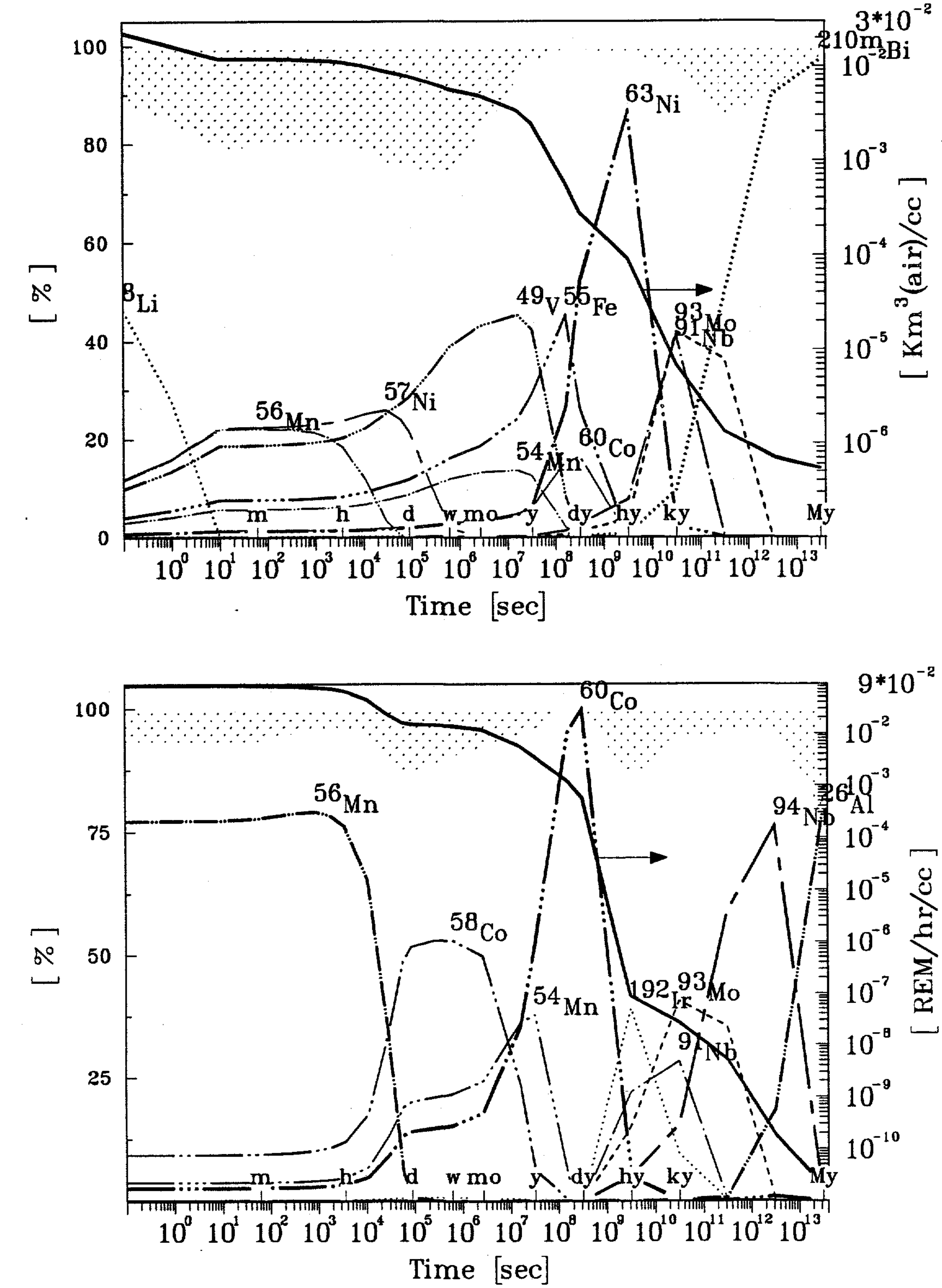

Figure 38. The specific air-BHP (top) and the point-source contact dose (bottom) in zone # 7 (I_SS - SS/water).

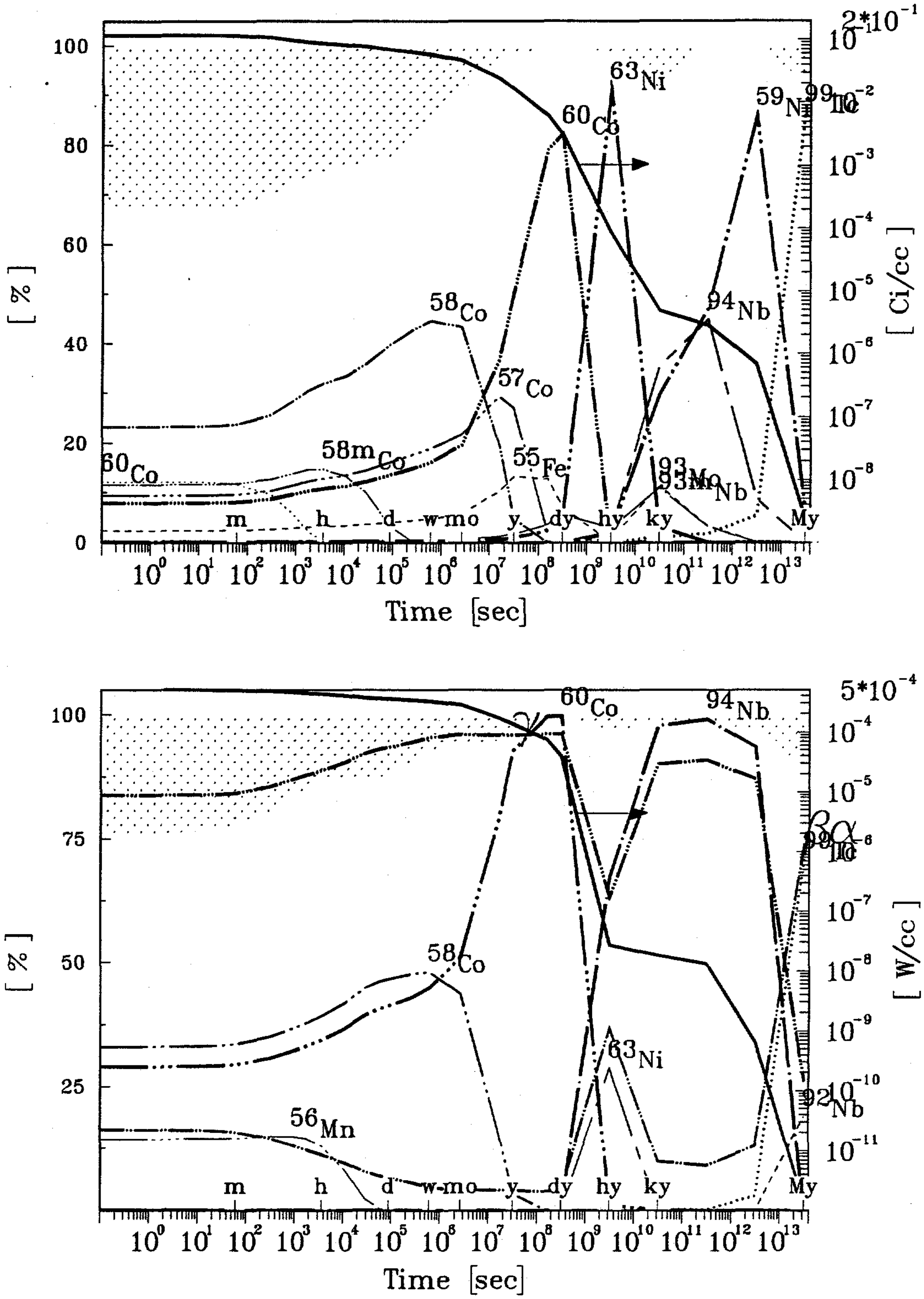

6

Figure 39. The specific radioactivity (top) and the specific decay heat (bottom) in zone # 6 (I_VV - SS/water).

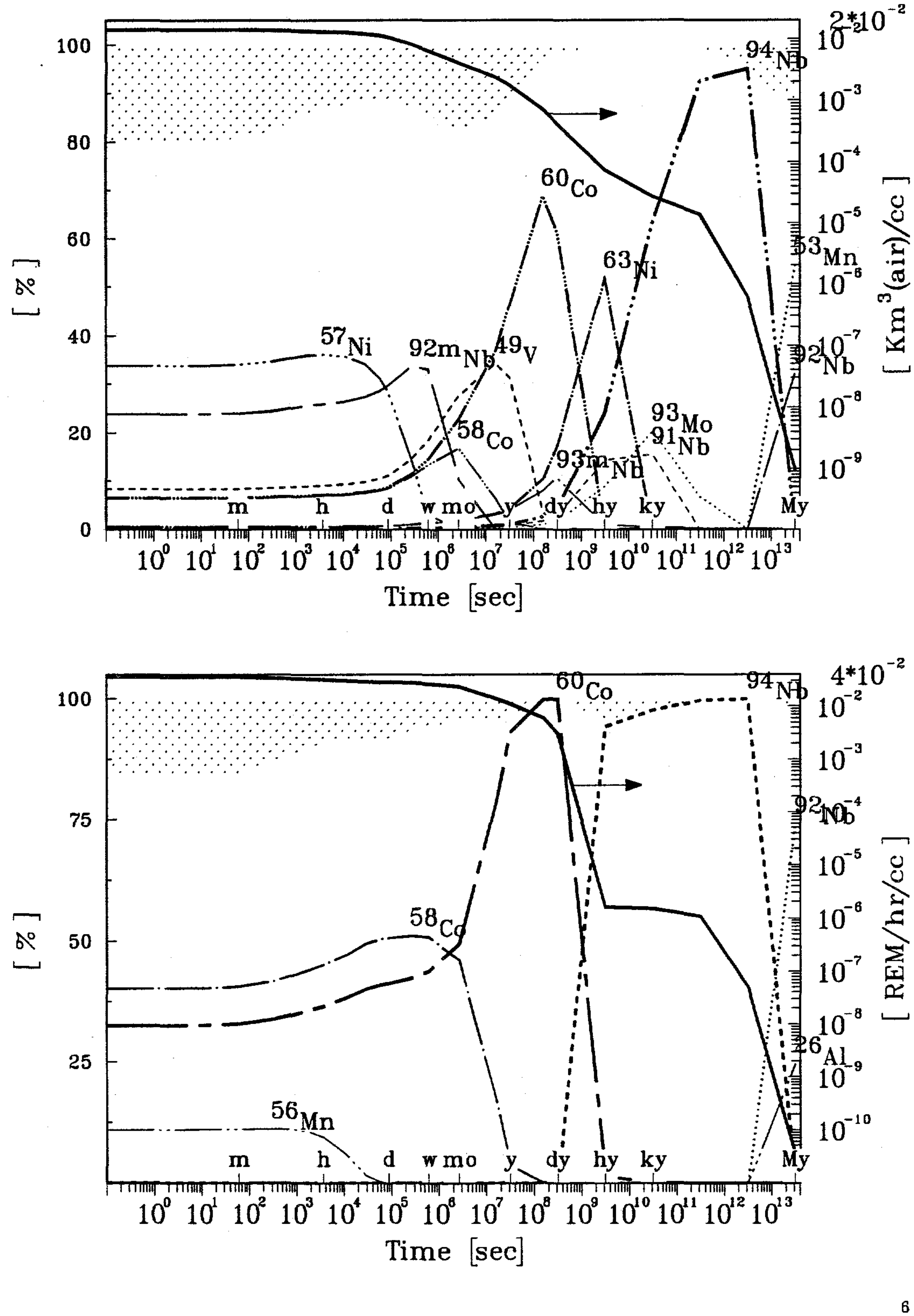

Figure 40. The specific air-BHP (top) and the point-source contact dose (bottom) in zone # 6 (I_VV - SS/water).

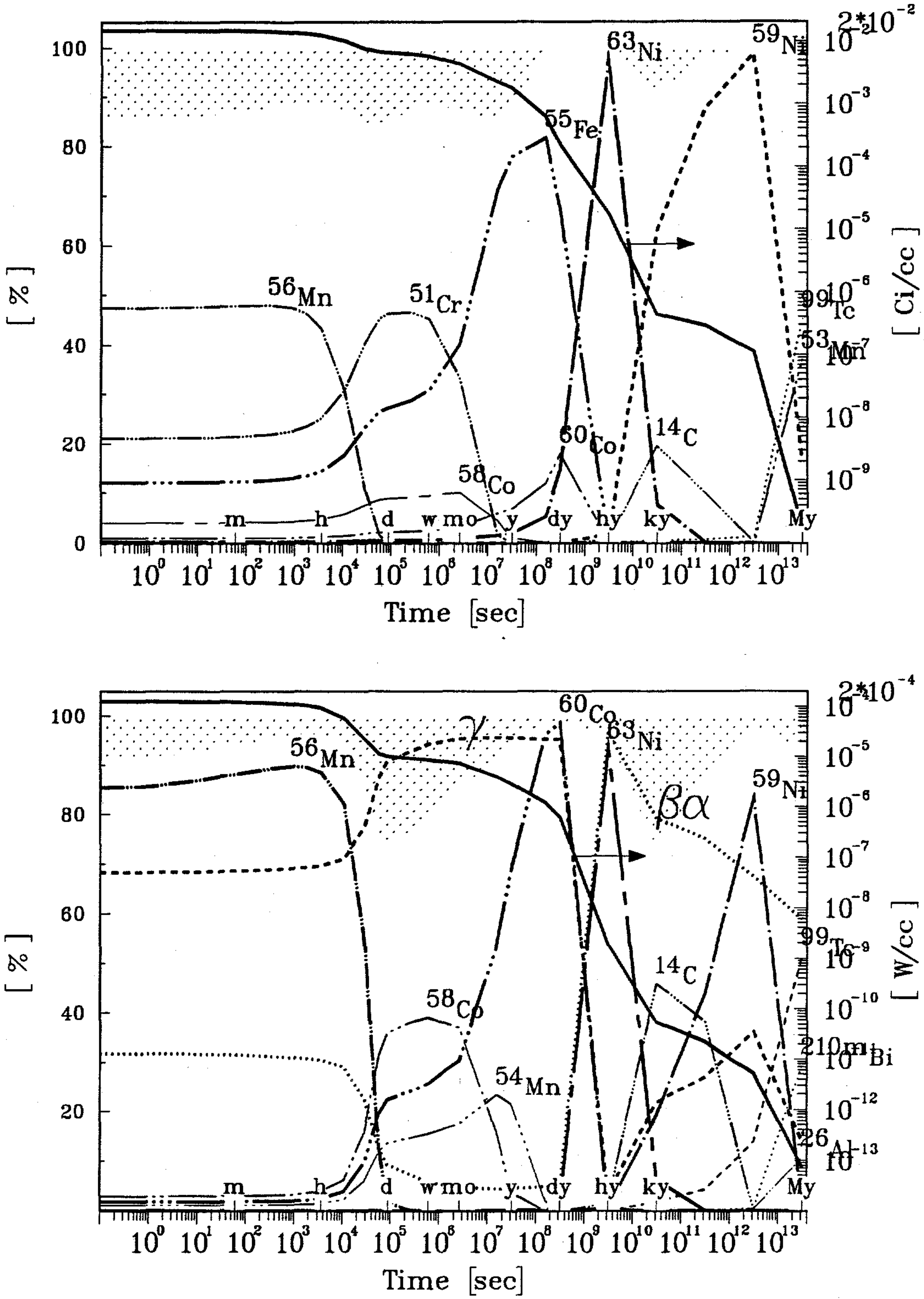

5

Figure 41. The specific radioactivity (top) and the specific decay heat (bottom) in zone # 5 (I_SS_H2O - SS/water).

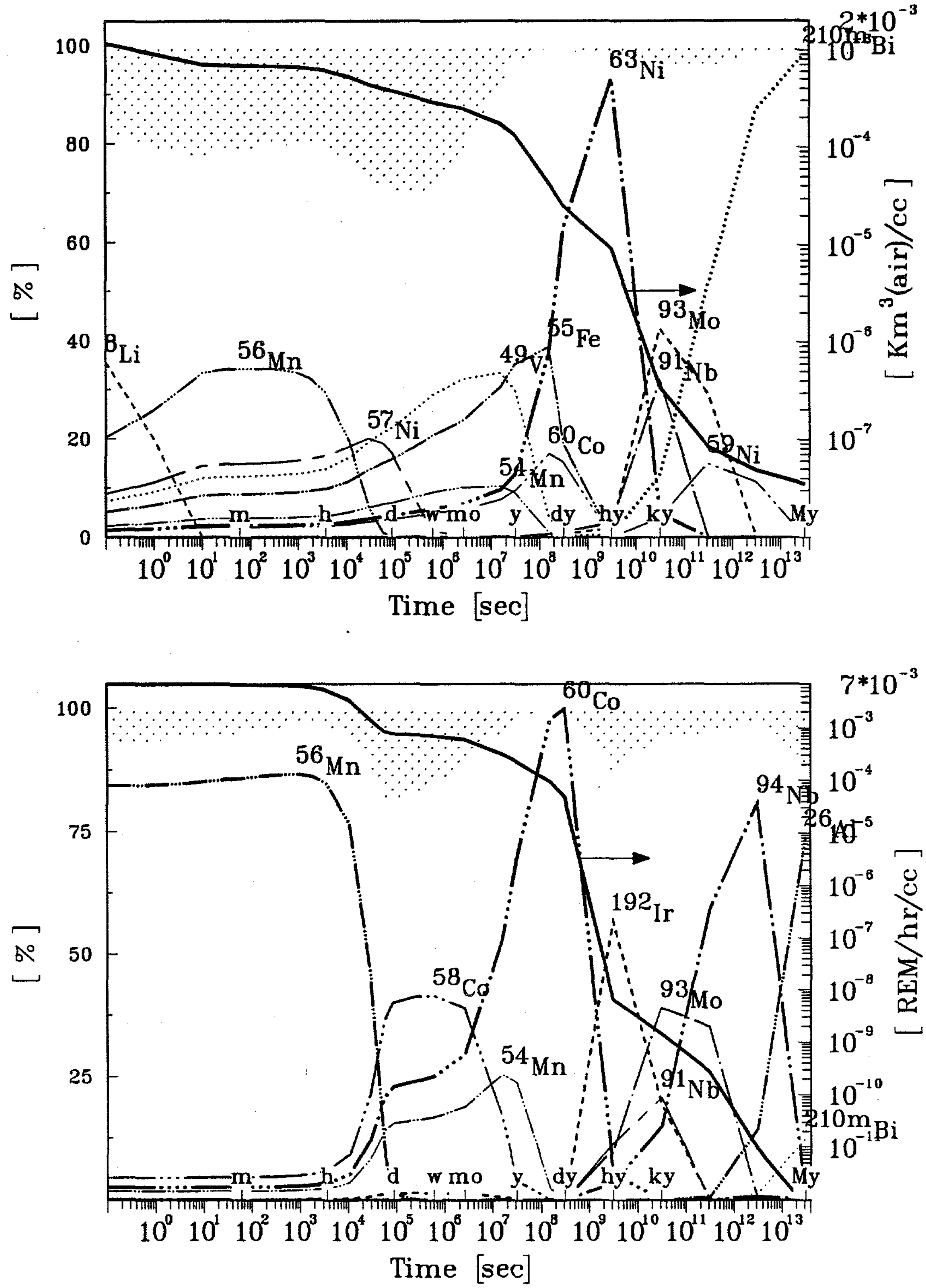

5

Figure 42. The specific air-BHP (top) and the point-source contact dose (bottom) in zone # 5 (I_SS_H2O - SS/water).

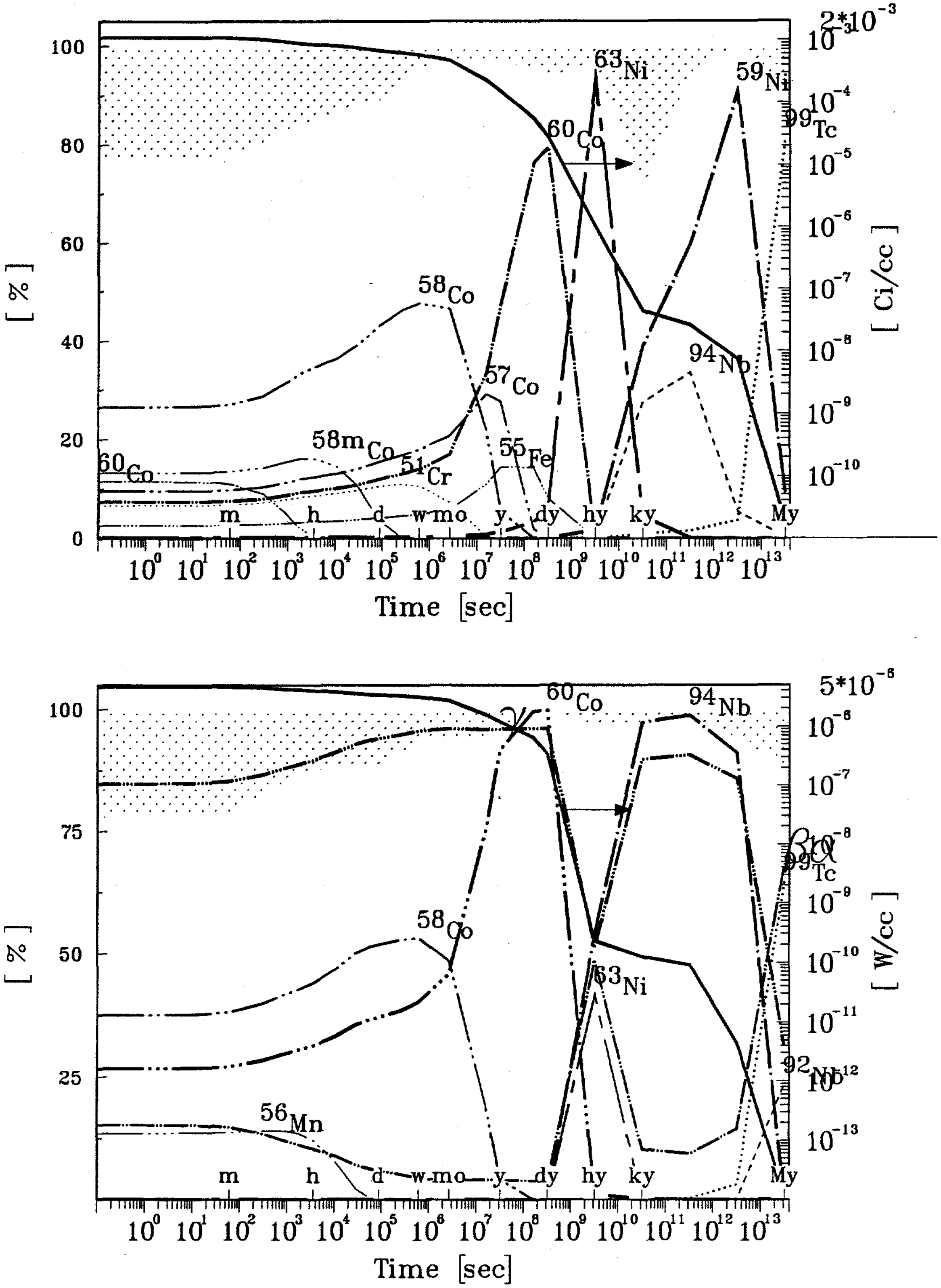

4

Figure 43. The specific radioactivity (top) and the specific decay heat (bottom) in zone # 4 (I_VV - SS/water).

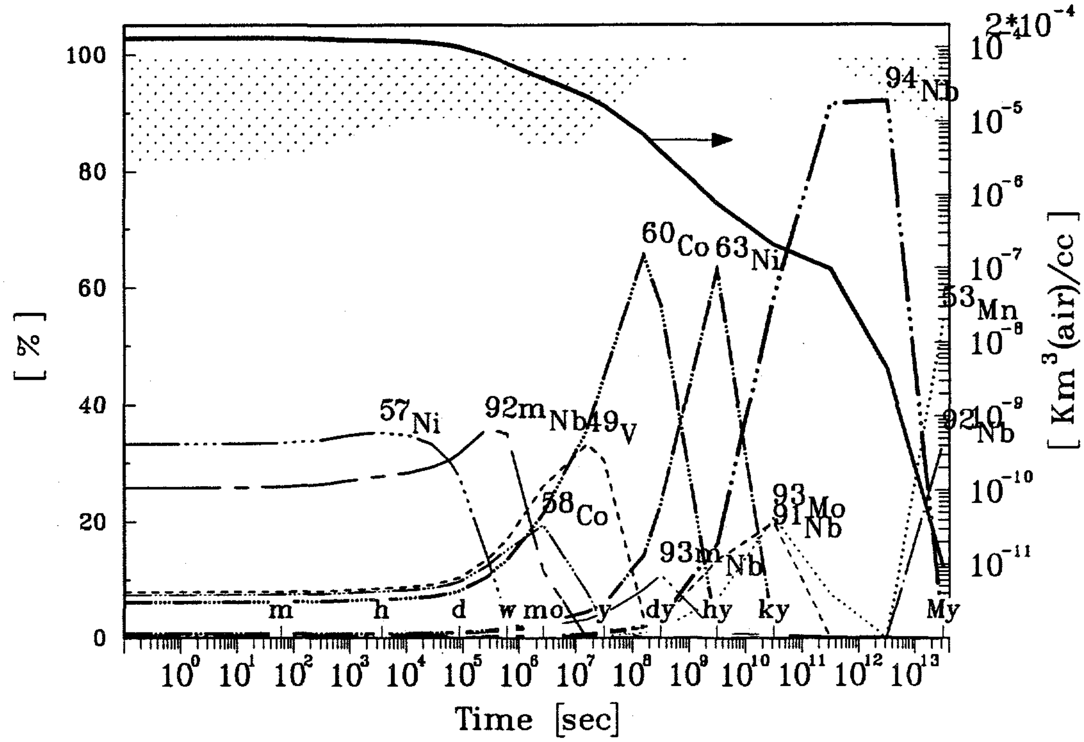

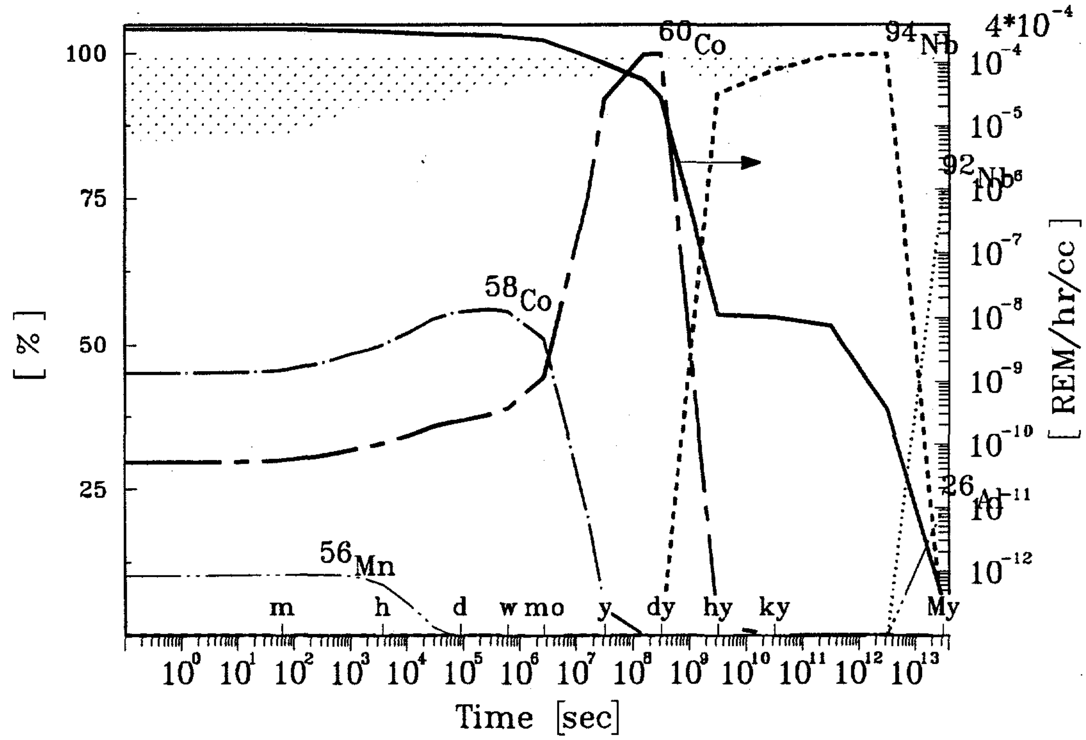

Figure 44. The specific air-BHP (top) and the point-source contact dose (bottom) in zone # 4 (I_VV - SS/water).

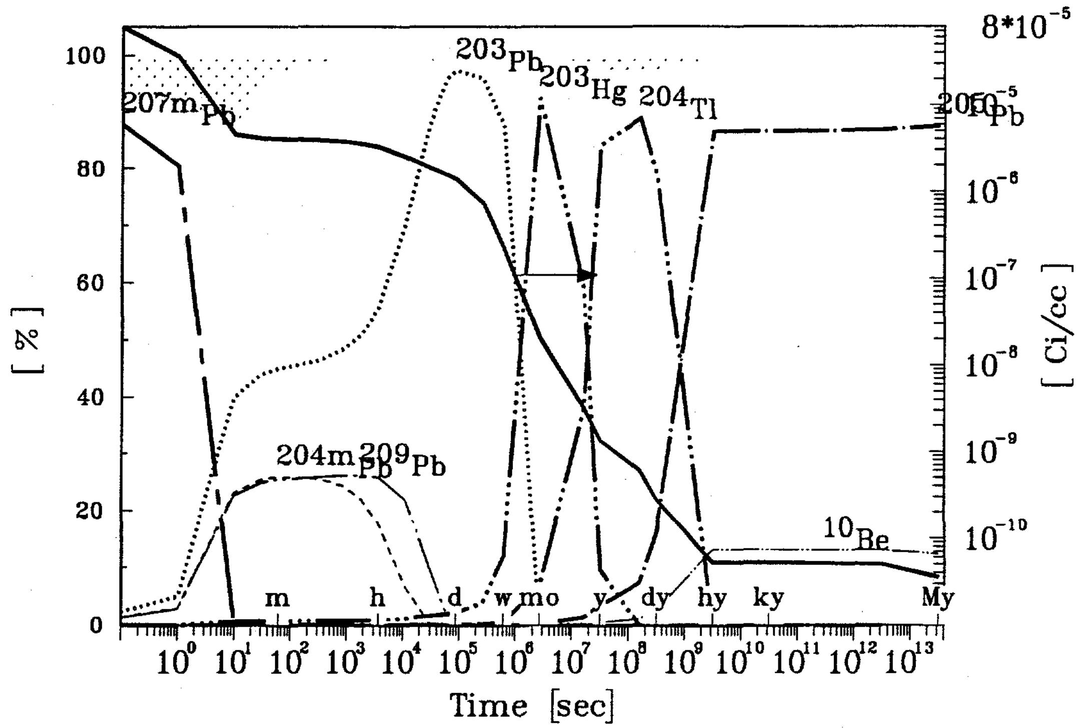

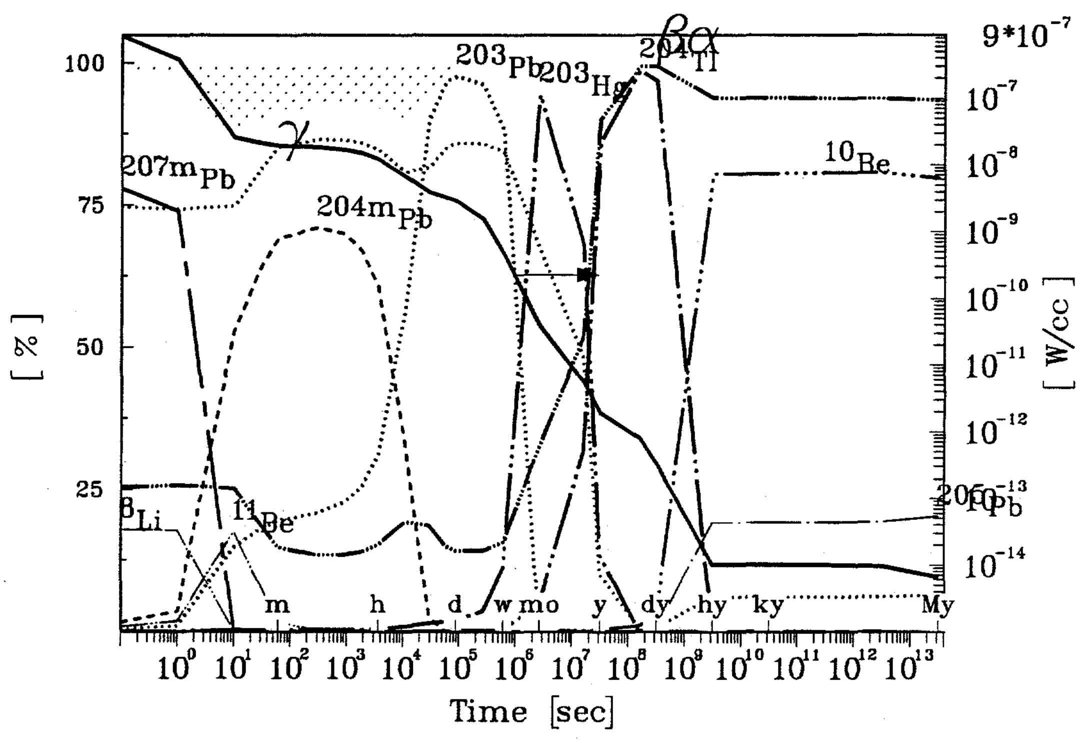

Figure 45. The specific radioactivity (top) and the specific decay heat (bottom) in zone # 3 (I_B4C_Pb - SS/water).

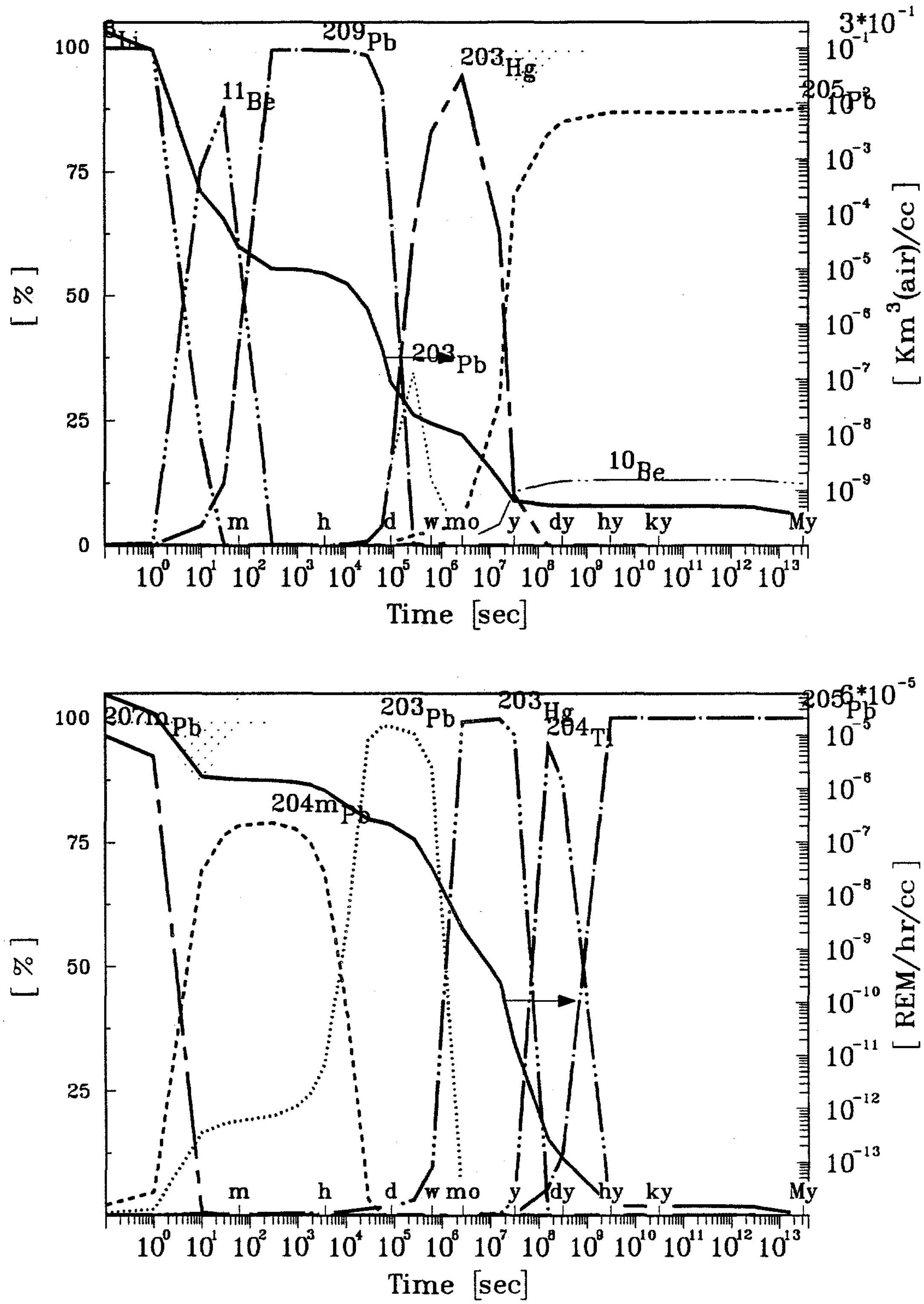

3

Figure 46. The specific air-BHP (top) and the point-source contact dose (bottom) in zone # 3 (I_B4C_Pb - SS/water).

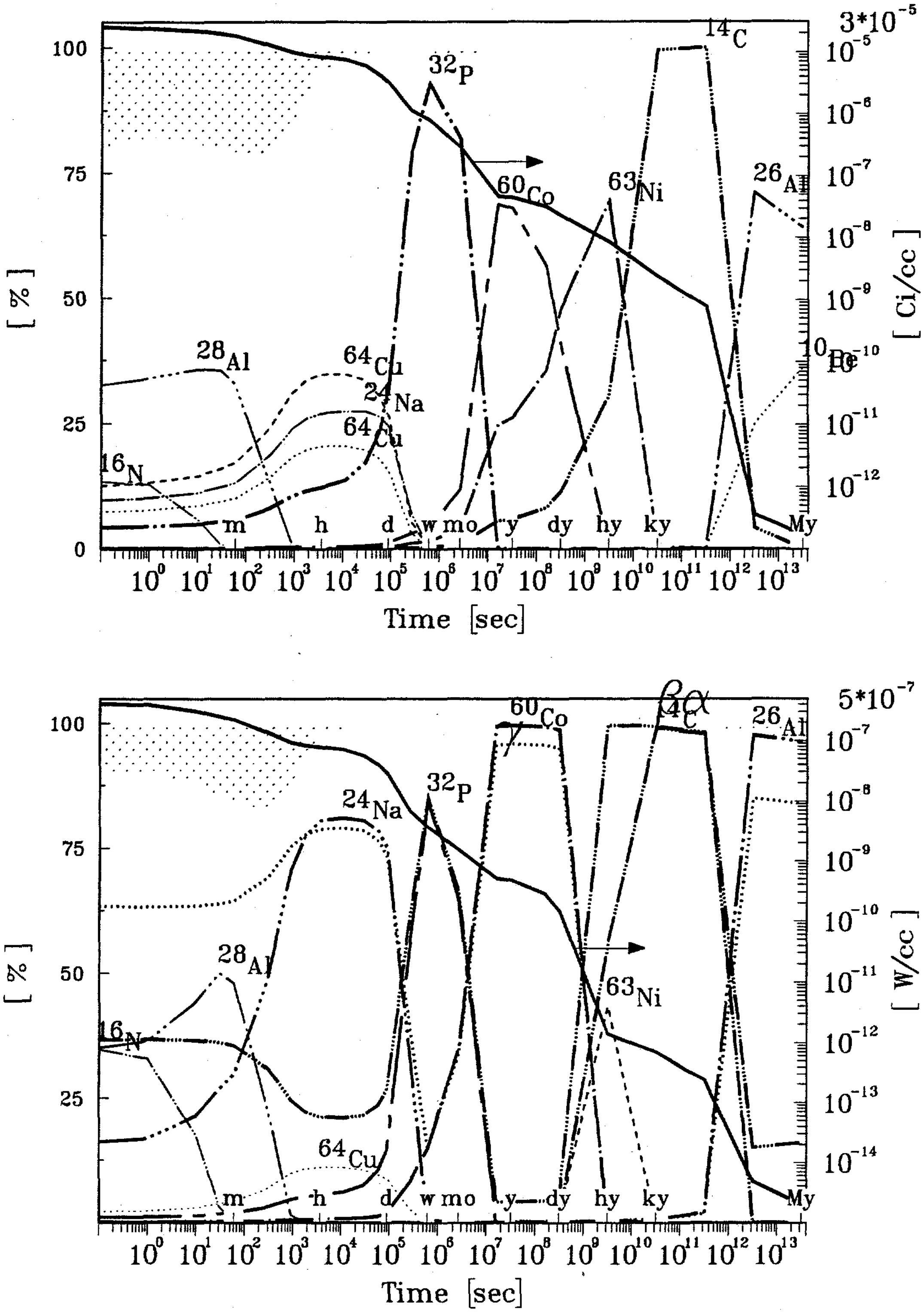

Figure 47. The specific radioactivity (top) and the specific decay heat (bottom) in zone # 2 (I_INSUL - SS/water).

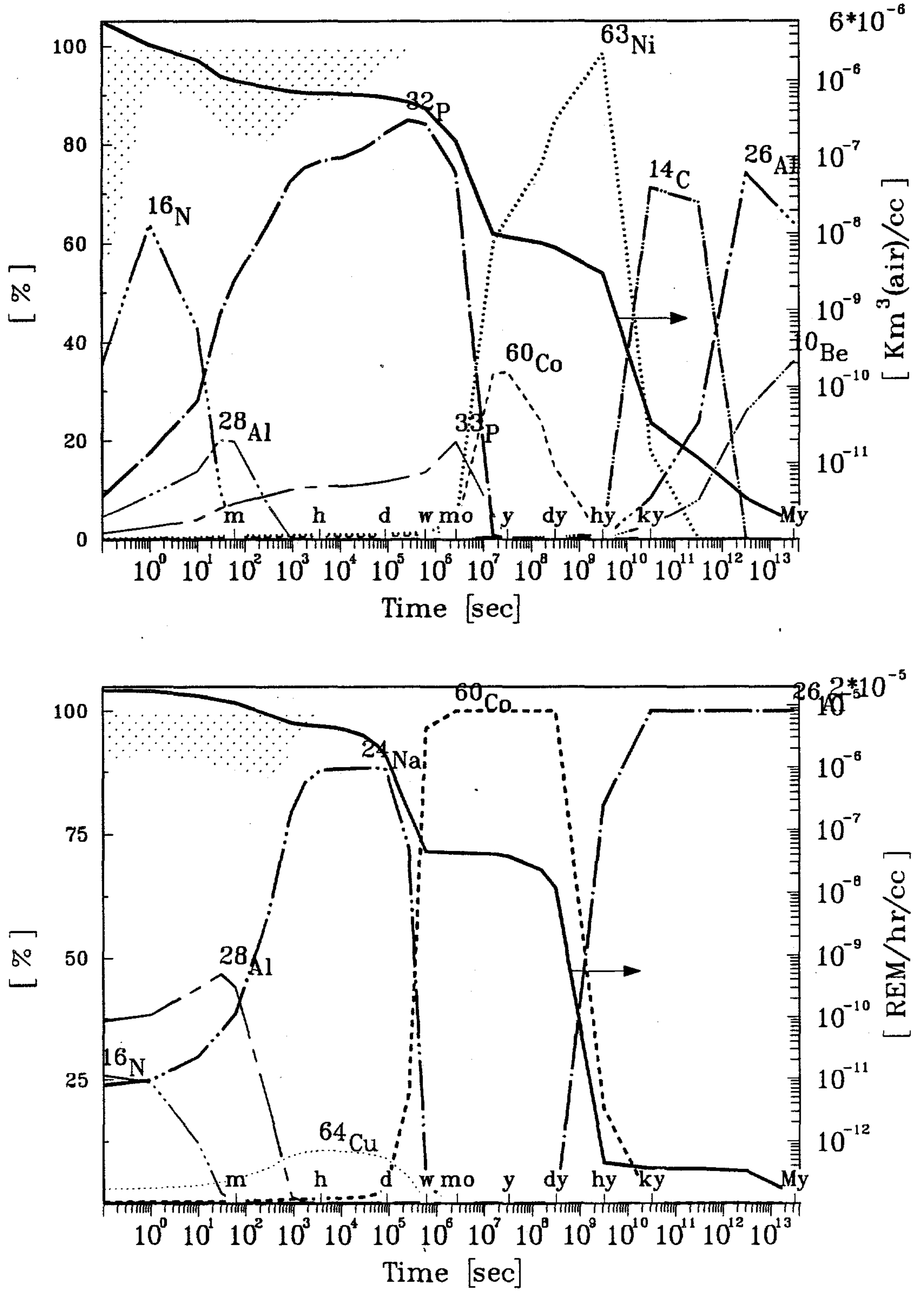

Figure 48. The specific air-BHP (top) and the point-source contact dose (bottom) in zone # 2 (I_INSUL - SS/water).

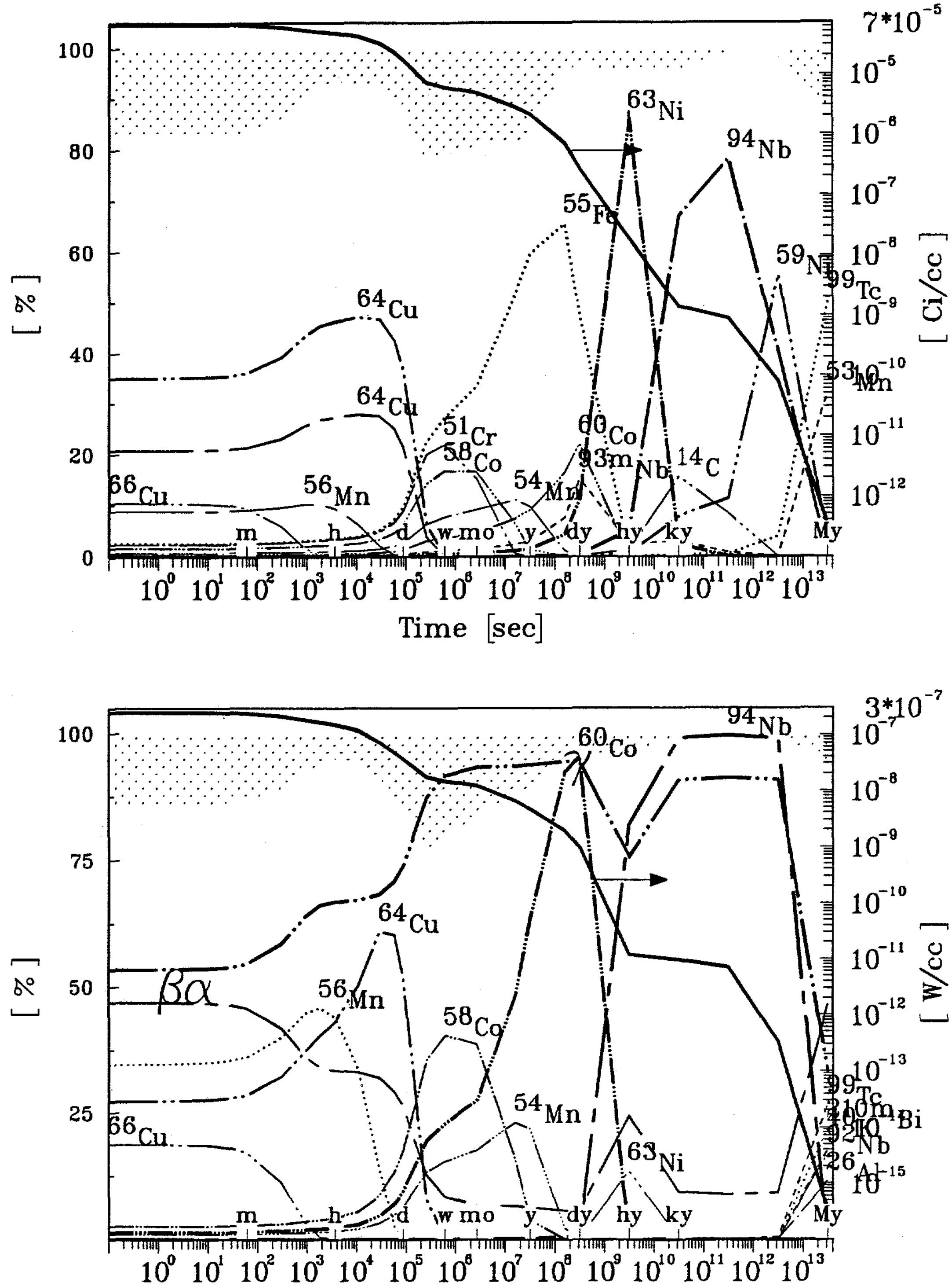

Figure 49. The specific radioactivity (top) and the specific decay heat (bottom) in zone # 1 (I_Magnet - SS/water).

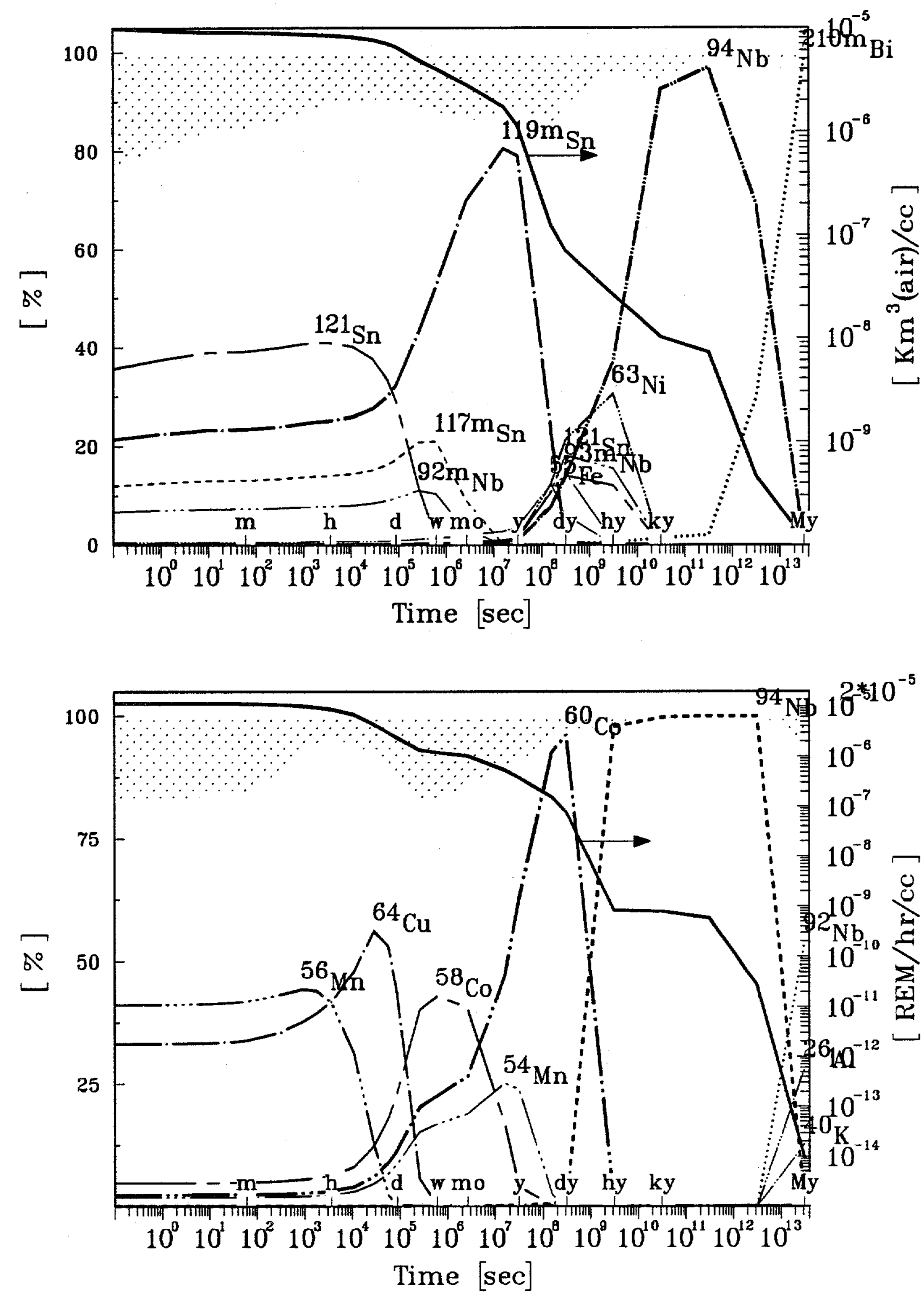

Figure 50. The specific air-BHP (top) and the point-source contact dose (bottom) in zone # 1 (I_Magnet - SS/water).

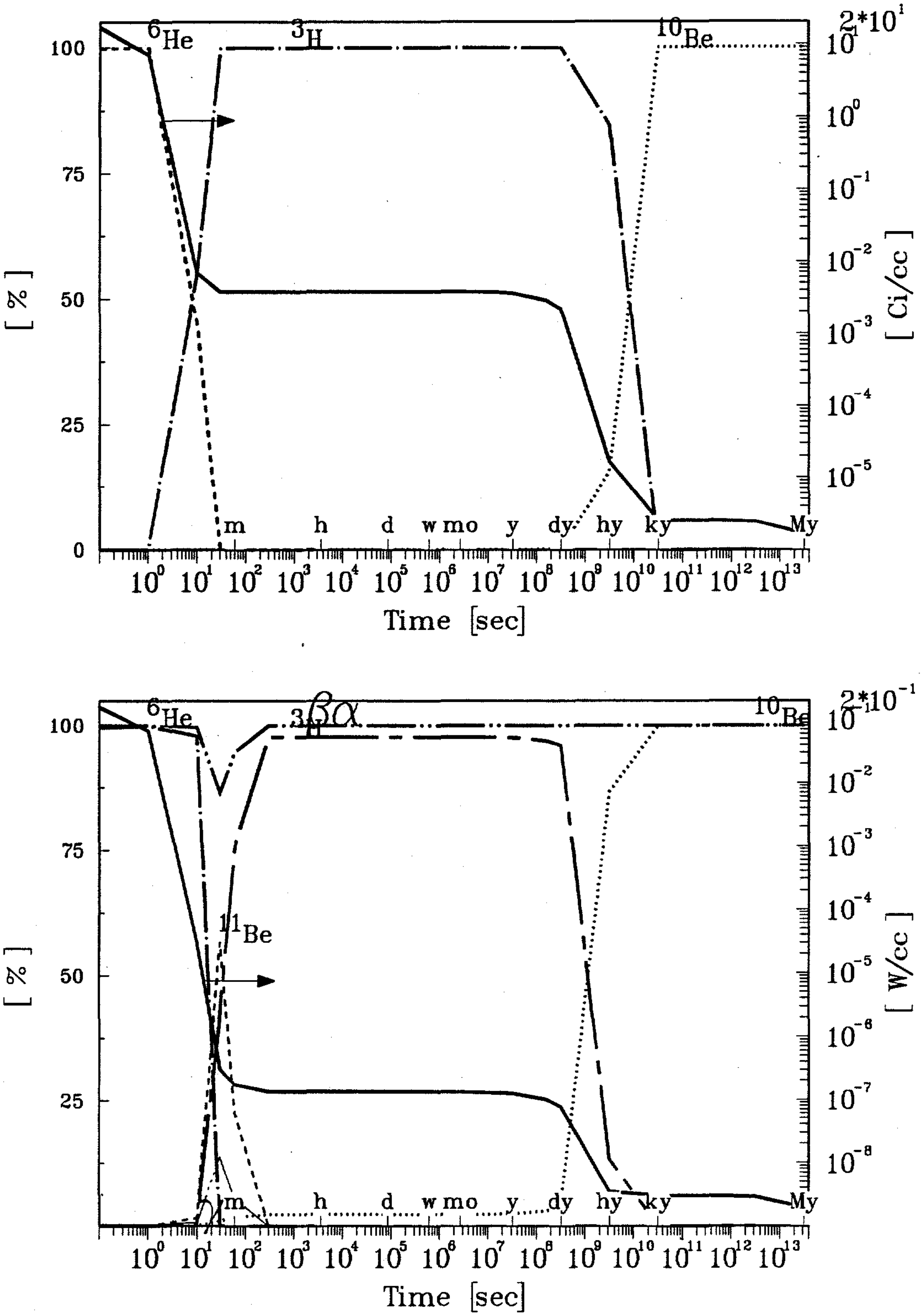

24

Figure 51. The specific radioactivity (top) and the specific decay heat (bottom) in zone # 24 (O_Be - SS/water).

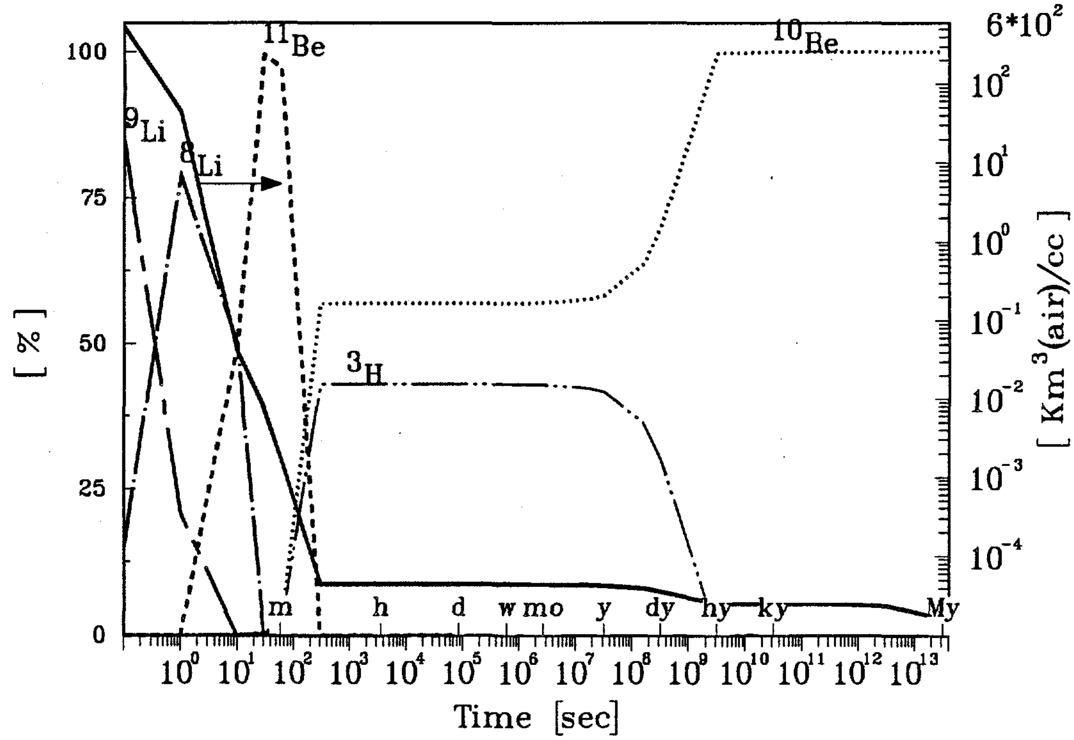

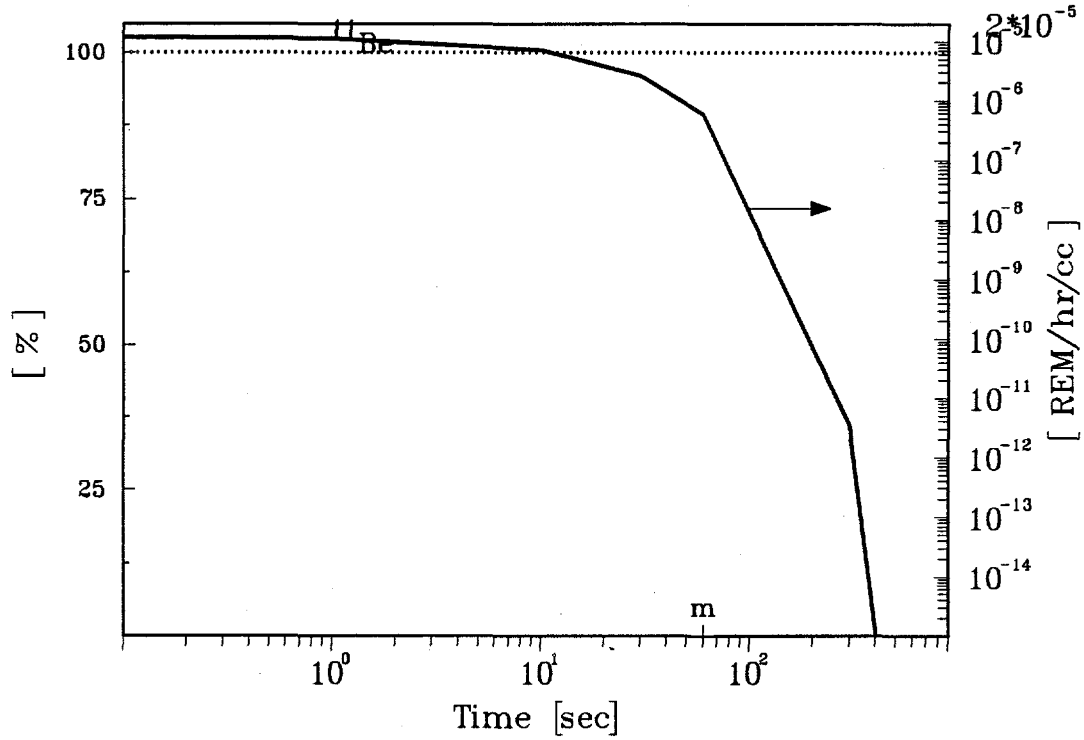

24

Figure 52. The specific air-BHP (top) and the point-source contact dose (bottom) in zone # 24 (O_Be - SS/water).

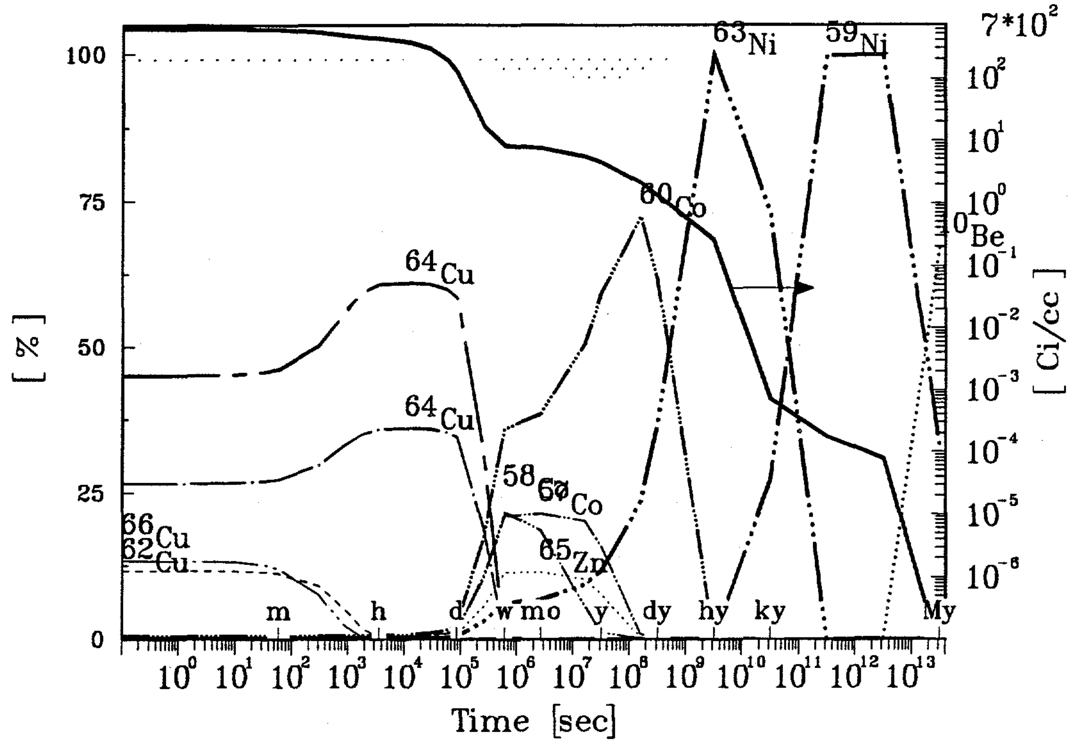

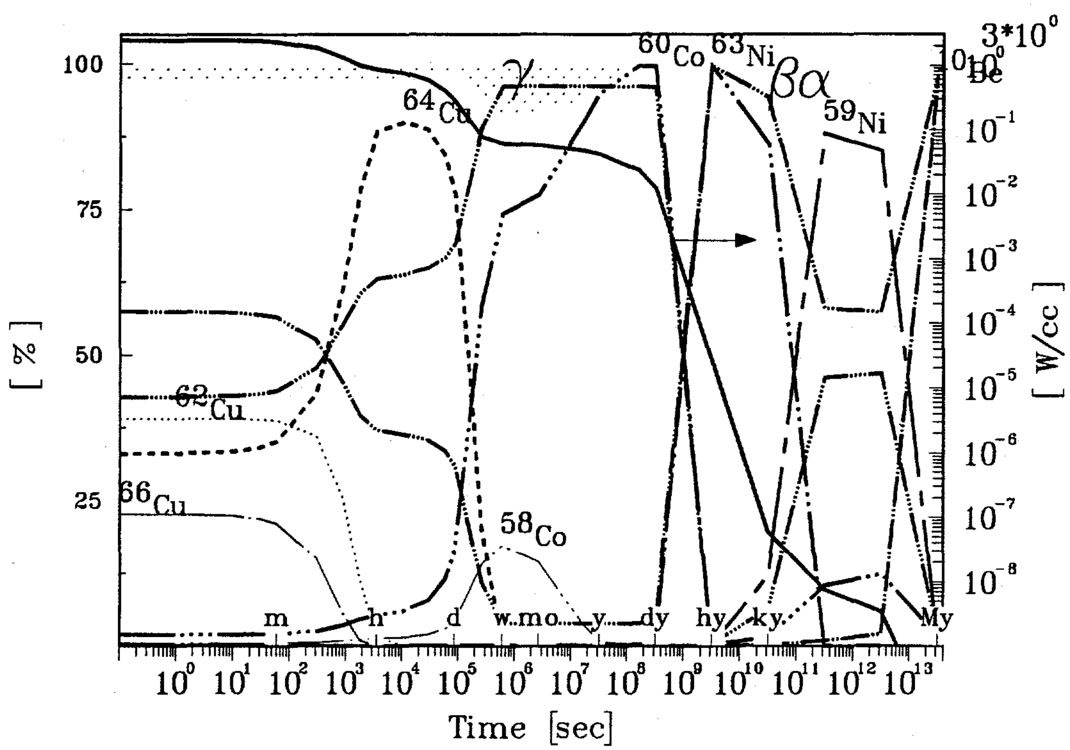

25

Figure 53. The specific radioactivity (top) and the specific decay heat (bottom) in zone # 25 (O_Cua - SS/water).

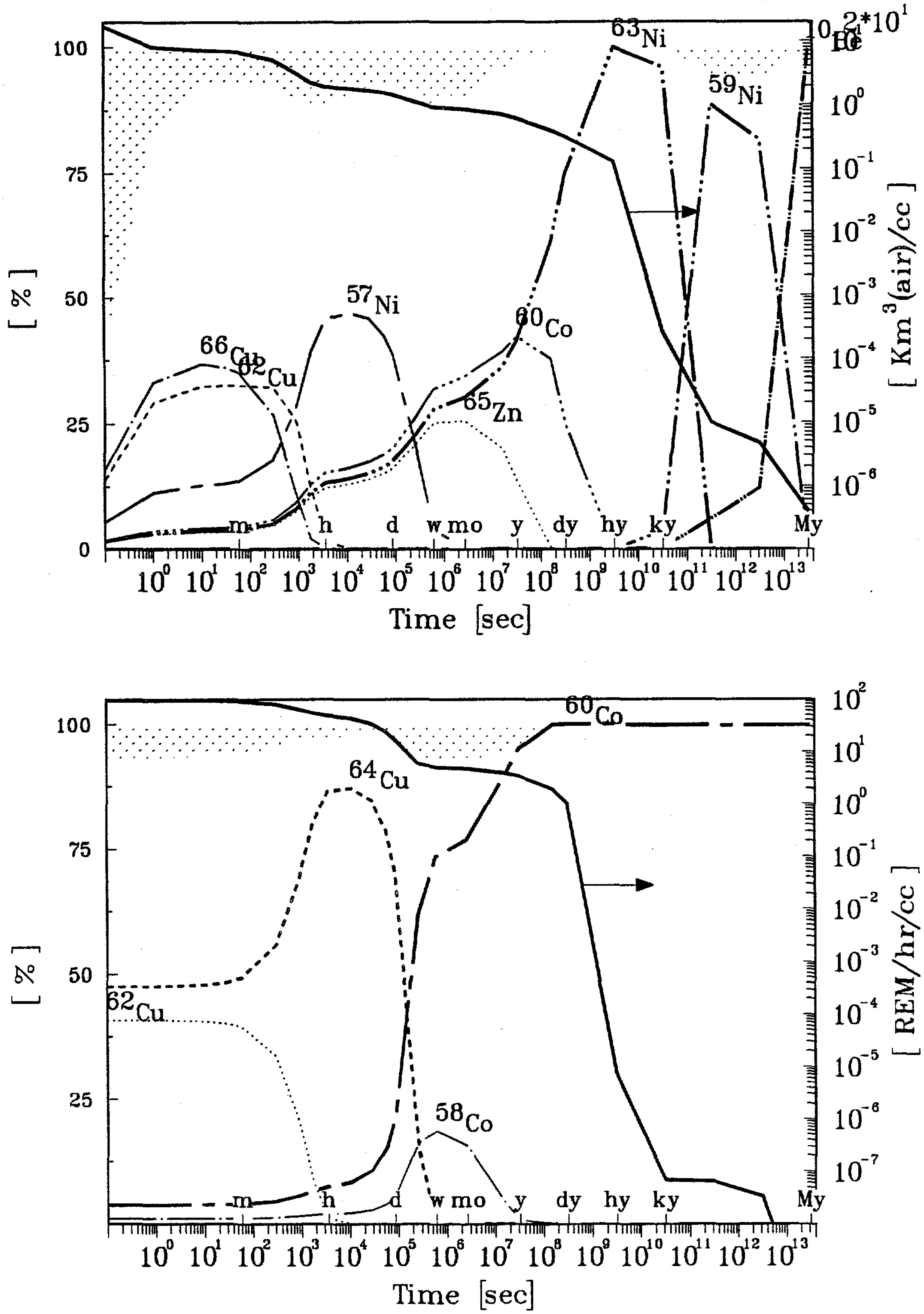

25

Figure 54. The specific air-BHP (top) and the point-source contact dose (bottom) in zone # 25 (O_Cua - SS/water).

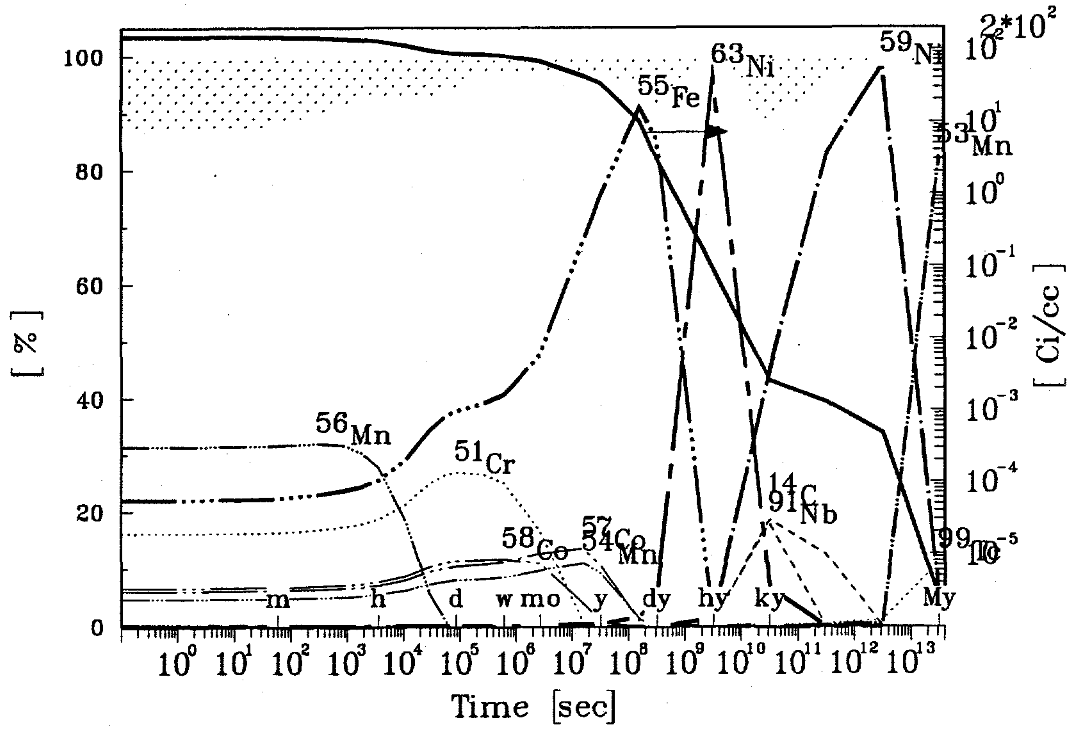

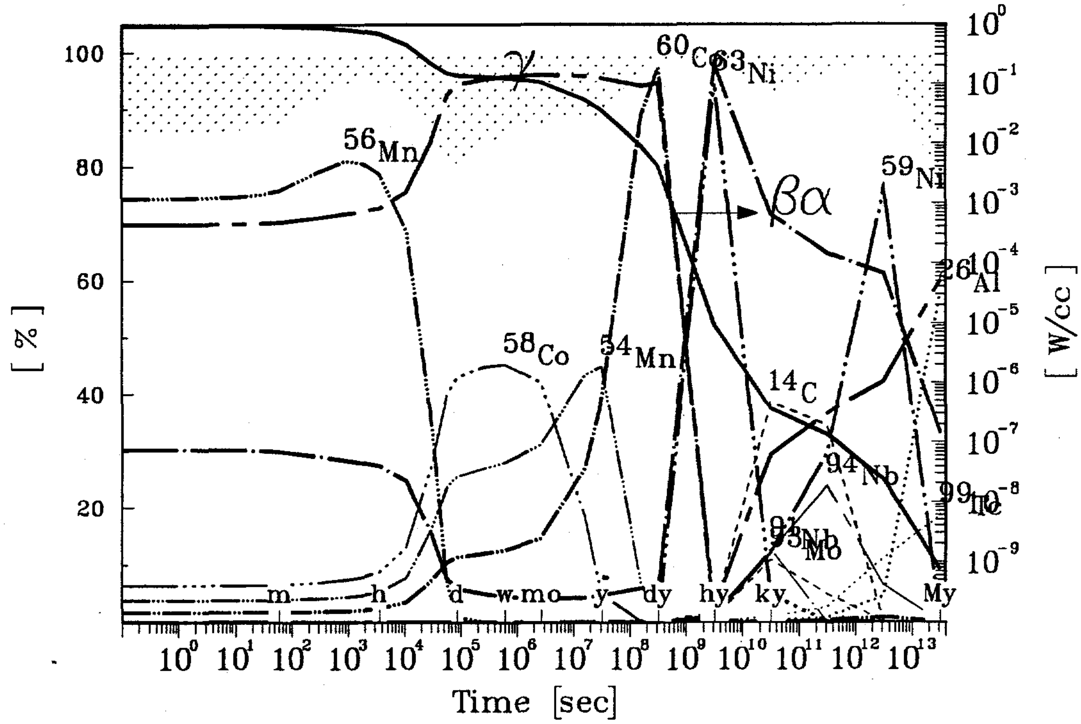

26

Figure 55. The specific radioactivity (top) and the specific decay heat (bottom) in zone # 26 (O_SS (FW)- SS/water).

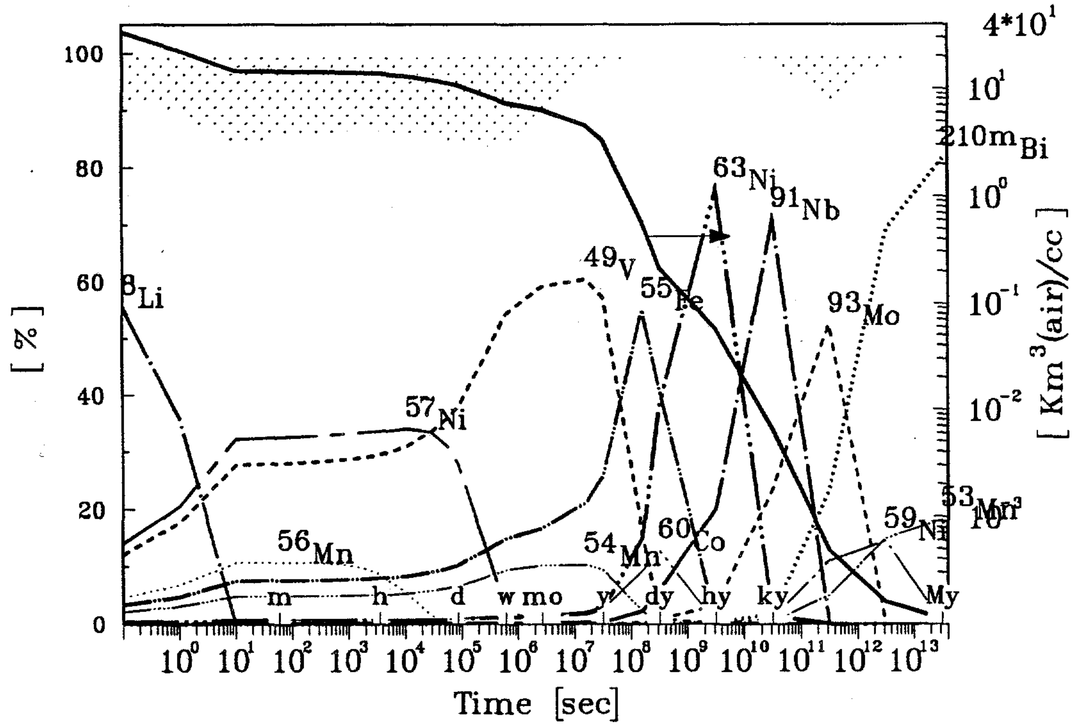

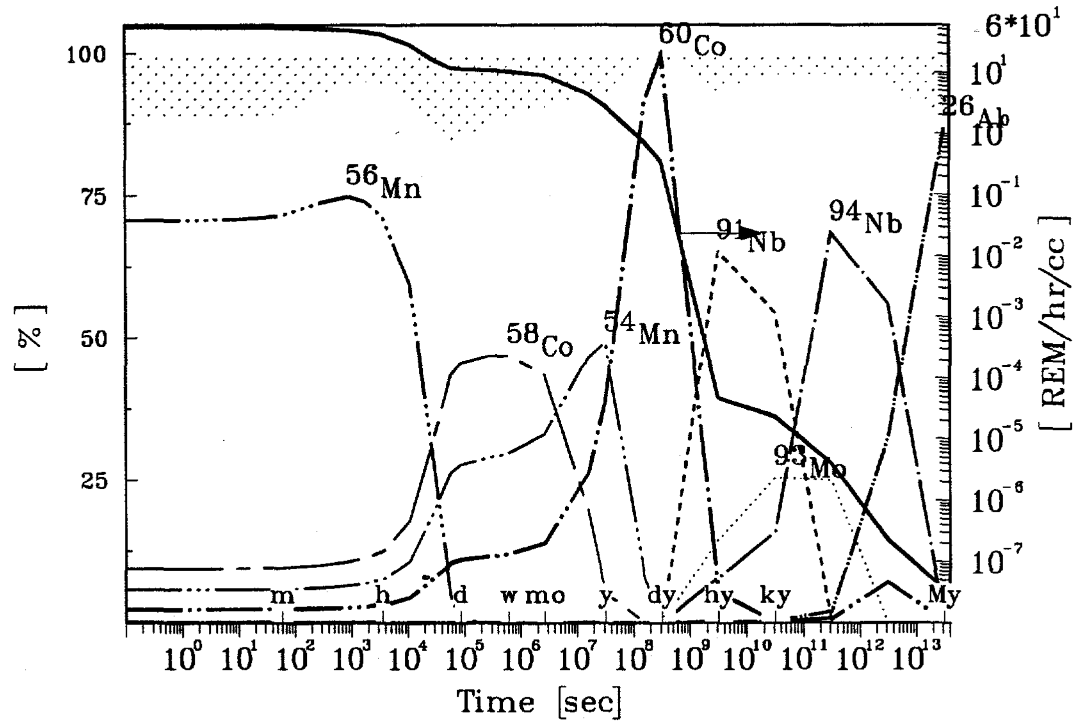

26

Figure 56. The specific air-BHP (top) and the point-source contact dose (bottom) in zone # 26 (O_SS (FW)- SS/water).

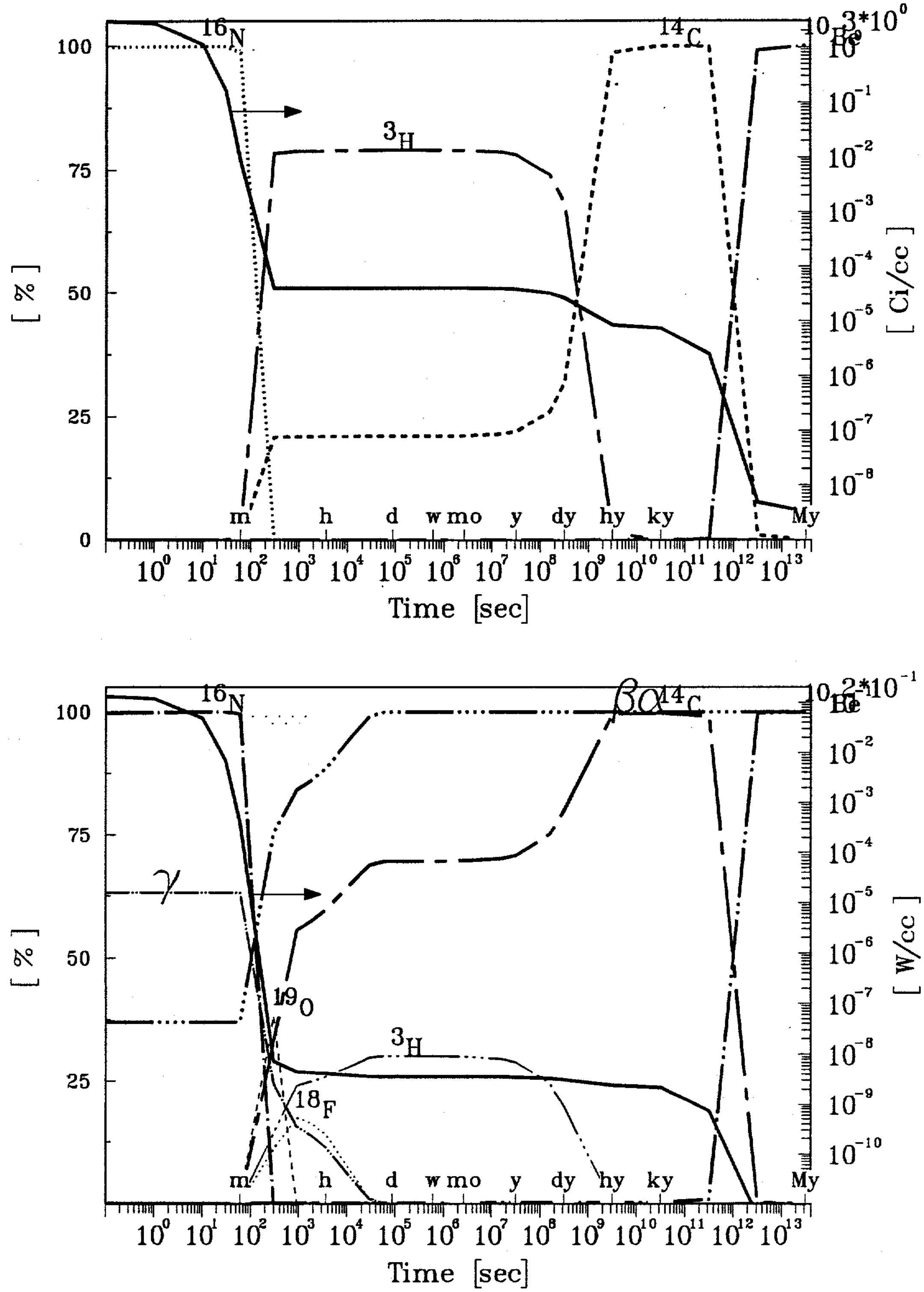

27

Figure 57. The specific radioactivity (top) and the specific decay heat (bottom) in zone # 27 (O_H2O - SS/water).

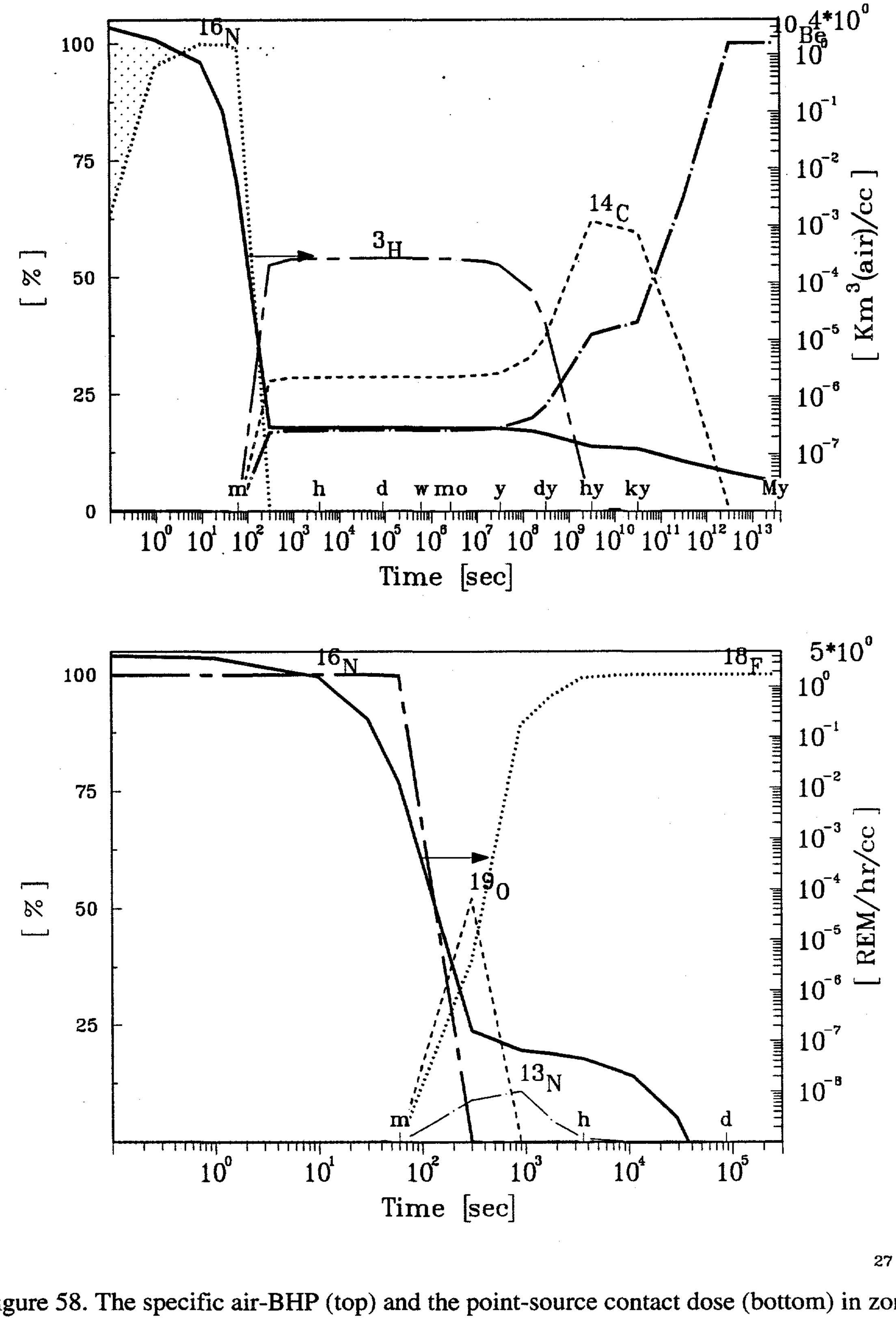

Figure 58. The specific air-BHP (top) and the point-source contact dose (bottom) in zone # 27 (O_H2O - SS/water).

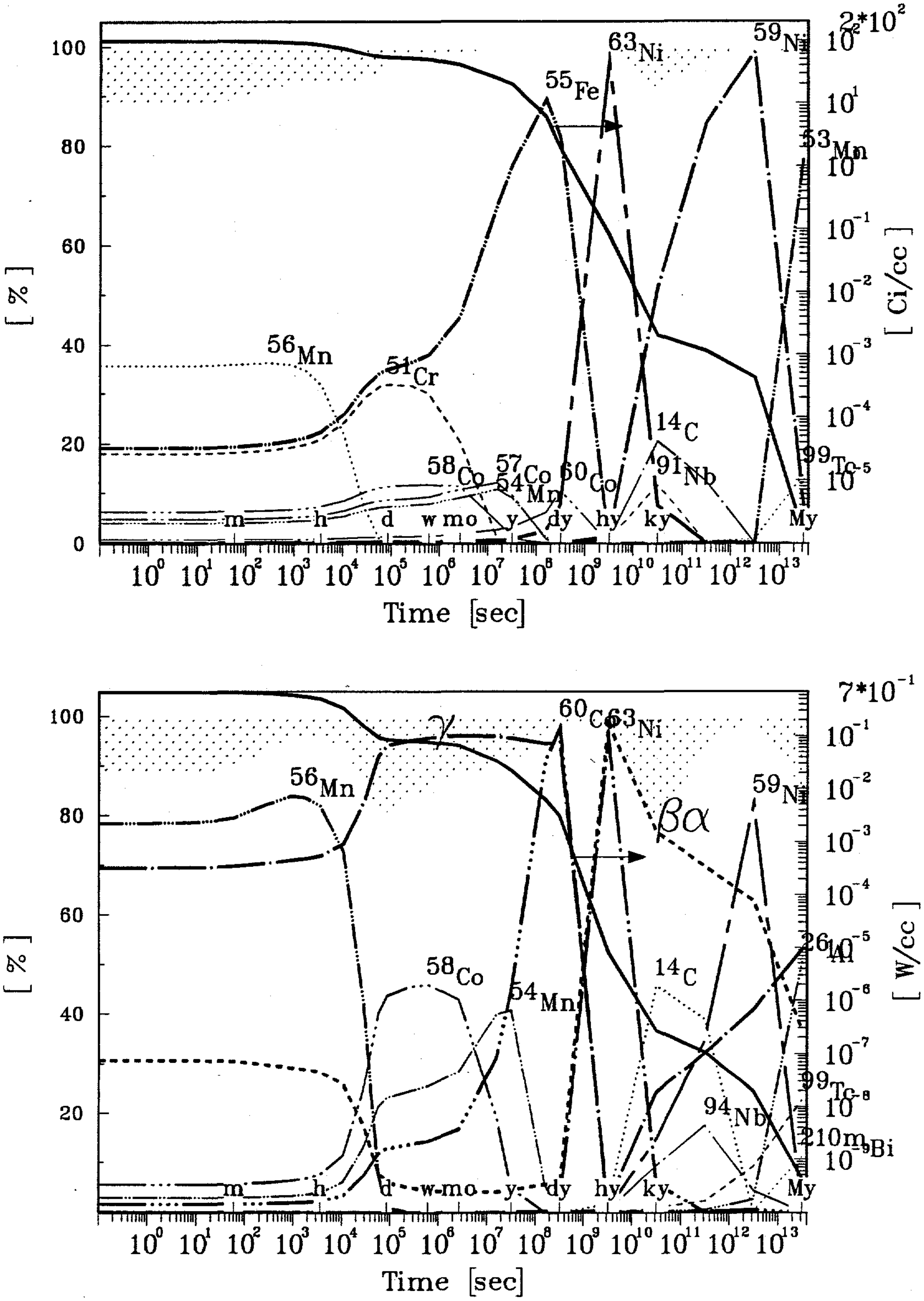

Figure 59. The specific radioactivity (top) and the specific decay heat (bottom) in zone # 28 (O_SS - SS/water).

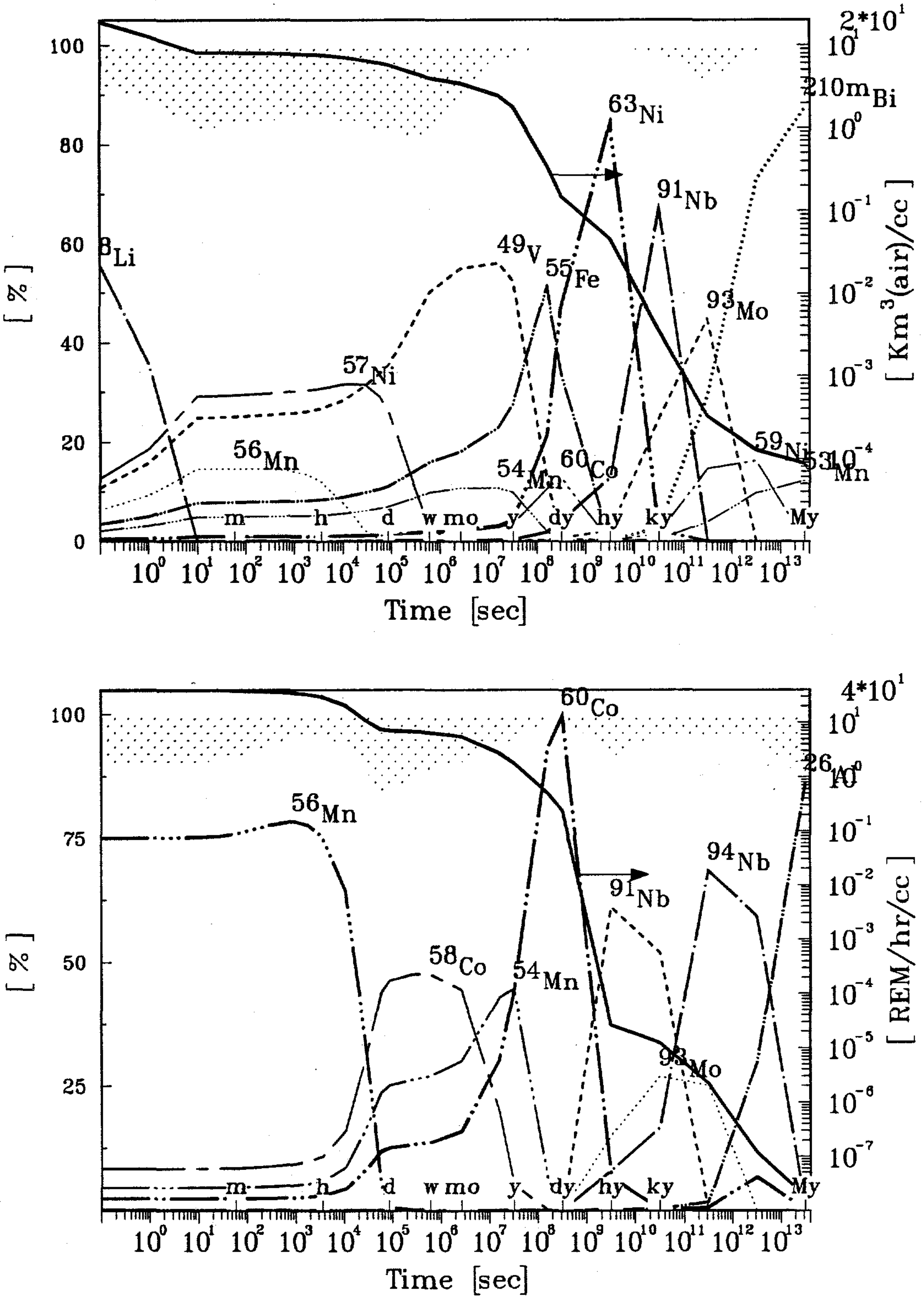

28

Figure 60. The specific air-BHP (top) and the point-source contact dose (bottom) in zone # 28 (O_SS - SS/water).

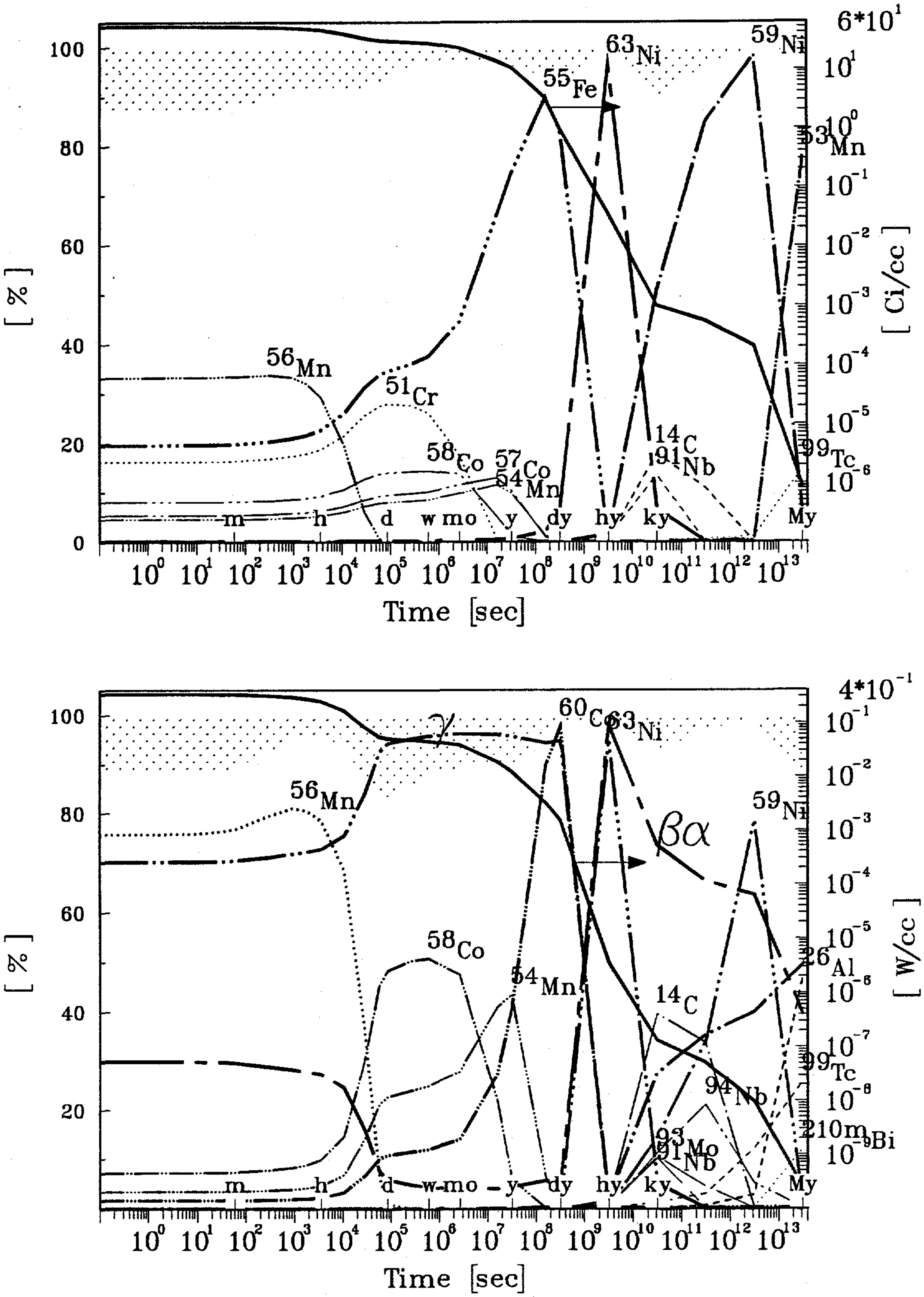

30

Figure 61. The specific radioactivity (top) and the specific decay heat (bottom) in zone # 30 (O_SS - SS/water).

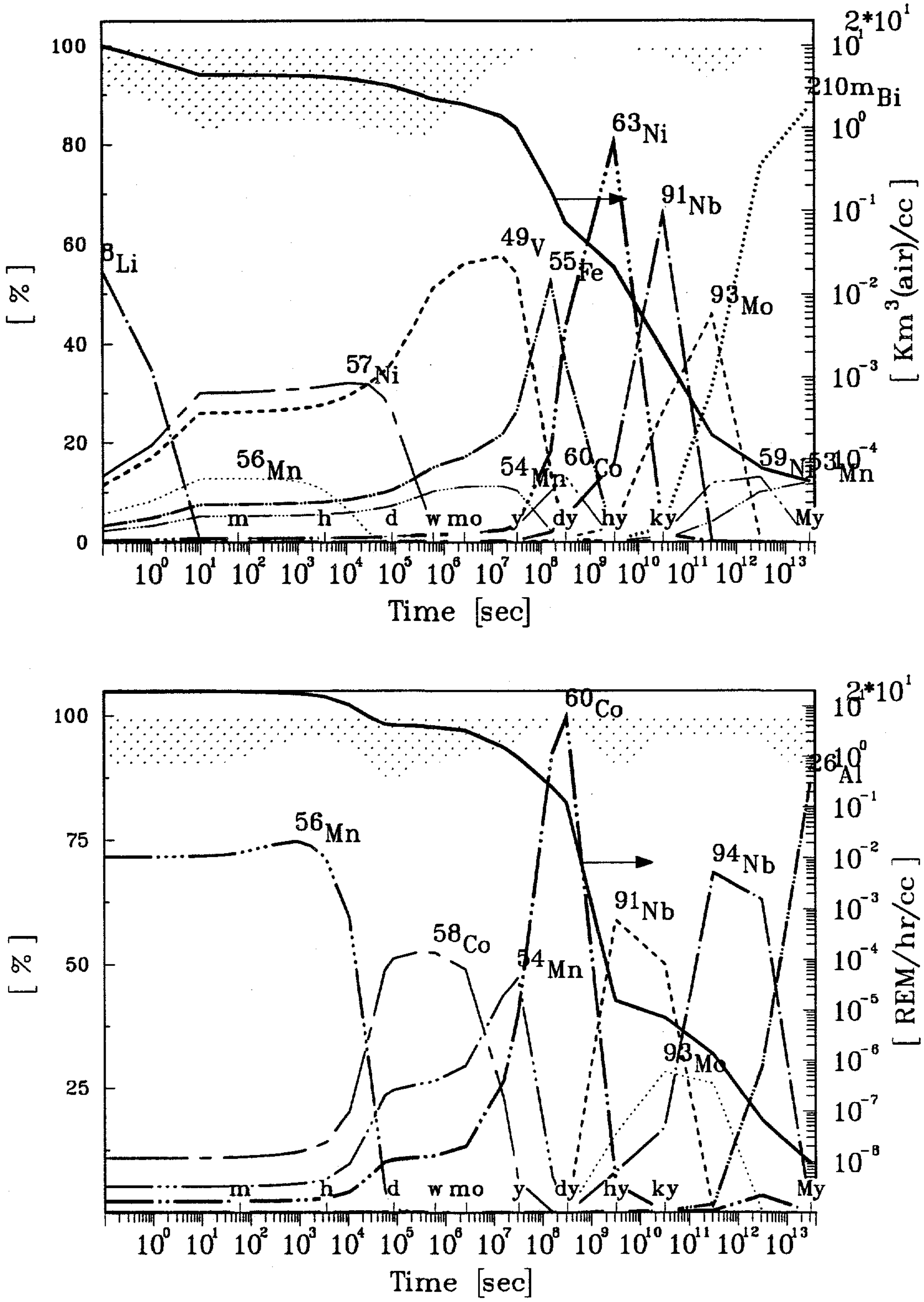

30

Figure 62. The specific air-BHP (top) and the point-source contact dose (bottom) in zone # 30 (O_SS - SS/water).

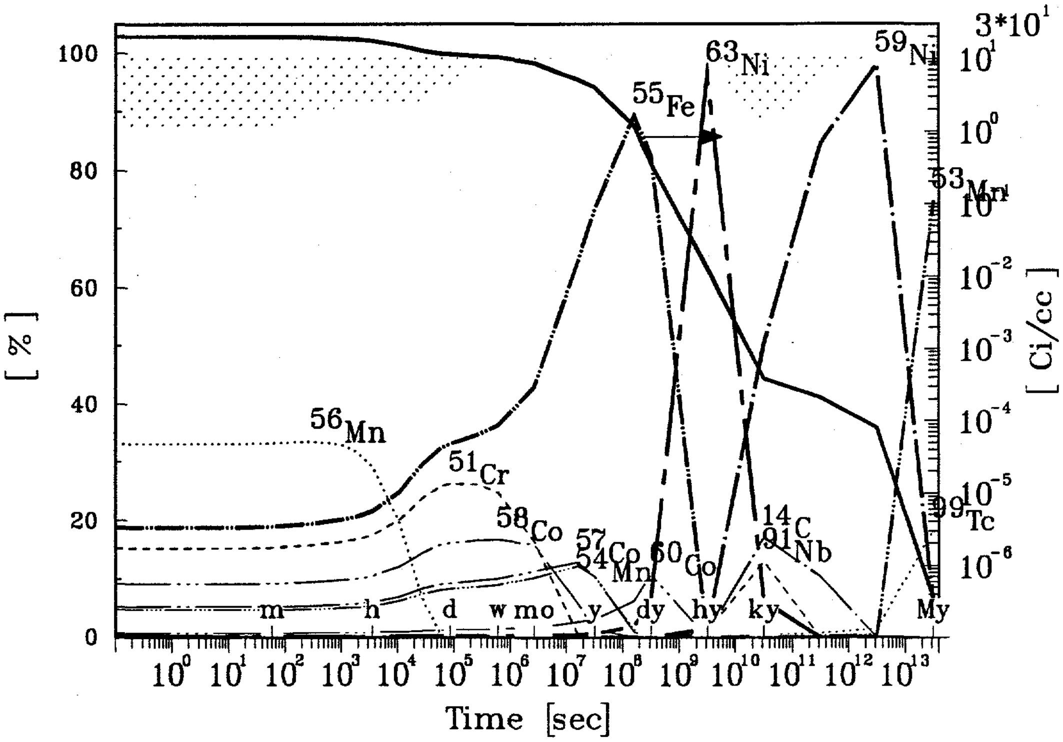

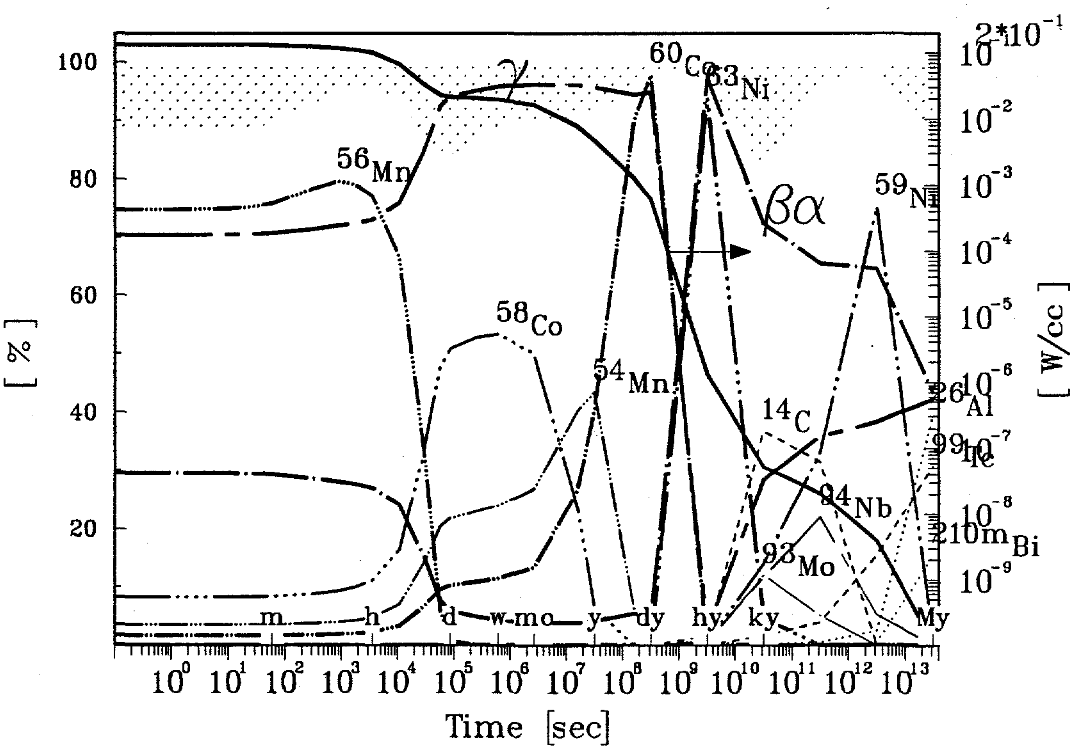

32

Figure 63. The specific radioactivity (top) and the specific decay heat (bottom) in zone # 32 (O_SS - SS/water).

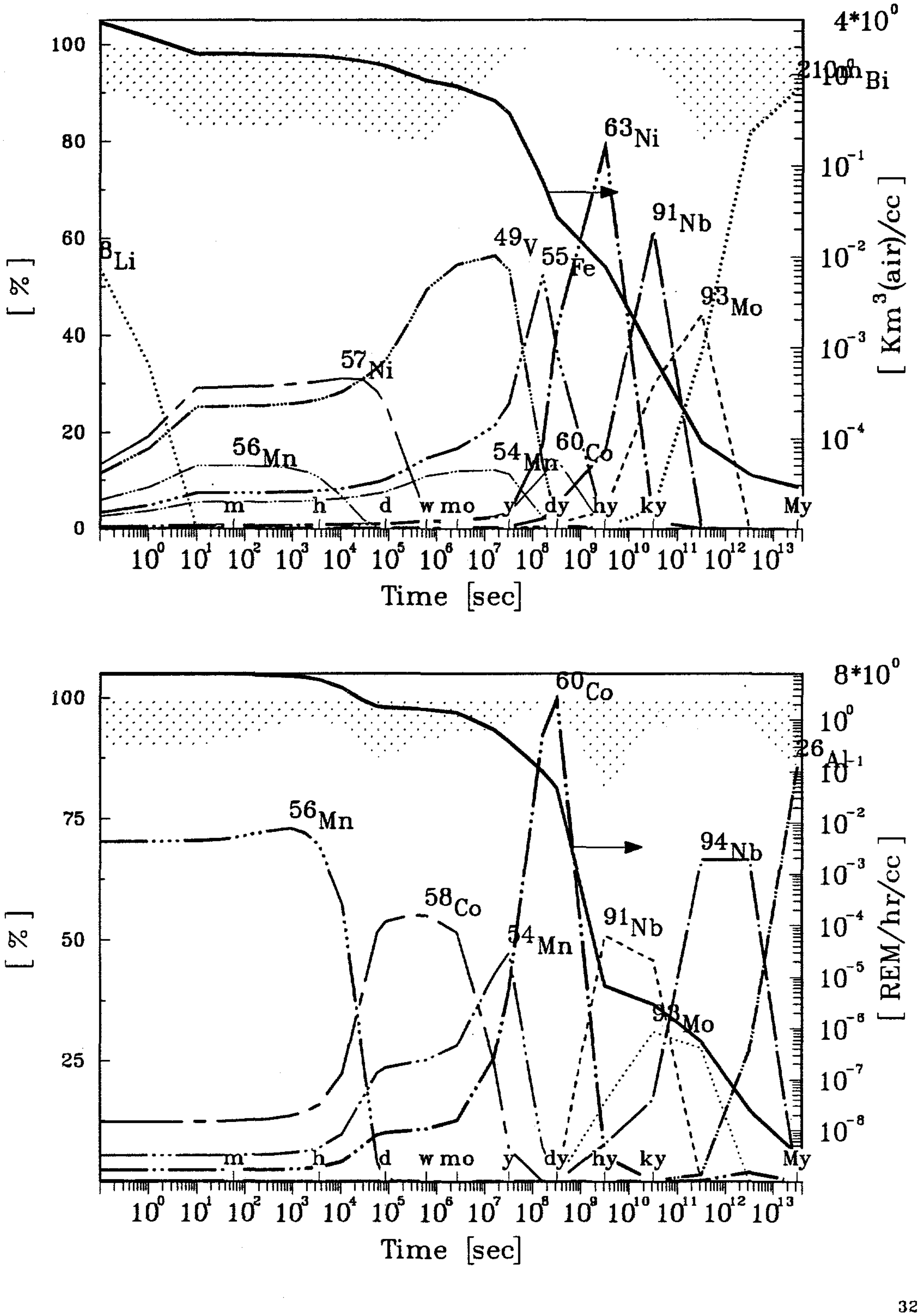

Figure 64. The specific air-BHP (top) and the point-source contact dose (bottom) in zone # 32 (O_SS - SS/water).

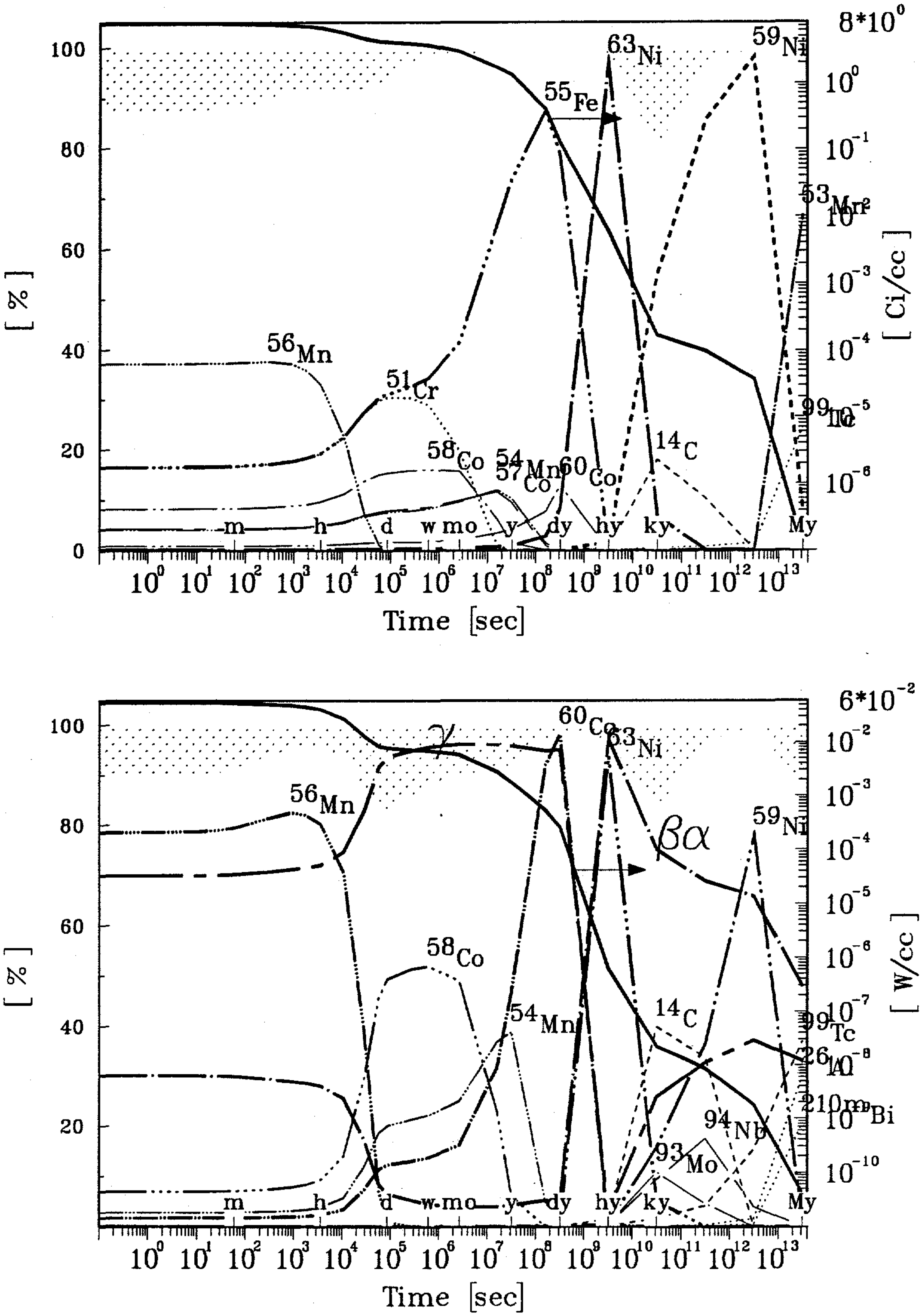

34

Figure 65. The specific radioactivity (top) and the specific decay heat (bottom) in zone # 34 (O_SS - SS/water).

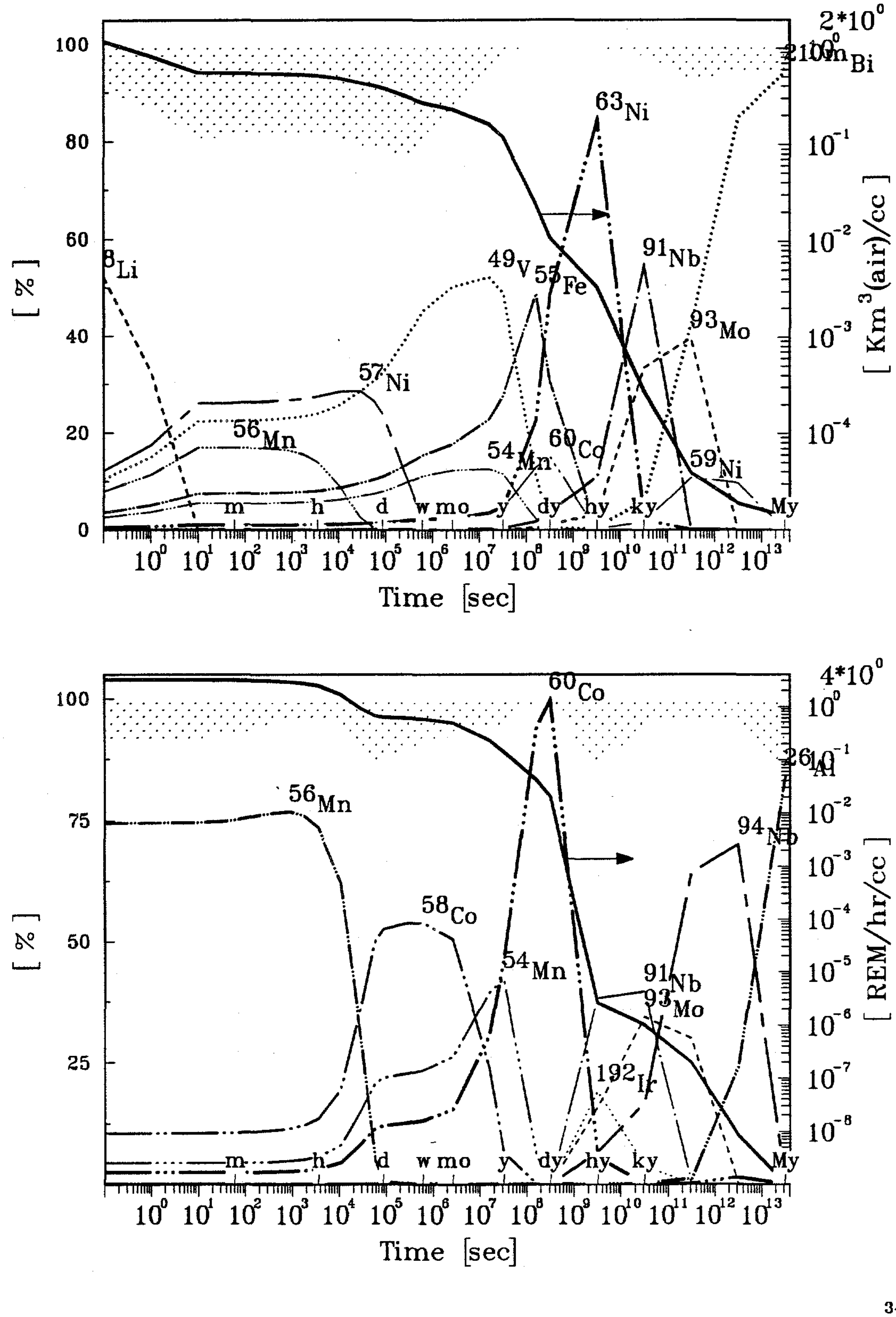

Figure 66. The specific air-BHP (top) and the point-source contact dose (bottom) in zone # 34 (O_SS - SS/water).

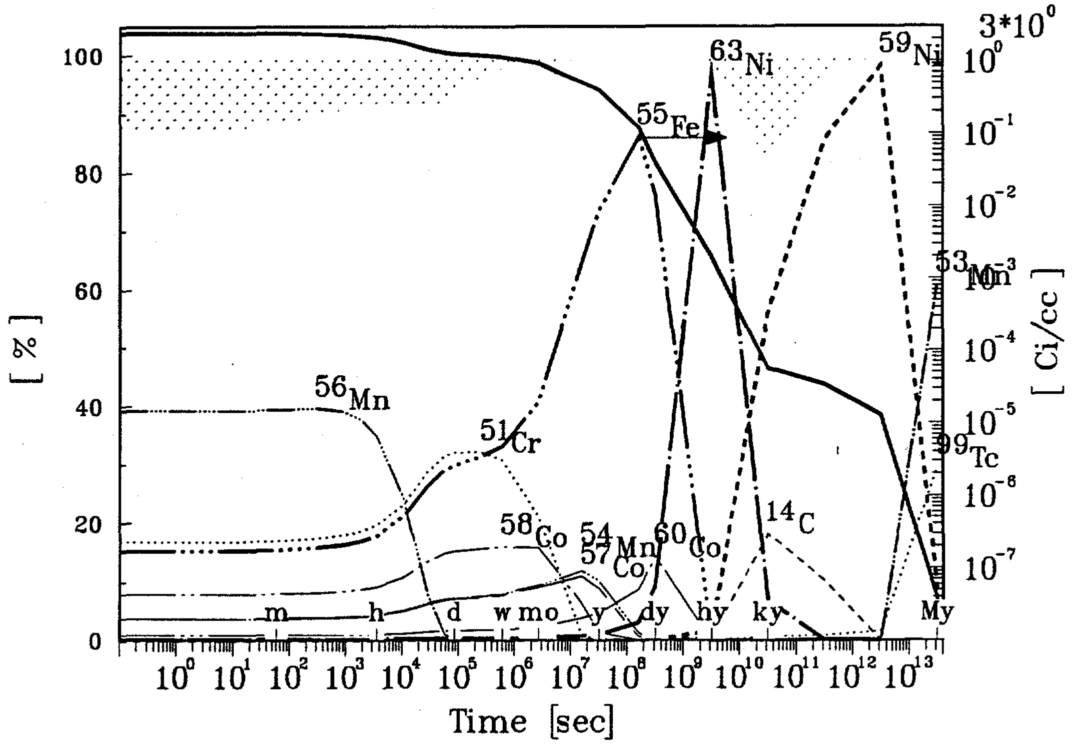

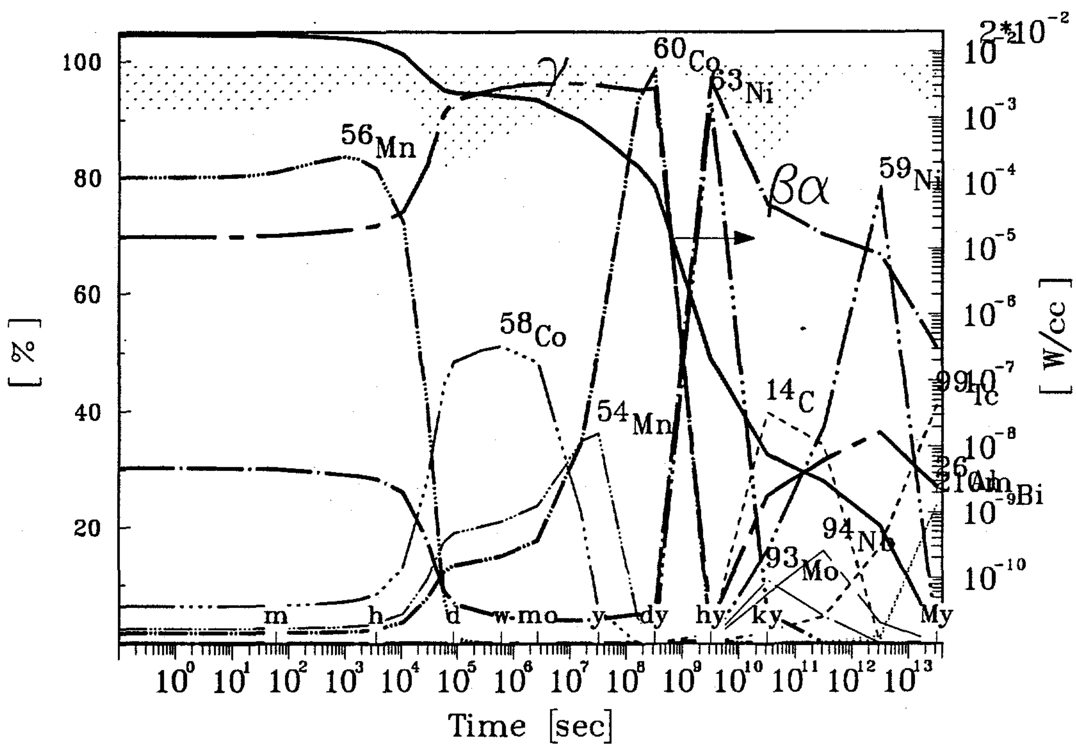

36

Figure 67. The specific radioactivity (top) and the specific decay heat (bottom) in zone # 36 (O_SS - SS/water).

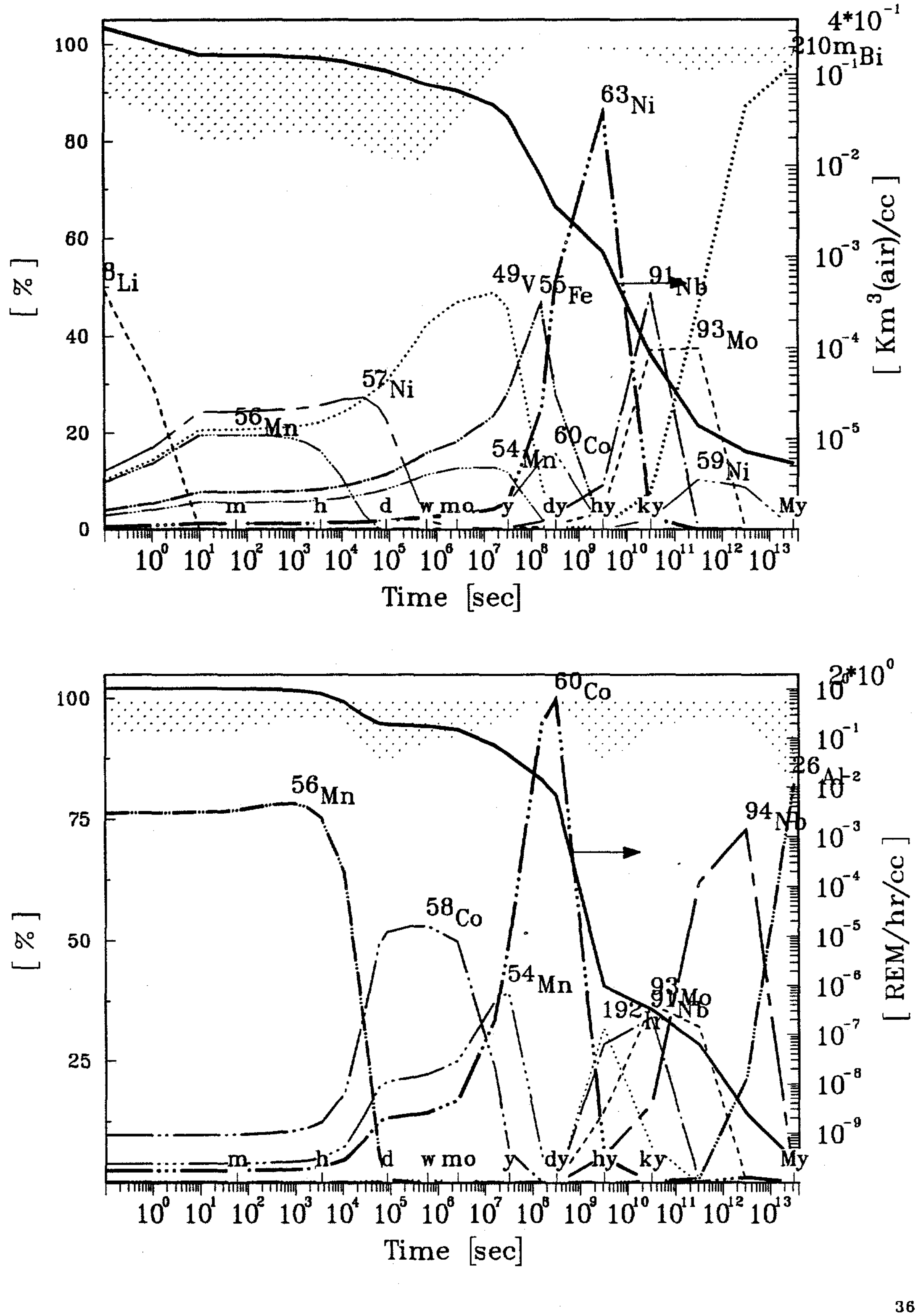

Figure 68. The specific air-BHP (top) and the point-source contact dose (bottom) in zone # 36 (O_SS - SS/water).

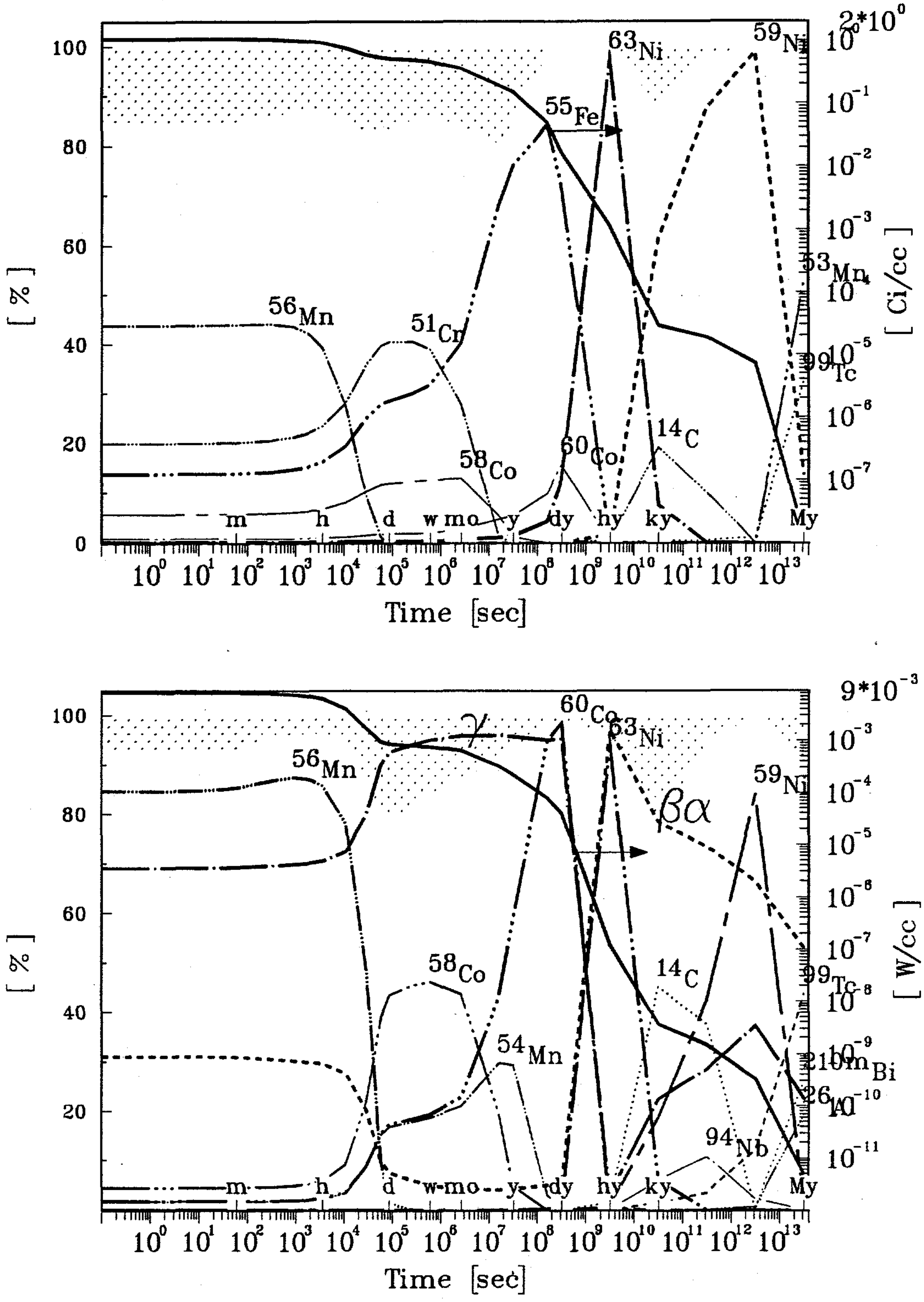

38

Figure 69. The specific radioactivity (top) and the specific decay heat (bottom) in zone # 38 (O_SS - SS/water).

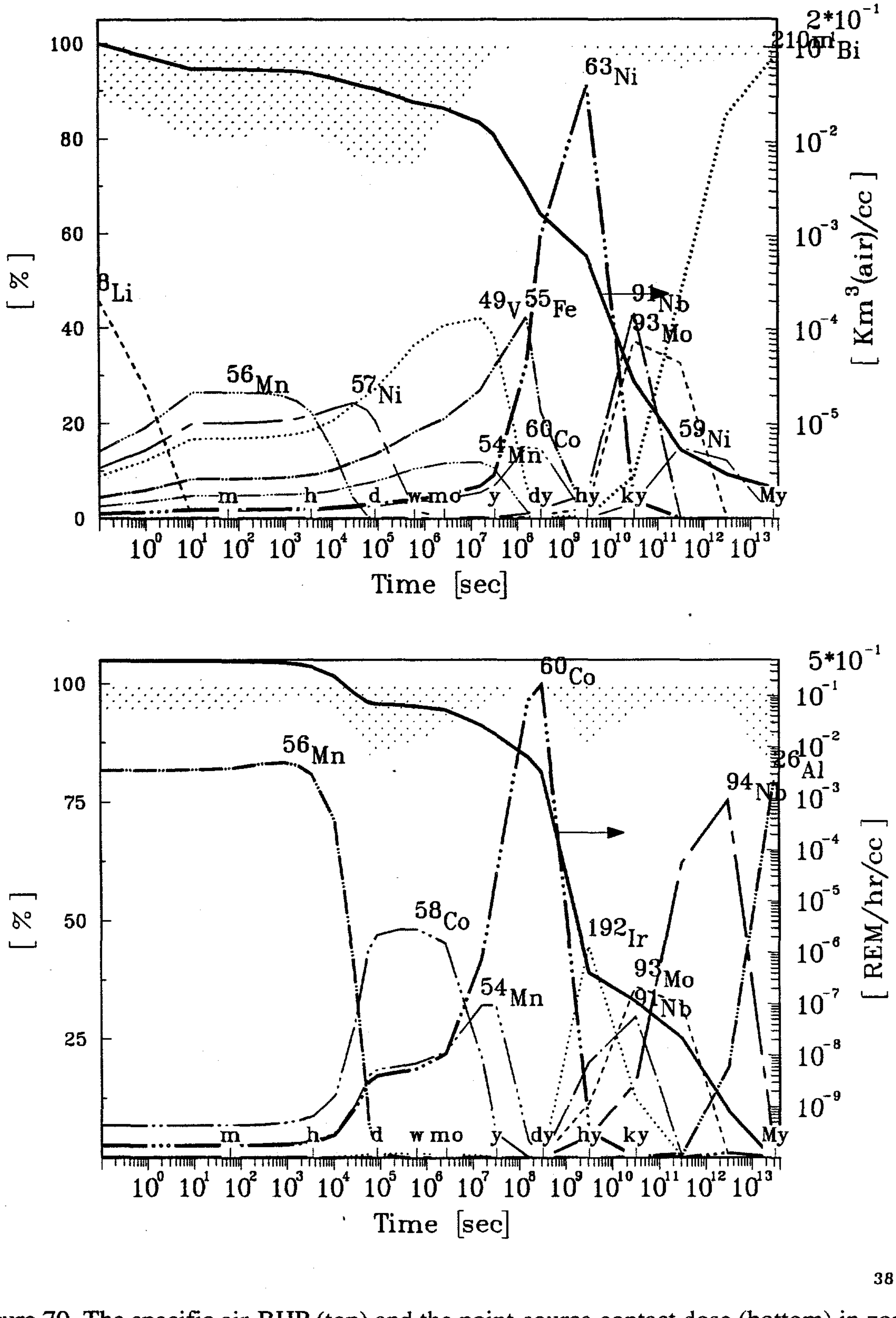

Figure 70. The specific air-BHP (top) and the point-source contact dose (bottom) in zone # 38 (O_SS - SS/water).

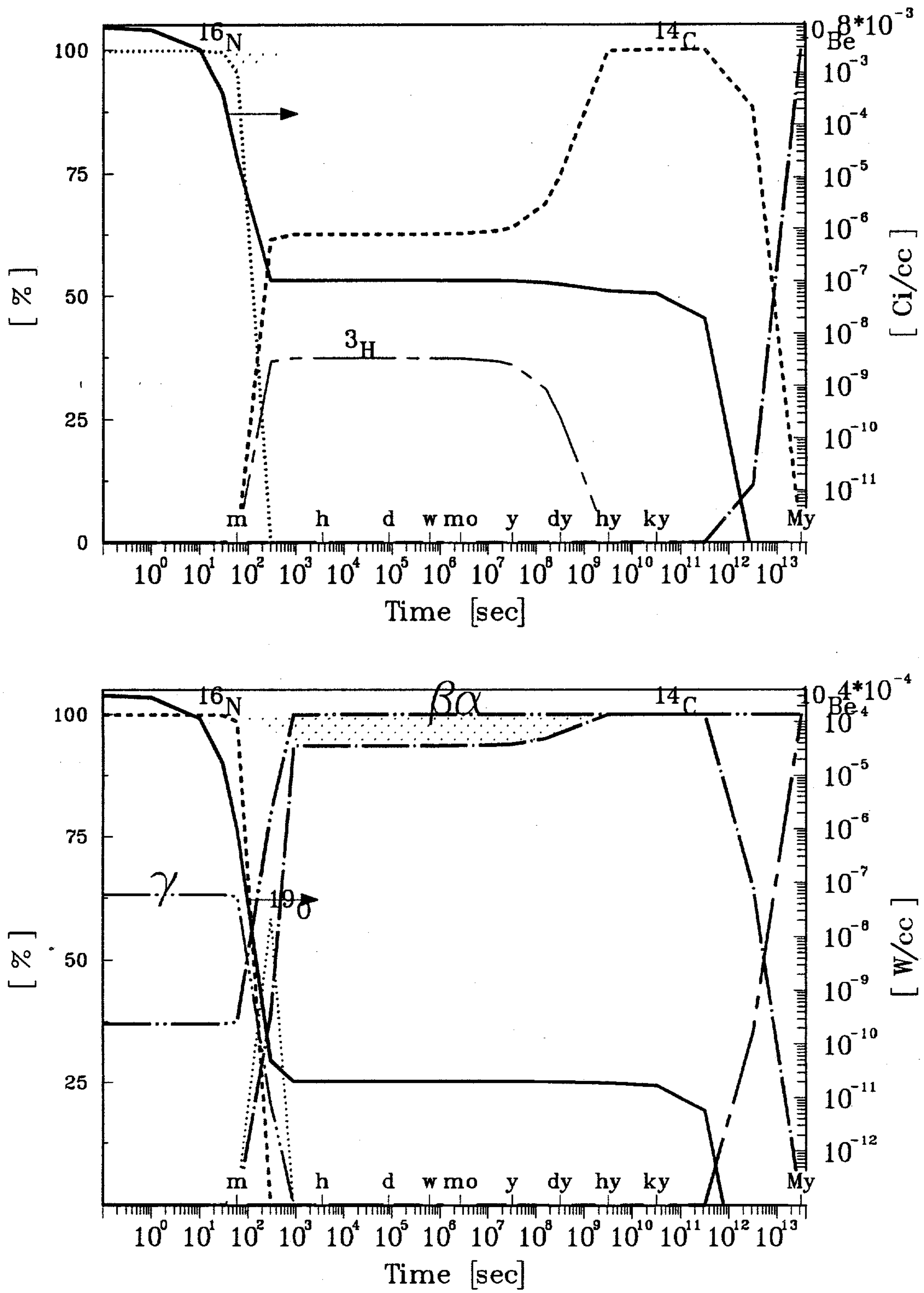

39

Figure 71. The specific radioactivity (top) and the specific decay heat (bottom) in zone # 39 (O_H2O - SS/water).

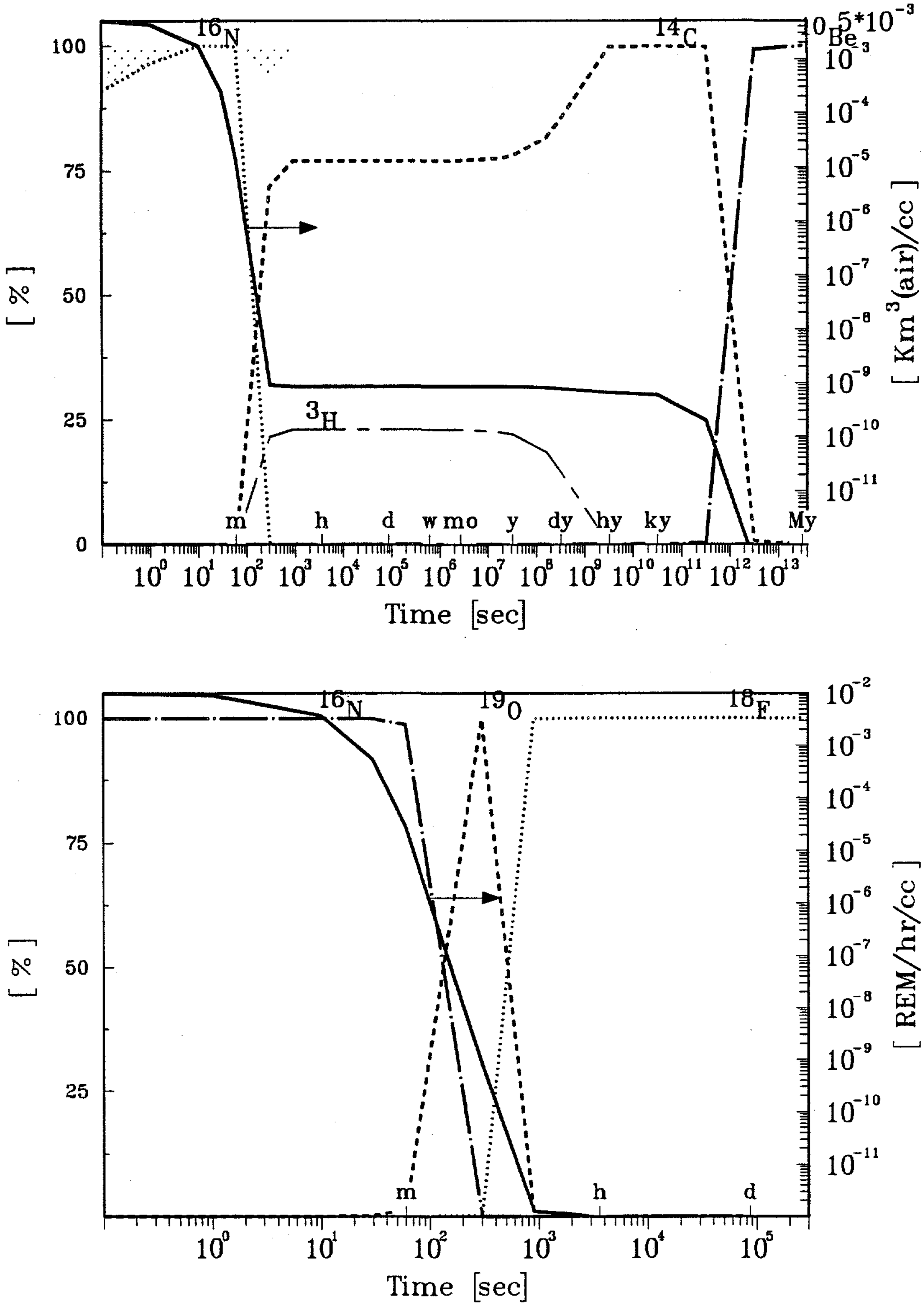

39

Figure 72. The specific air-BHP (top) and the point-source contact dose (bottom) in zone # 39 (O_H2O - SS/water).

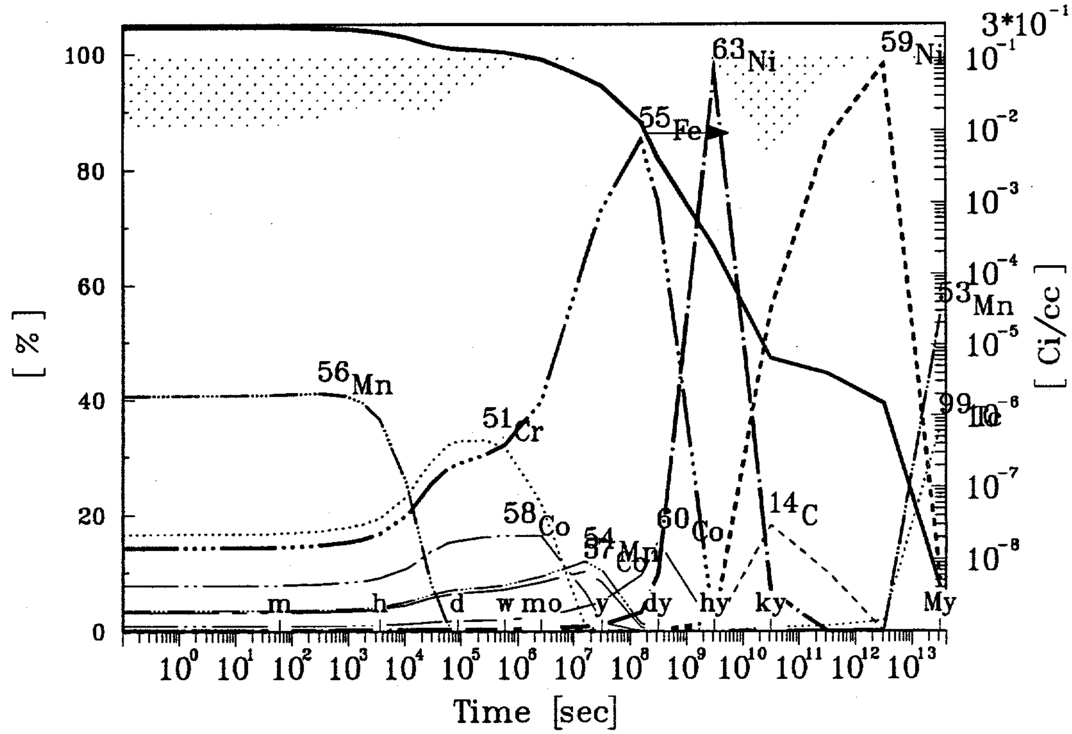

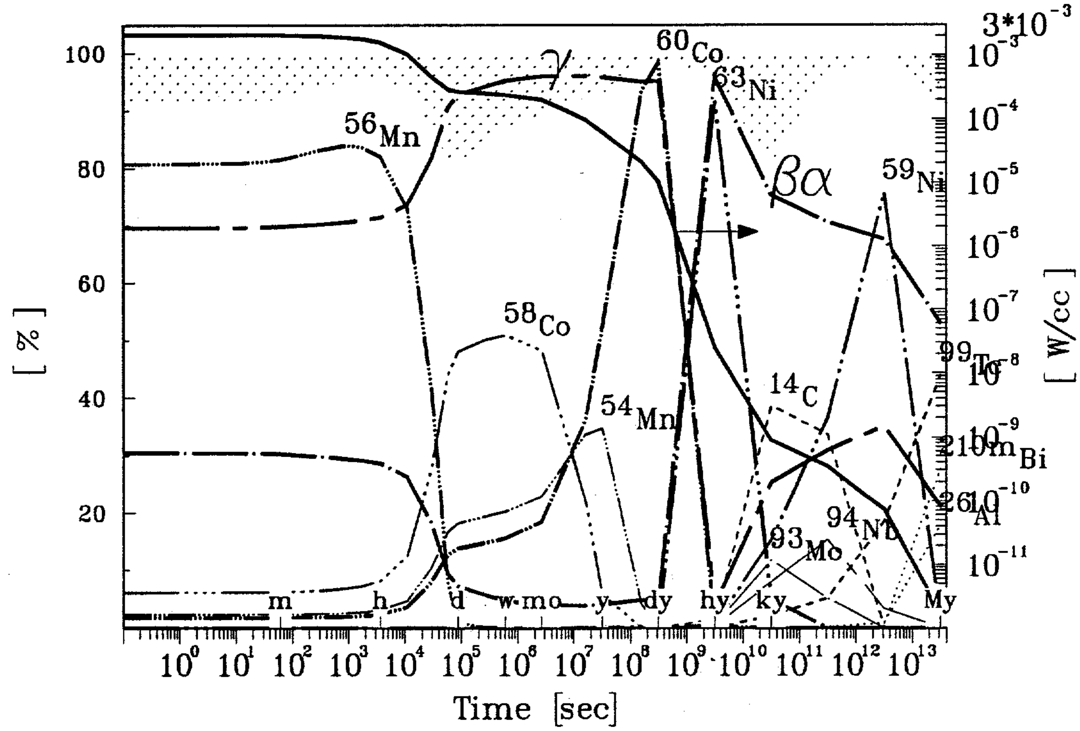

40

Figure 73. The specific radioactivity (top) and the specific decay heat (bottom) in zone # 40 (O_SS - SS/water).

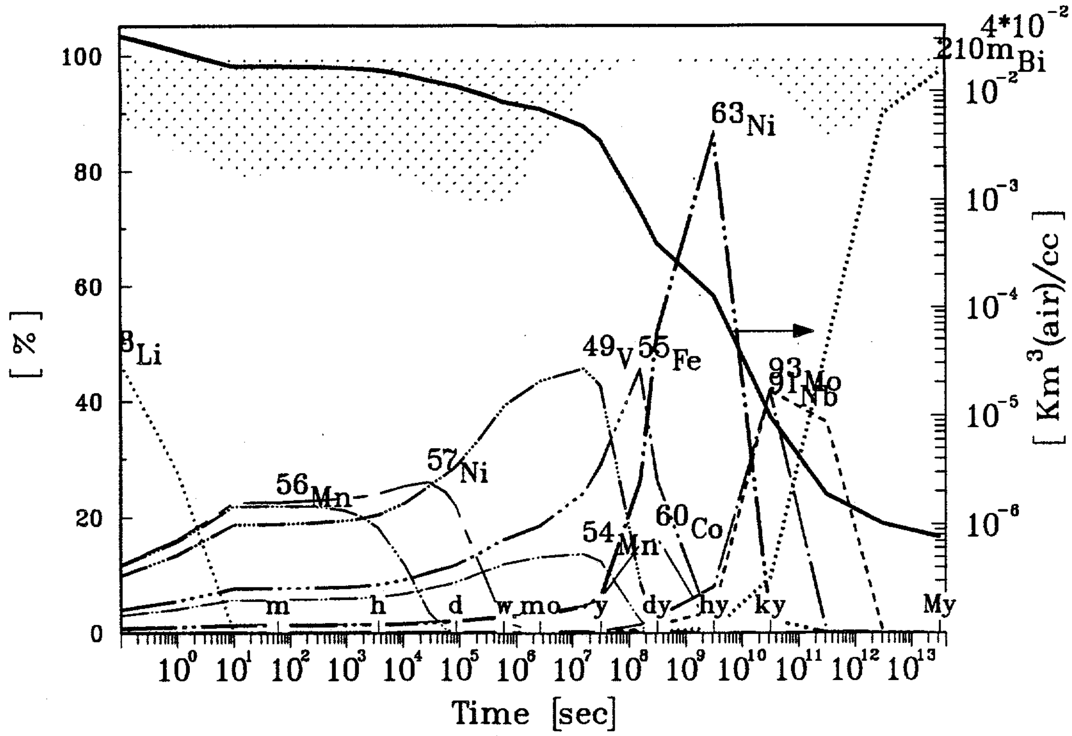

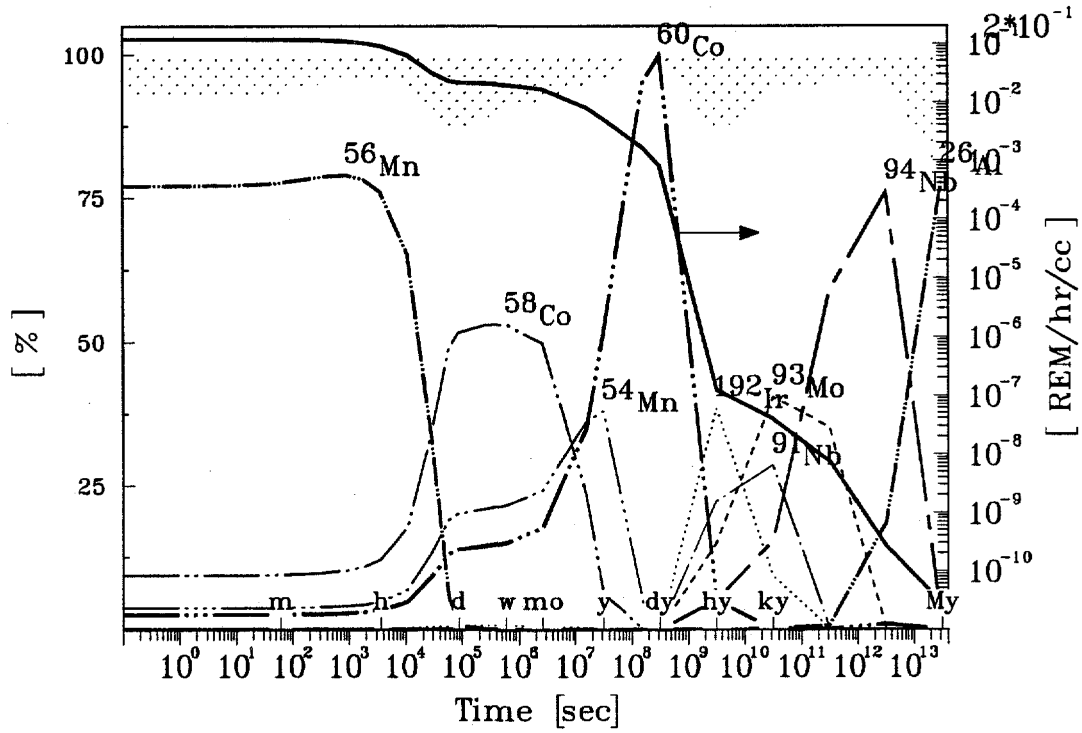

40

Figure 74. The specific air-BHP (top) and the point-source contact dose (bottom) in zone # 40 (O_SS - SS/water).

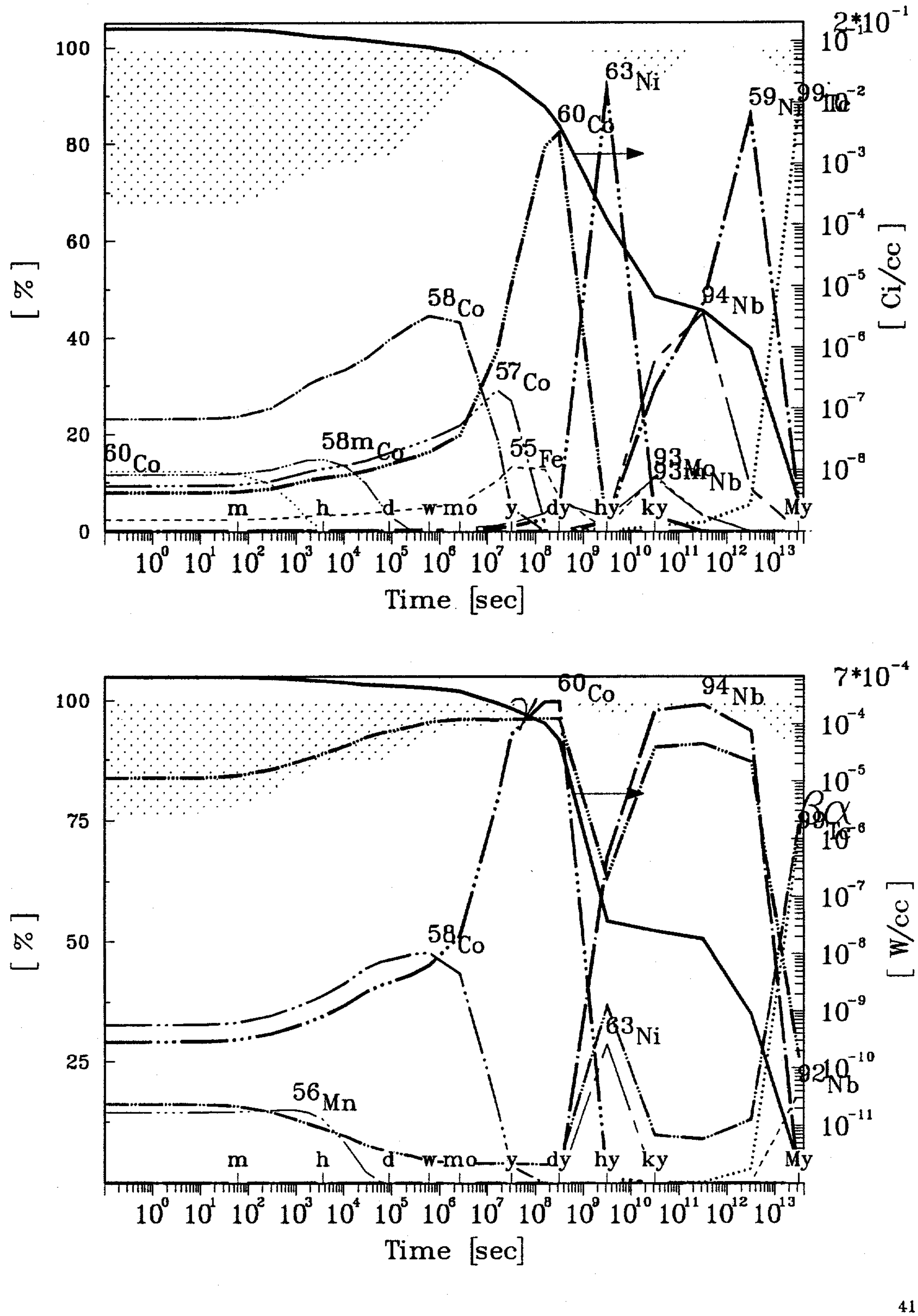

Figure 75. The specific radioactivity (top) and the specific decay heat (bottom) in zone # 41 (O_VV - SS/water).

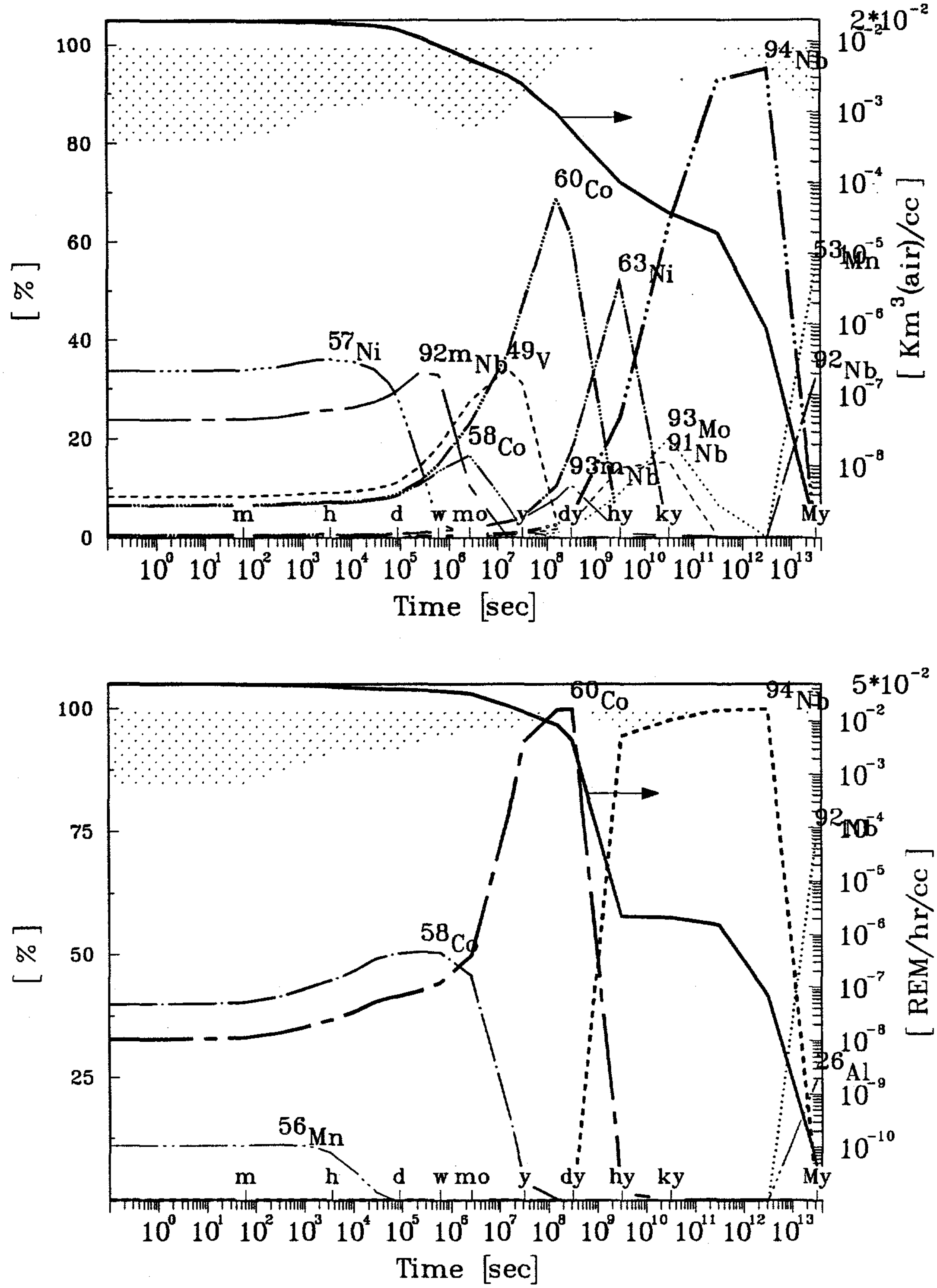

41

Figure 76. The specific air-BHP (top) and the point-source contact dose (bottom) in zone # 41 (O_VV - SS/water).

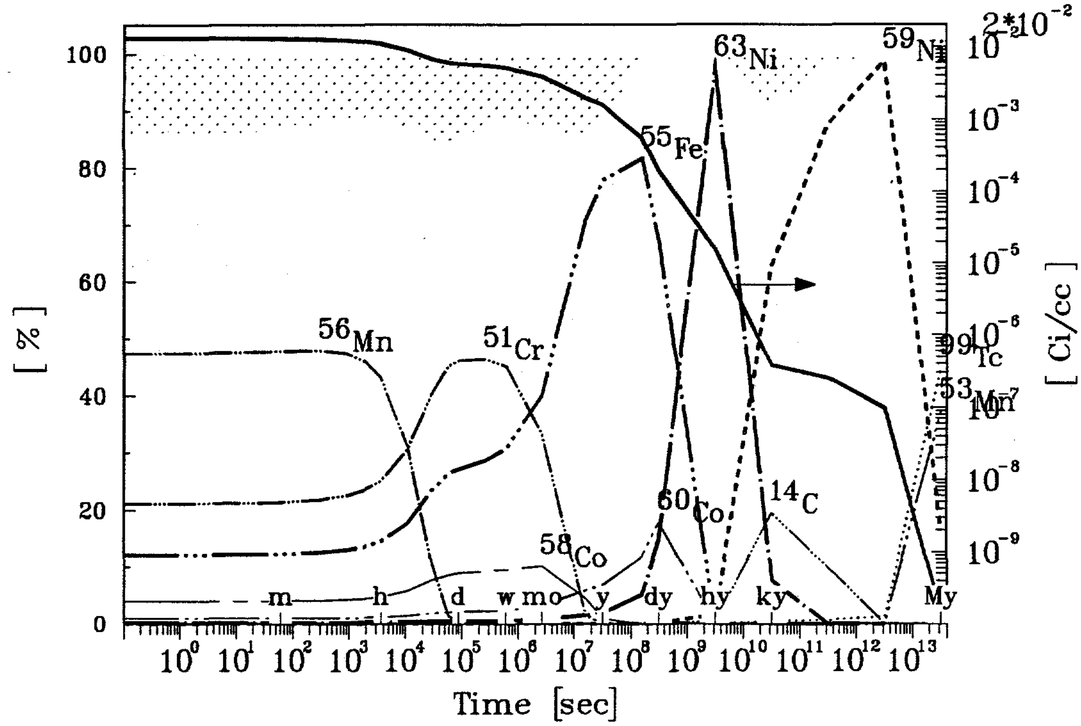

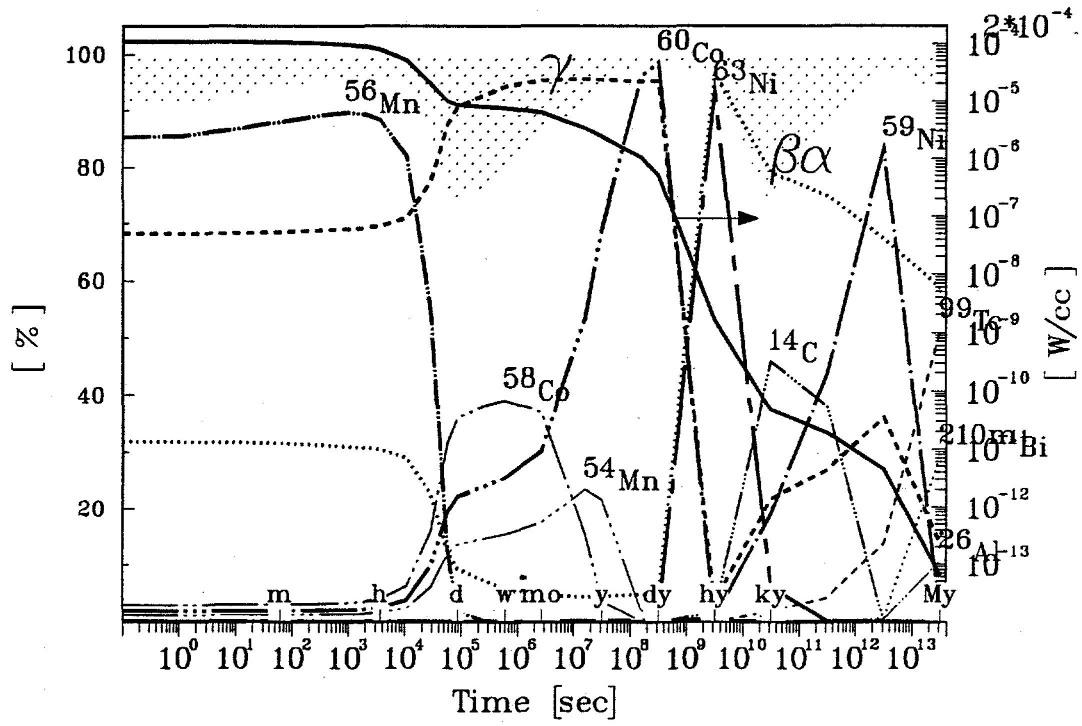

42

Figure 77. The specific radioactivity (top) and the specific decay heat (bottom) in zone # 42 (O_SS_H2O - SS/water).

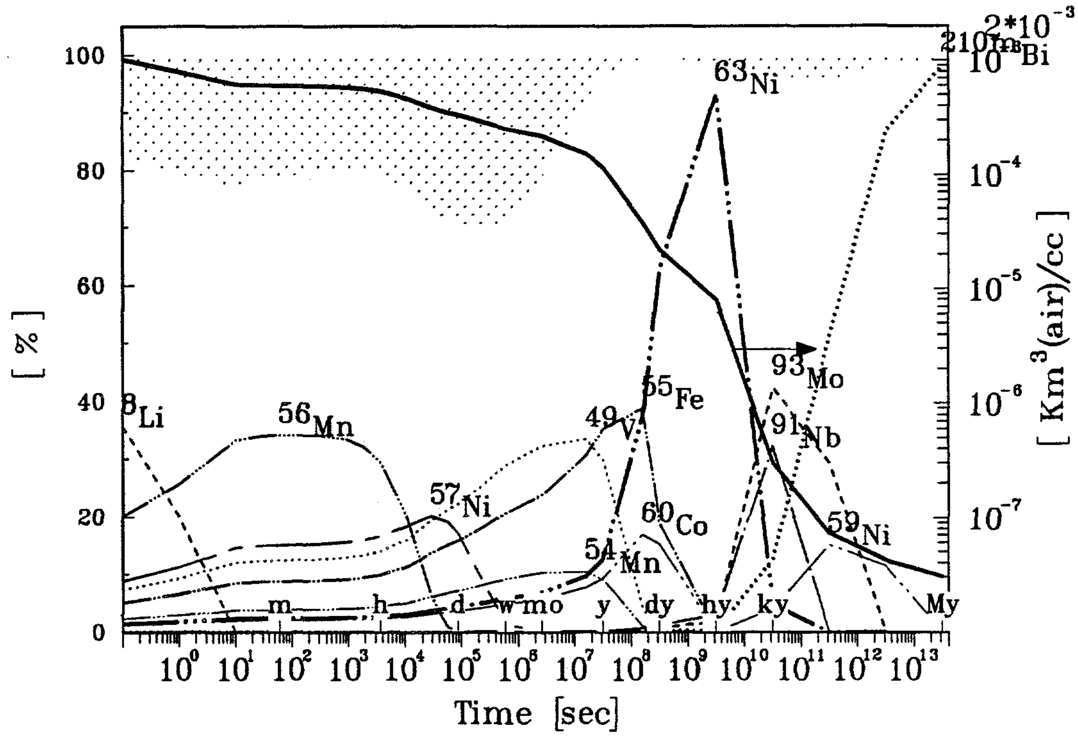

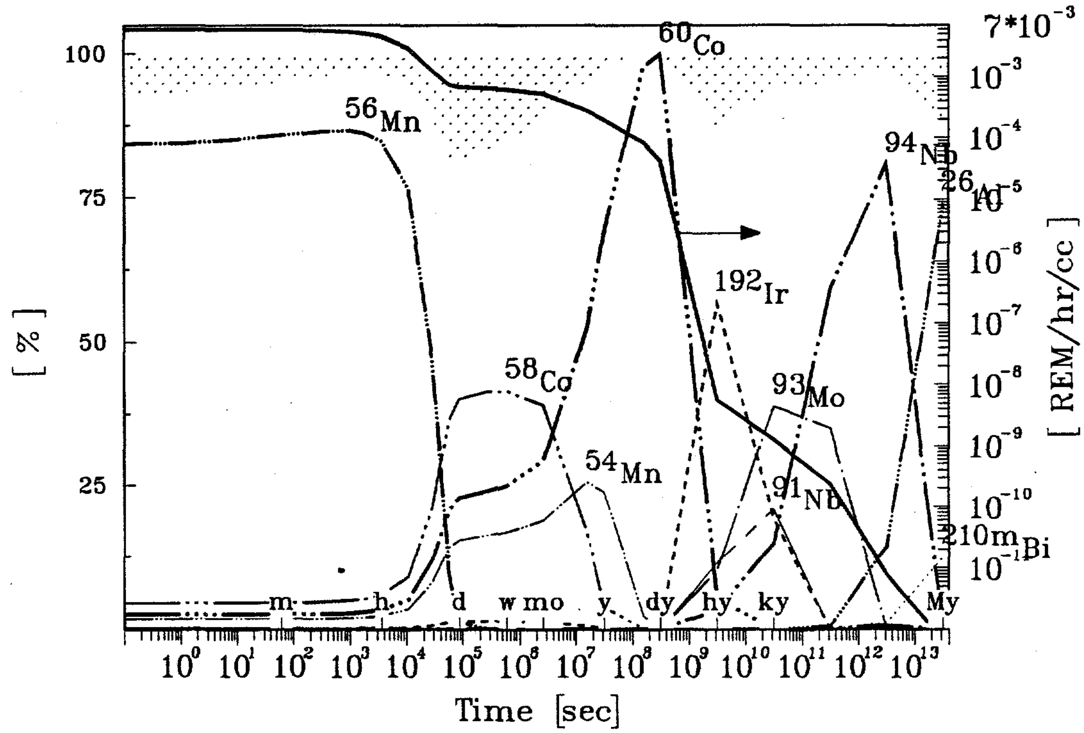

42

Figure 78. The specific air-BHP (top) and the point-source contact dose (bottom) in zone # 42 (O_SS_H2O - SS/water).

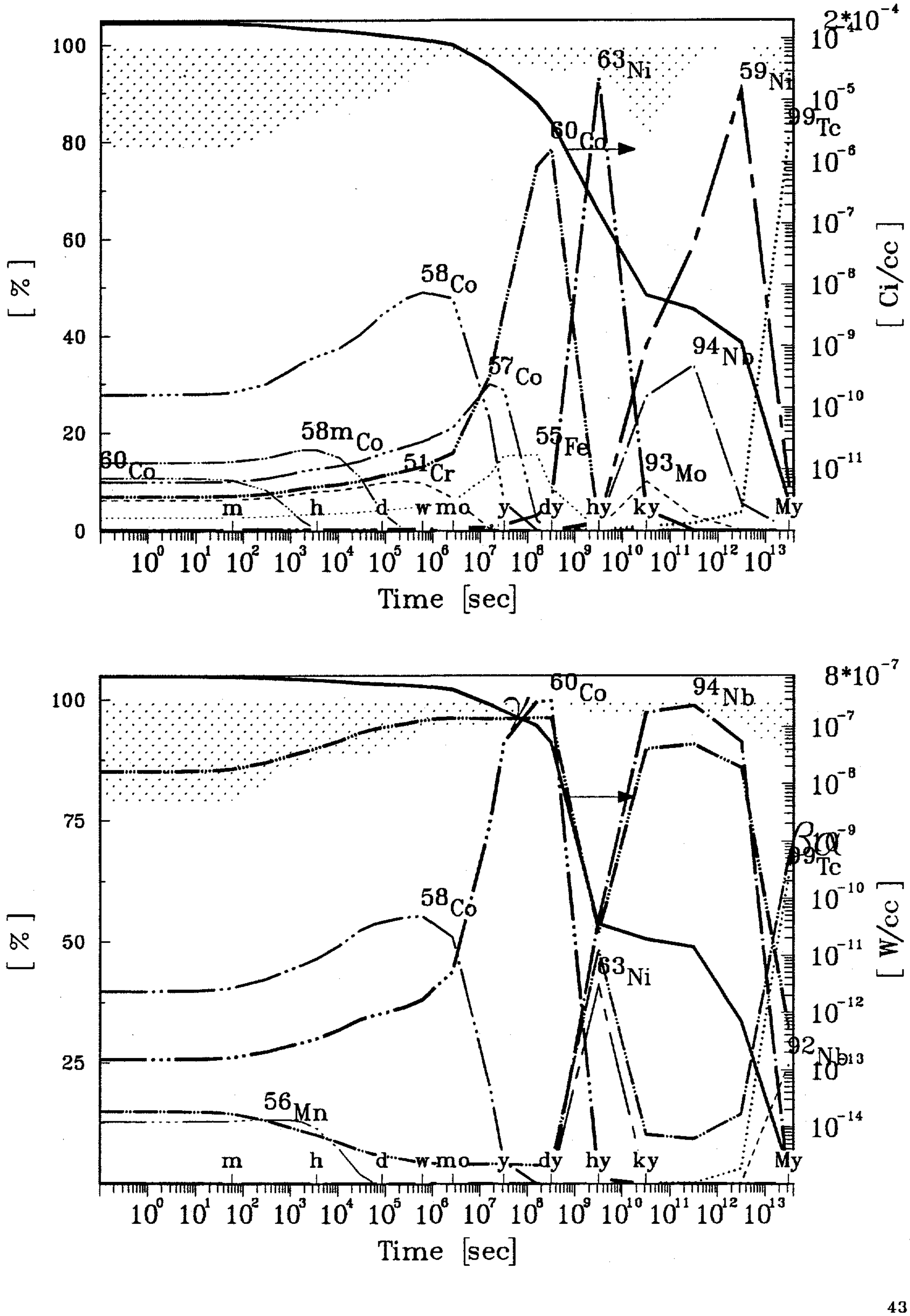

Figure 79. The specific radioactivity (top) and the specific decay heat (bottom) in zone # 43 (O_VV - SS/water).

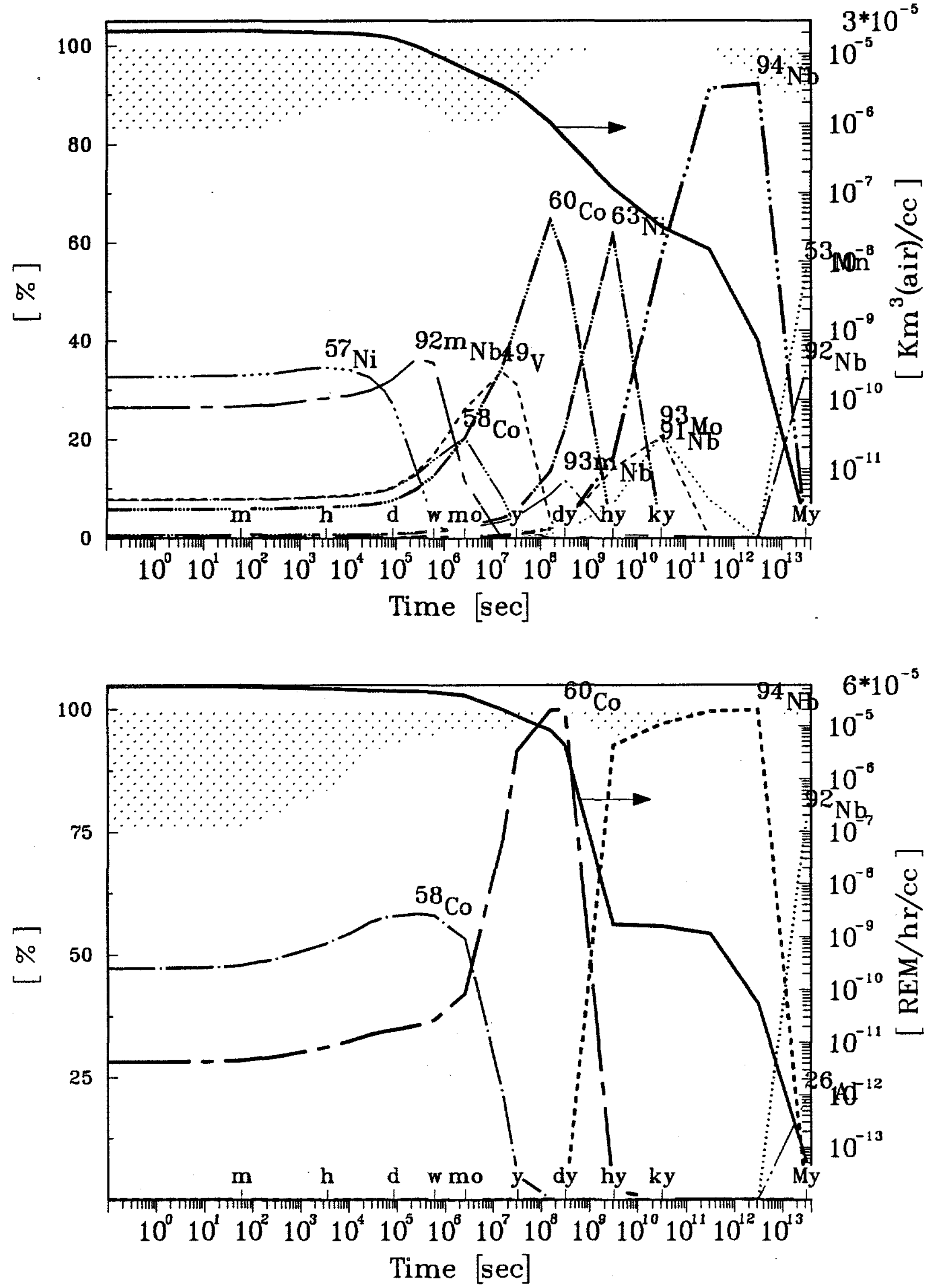

43

Figure 80. The specific air-BHP (top) and the point-source contact dose (bottom) in zone # 43 (O_VV - SS/water).

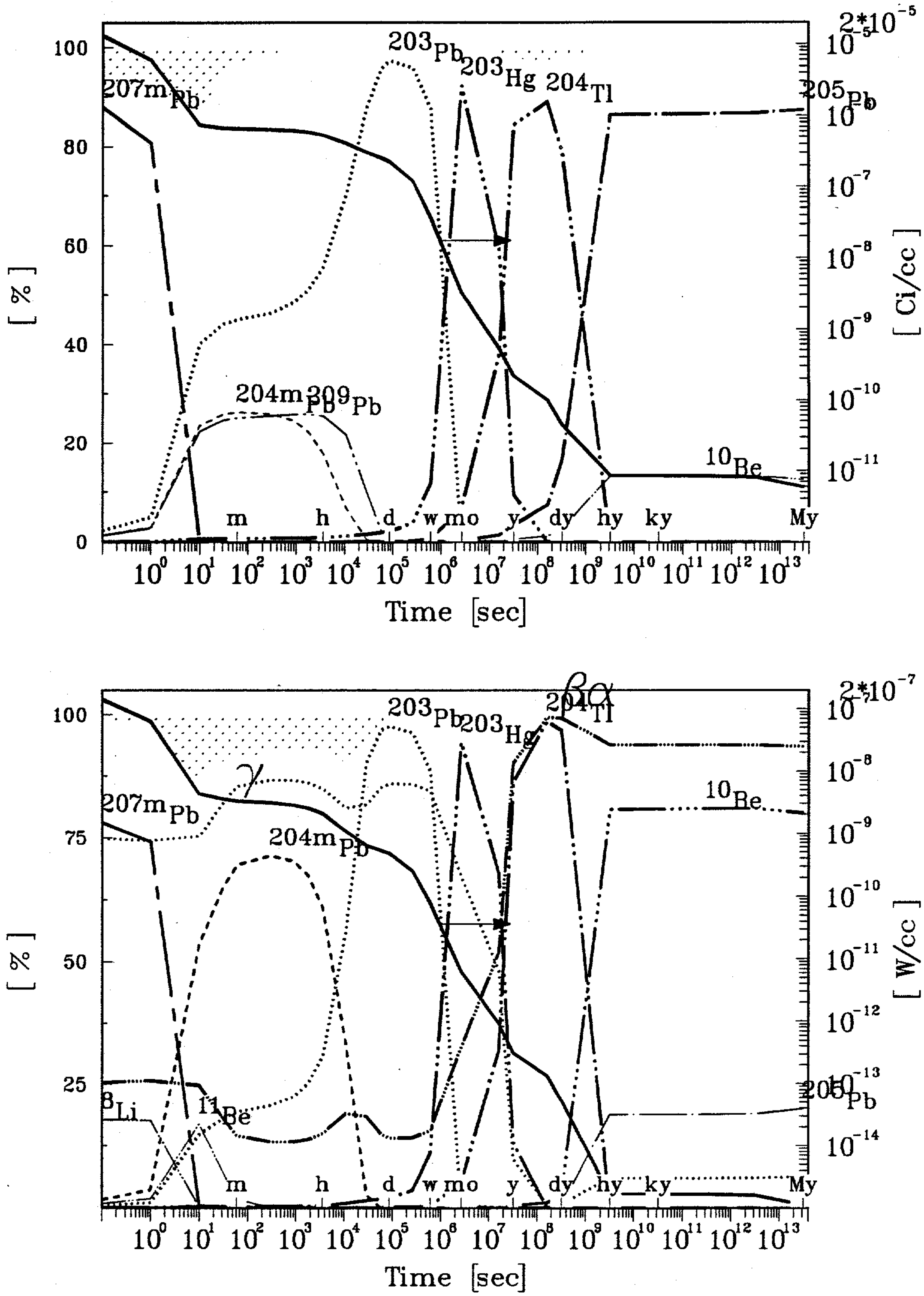

44

Figure 81. The specific radioactivity (top) and the specific decay heat (bottom) in zone # 44 (O_B4C_Pb - SS/water).

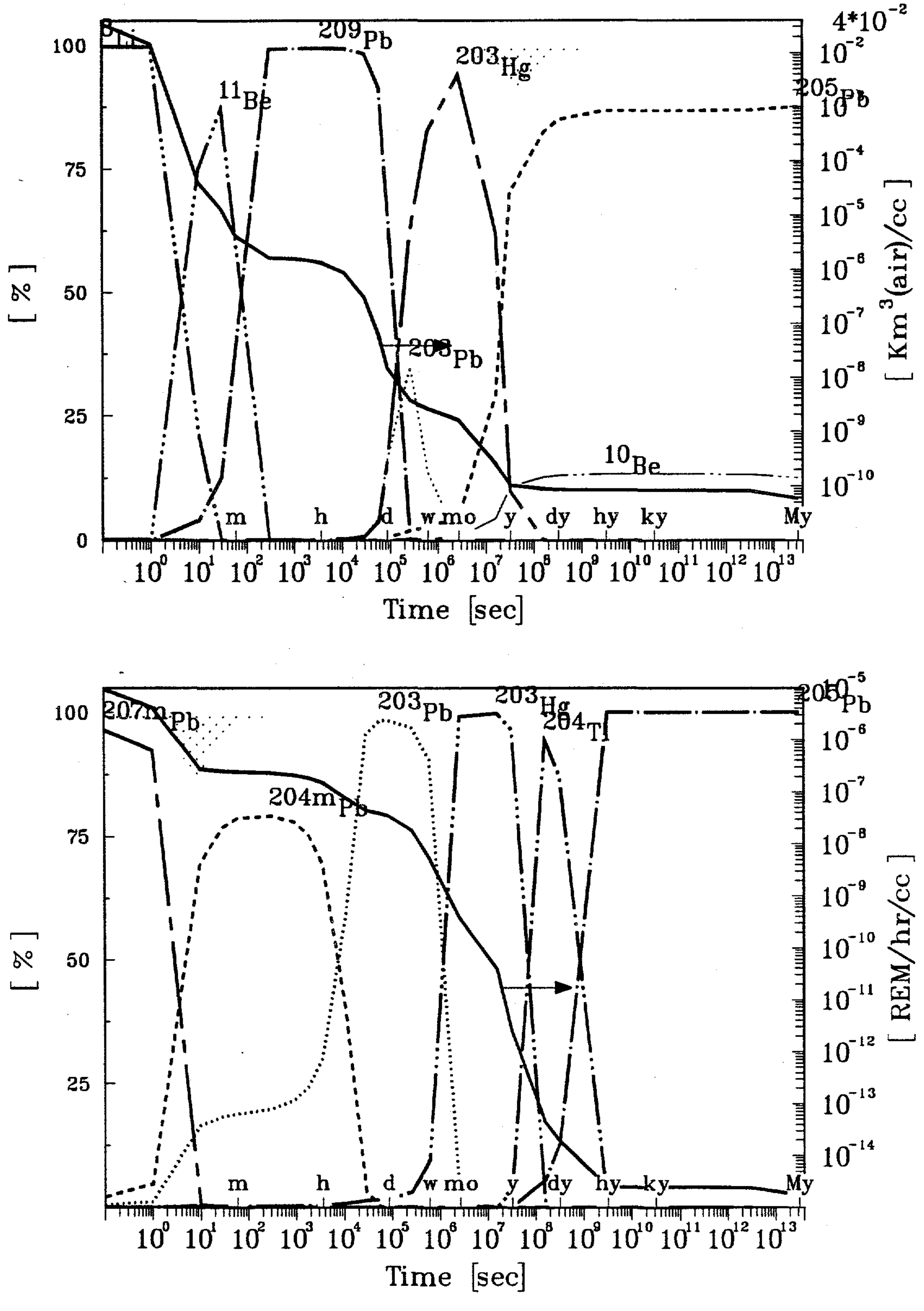

Figure 82. The specific air-BHP (top) and the point-source contact dose (bottom) in zone # 44 (O_B4C_Pb - SS/water).

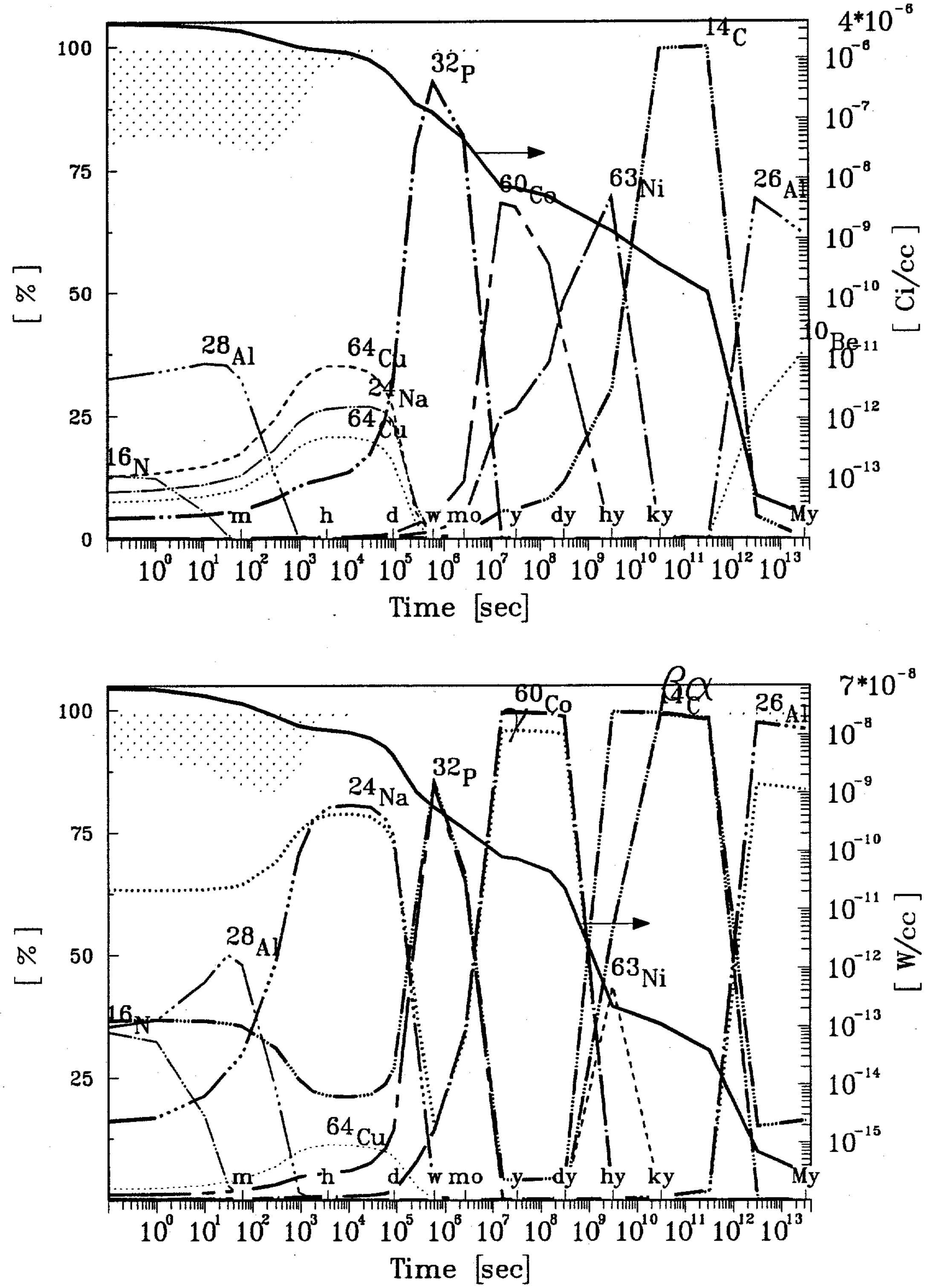

45

Figure 83. The specific radioactivity (top) and the specific decay heat (bottom) in zone # 45 (O_INSUL - SS/water).

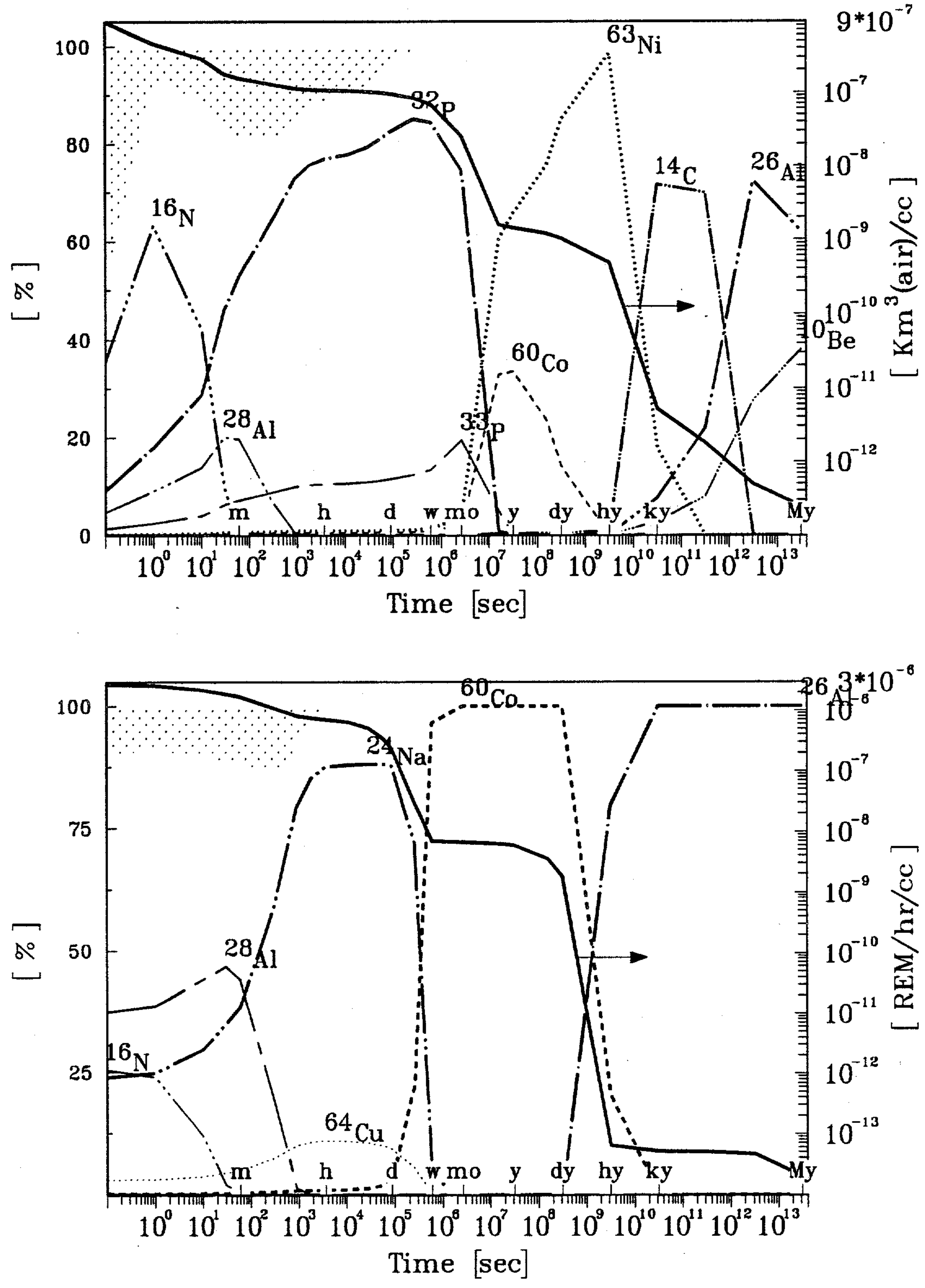

45

Figure 84. The specific air-BHP (top) and the point-source contact dose (bottom) in zone # 45 (O_INSUL - SS/water).

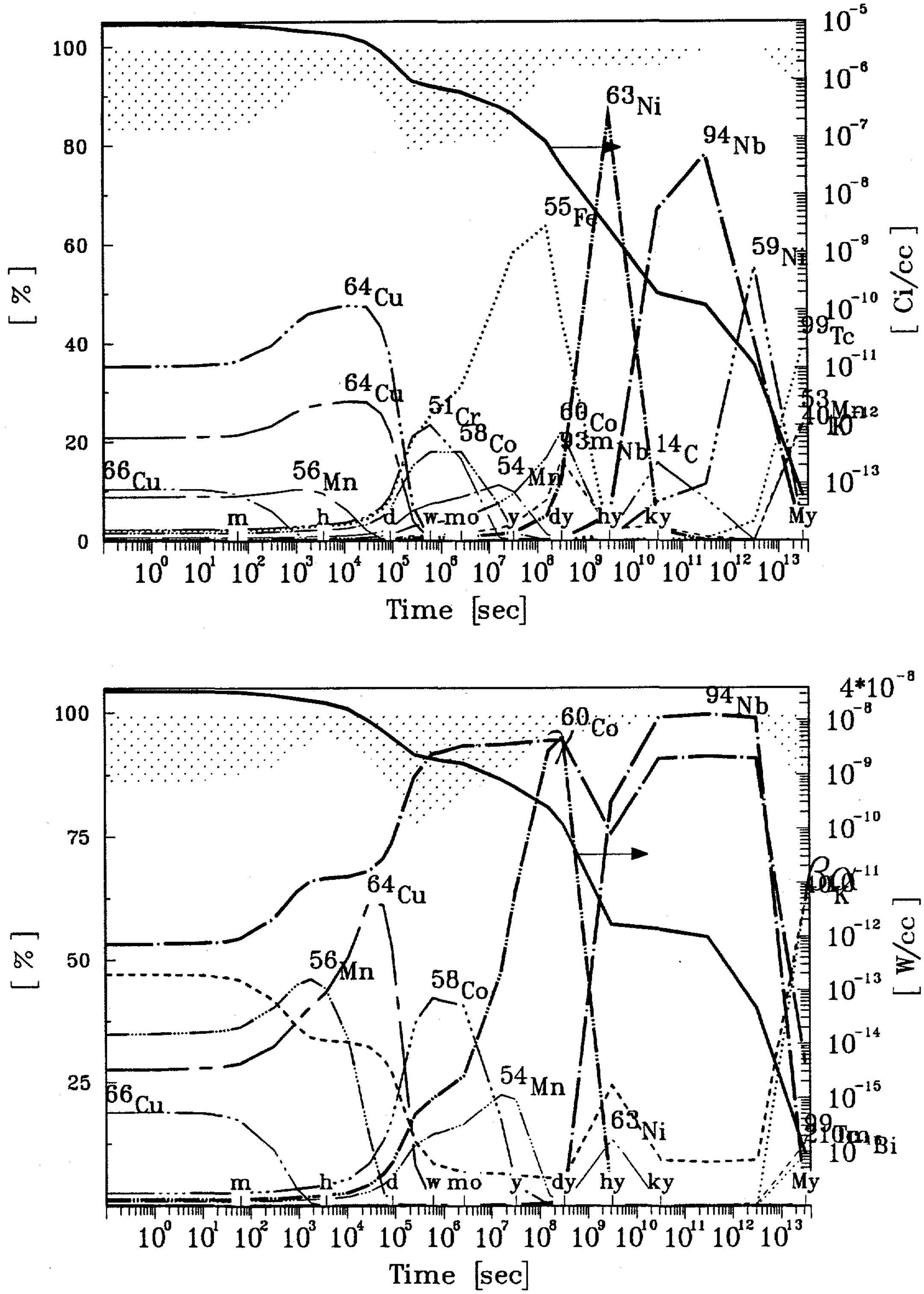

Figure 85. The specific radioactivity (top) and the specific decay heat (bottom) in zone # 46 (O_Magnet - SS/water).

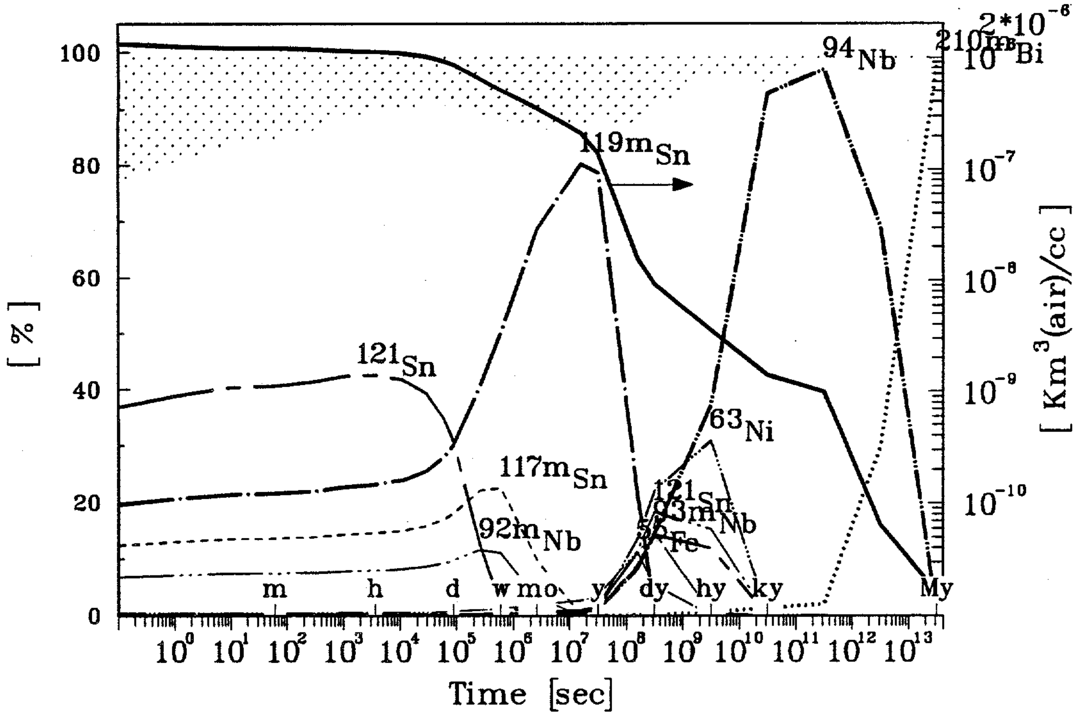

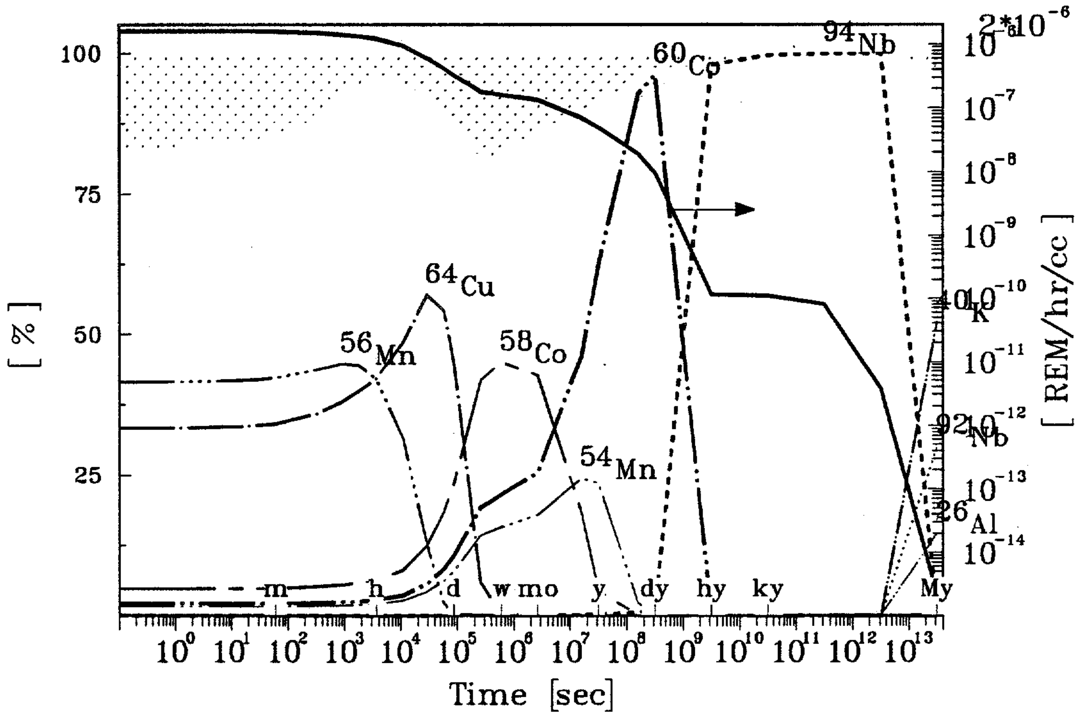

Figure 86. The specific air-BHP (top) and the point-source contact dose (bottom) in zone # 46 (O_Magnet - SS/water).

References

1. H. Attaya, "Input Instructions for RACC-P," Argonne National Laboratory, ANL/FPP/TM-270 (1994).

2. H. Attaya, "Radioactivity Computation of Steady-State and Pulsed Fusion Reactors Operation," Argonne National Laboratory, ANL/FPP/TM-273 (1995).

3. R.D. O'Dell et al., "User's Manual for ONEDANT: a code package for one-dimensional, diffusion-accelerated neutral particle transport," Los Alamos National Laboratory Report, LA-9184-M (1989).

4. H. Attaya et al., "Two Dimensional LOCA Analysis for Fusion Reactors," Proc. Of 13th IEEE Symposium on Fusion Engineering, Knoxville, TN, IEEE Cat. No. 89CH2820, 1120 (1989).

5. H. Attaya, "LOCA Analysis for Manganese-Stabilized Steel," Fusion Technology Vol. 19, 1331 (1991).

6. H. Attaya et al., "US-ITER Activation Analysis," Fusion Technology Vol. 19, 1837 (1991).

DISTRIBUTION LIST FOR ANL/FPP/TM-276

Internal

H. Attaya (5)
S. Bhattacharyya
M. Billone
J. Brooks
D. Ehst
Y. Gohar
I. Gomes
A. Hassanein
T. Hua
C. Johnson
M. Lineberry
R. Mattas
B. Micklich
Dale L. Smith
D.-K. Sze
T. Yule

FPP Files (5)
TIS Files (1)

External

DOE/OSTI for distribution per UC-424 (41)
Manager, Chicago Operations Office
ANL-E Libraries (2)
ANL-W Library
M. Abdou, University of California, Los Angeles
C. Baker, University of California, San Diego
S. Berk, U.S. Department of Energy
W. Daenner, ITER, Germany
J. Davis, McDonnell Douglas Aerospace
J. Doggett, Lawrence Livermore National Laboratory
L. El-Guebaly, University of Wisconsin
U. Fischer, Forschungszentrum Karlsruhe, Germany
W. Gauster, ITER JCT, Garching, Germany
L. Greenwood, Battelle Pacific Northwest Laboratory
I. Kirillov, D.V. Efremov Scientific Research Institute, Russia
D. Lousteau, ITER JCT, Garching, Germany
H. Maekawa, Japan Atomic Energy Research Institute, Japan
S. Malang, Forschungszentrum Karlsruhe, Germany
D. Muntz, Forschungszentrum Karlsruhe, Germany
R. Parker, ITER JCT, Garching, Germany
S. Piet, ITER JCT, San Diego, California
R. Price, U.S. Department of Energy
A. Raffray, ITER JCT, Garching, Germany
G. Saji, ITER JCT, San Diego, California
M. Sawan, University of Wisconsin
M. Seki, Japan Atomic Energy Research Institute, Japan
W. Stacey, Georgia Institute of Technology
D. Steiner, Rensselaer Polytechnic Institute
I. Sviatoslavsky, University of Wisconsin
M. Tillack, University of California, San Diego
J. Vetter, Forschungszentrum Karlsruhe, Germany
G. Vieider, ITER, Germany
R. Watson, Sandia National Laboratories, Albuquerque

F.W. Wiffen, U.S. Department of Energy
K. Wilson, Sandia National Laboratories, Livermore
M. Youssef, University of California, Los Angeles
C.E.A. Library, Fontenay-aux-Roses, France
Librarian, Culham Laboratory, England
Thermonuclear Library, Japan Atomic Energy Research Institute, Japan